Real-Time Measurements of Non-Refractory Particle Composition and Interactions at Forested Sites

By

Alice Elizabeth Delia

B.A., Kalamazoo College, Kalamazoo, MI, 1997

M.S., University of Colorado at Boulder, 2001

A thesis submitted to the Faculty of the Graduate School of the University of Colorado in partial fulfillment of the requirement for the degree of Doctor of Philosophy

Department of Astrophysical, Planetary and Atmospheric Sciences

May 2004

This thesis entitled:

Real-Time Measurements of Non-Refractory Particle Composition and Interactions at Rural and Semi-Rural Sites

Written by: Alice Elizabeth Delia

has been approved for the Department of Astrophysical, Planetary, and Atmospheric Sciences

---

Dr. Darin W. Toohey

Date _____

The final copy of this thesis has been examined by the signatories, and we find that both the content and the form meet acceptable presentation standards of scholarly work in the above-mentioned discipline

Delia, Alice Elizabeth (Ph.D., Department of Astrophysical, Planetary and Atmospheric Sciences)
Real-Time Measurements of Non-Refractory Particle Composition and Interactions at Forested Sites

Thesis directed by Professor Darin W. Toohey

ABSTRACT

Aerosols can have a significant influence on air quality, visibility, health, and regional and global climate. As is evident from the Intergovernmental Panel on Climate Change report [2001], the effect of aerosols on climate are the most uncertain, could be positive or negative depending on the chemical composition, can have secondary effects that are poorly understood, and could be as large as that of the greenhouse gases. However, aerosol properties are difficult to measure because there is so much variability in size, composition, and other properties. The more local effects, such as air quality, visibility, and health, are also difficult to determine because aerosols are strongly influenced by local conditions as well as long-range transport.

Currently, there are no instruments capable of measuring all aerosol properties, either in-situ or remotely. Most measurements are restricted to a certain size range, to only one property, or multiple properties (e.g., an impactor with size and chemical composition) with low time resolution. In 1999, the Aerosol Mass Spectrometer (AMS) developed by Aerodyne Research, Inc., was deployed for the first time in the Atlanta Supersites Project. The AMS provides real time in-situ quantitative chemical composition and size data of submicron non-refractory aerosols. The compositional information is obtained with standard quadrupole mass

spectrometry and the size data by particle time of flight across a vacuum chamber. Particles are first vaporized, typically at a temperature of approximately 600 °C, and then ionized by electron impact before being analyzed by the quadrupole mass spectrometer. It is this separation of vaporization and ionization that allows the AMS to produce quantitative data. During the last four years, the AMS has progressed from a pilot instrument with several unresolved issues to a self-sufficient, tested, instrument that provides more complete information about fine aerosols than most other instruments.

This thesis presents the operation and development of the Aerodyne Research Aerosol Mass Spectrometer (AMS) and results from several field campaigns. The main focus will be two large field campaigns at which the AMS was deployed, PROPHET 2001 at the University of Michigan Biological Station in northern Michigan and CELTIC 2003 at Duke Forest in North Carolina, are both located in forested areas. The PROPHET site is truly a remote site with no large population centers nearby while CELTIC is located just outside Raleigh, North Carolina, and has a much larger urban influence.

Aerosol properties at the PROPHET site are clearly dependent on wind direction, with large concentrations of aged, processed aerosols dominated by sulfate arriving from the south and low concentrations dominated by organic species arriving from the less populated region to the north. Aerosols at the CELTIC site are more of a mixture due to the variety of nearby sources, although large changes in air masses are also clearly apparent.

These measurements characterize the aerosols at a particular location, indicate the level of processing the aerosols have undergone and provide some information about sources.

ACKNOWLEDGEMENTS

First of all, I would like to thank my advisor, Dr. Darin Toohey, for providing advice, encouragement, the freedom to pursue my research interests freely, and many discussions of both scientific and trivial interests. He has helped me to understand the nature of scientific research and sparked my enthusiasm for discovering answers to some of the endless list of questions about the atmosphere. I have learned much from him and am looking forward to many more years of fascinating discussions.

Dr. Doug Worsnop has also been a wonderful mentor to me. He has helped me gain an understanding of the many aerosol issues as well as some of the broader implications. From my first confused experience at the Texas Air Quality Study in 2000, Doug has guided much of my research and helped me grow both as a scientist and a person. The rest of the Aerodyne Research people have also been instrumental in helping me to get a handle on all this AMS stuff, including John Jayne, Manjula Canagaratna, Tim Onasch, and Phil Silva (now at Utah State University).

Many thanks to my long-time office mate and fellow graduate student Brett Thornton, we have had a lot of fun commiserating together about research, university, and world problems. Dr. Linnea Avallone and her graduate students, Gannet Hallar, Lars Kalnajs, and Sean Davis, have also helped me with their advice and encouragement. My good friend and former roommate, Brenda Mulac, has been a source of great comfort and encouragement, as well as providing a lot of laughs. My undergraduate mentor, Dr. Sandra Laursen, has also offered a lot of advice and support and helped me put things in perspective. The PAOS staff (past and present) – Sherry Yearsley, Kelly Duong, Laurie Conway, and Lisa Burnham – have also been

instrumental in getting all the administrative details sorted out and providing some levity.

I could not have done any of this research without the help and resources of the many scientists I have worked with at the field campaigns that formed the core of my work. Although it may be repetitive, I would like to thank them all for their involvement in each campaign.

Texas Air Quality Study, Texas (2000): Doug Worsnop (ARI), Jose Jimenez (formerly ARI, currently CU), Manjula Canagaratna, Phil Silva, John Jayne, and Katie Purvis.

PROPHET, Michigan (2001): Doug Worsnop and Manjula Canagaratna (ARI), Rebecca Garland (CU), and Jonathan Allen and Umar Siddiqui (ASU) were the primary people I worked with on the AMS and SMPS measurements. Mary Anne Carroll (U of M) provided O_3, CO, NOx, and meteorological data and organized the study, Steve Bertman (Western Mich.) provided PAN, MPAN, PPN, and HONO data, Greg Huey and Dave Tanner (G. Tech) provided OH, H_2SO_4, and HNO_3 data and helped me a lot with my own instruments, Brian Lamb and Shelly Pressley (WSU) provided isoprene concentrations and fluxes, Jenny Moody and Mark Lilly (U. Virginia) provided vertical winds and back trajectories, Barry Lefer (NCAR) provided photolysis frequencies as well as assistance and advice, finally, the rest of the PROPHET scientists who made this a successful campaign.

CRYSTAL-FACE, Florida (2002): Although I did not present any of the work from this campaign, I learned many valuable lessons from this experience and especially

from Jose Jimenez (CU), Roya Bahreini Tomtor Varutbangkul, Rick Flagan, John Seinfeld and the rest of the CalTech and CIRPAS scientists.

Palmer School, Denver (2002): This experiment was on a much smaller scale than the organized studies, but was also a great learning experience. Many thanks to Shelly Miller and Mike Hannigan for their assistance with this project.

CELTIC, North Carolina (2003): Jose Jimenez and Alex Huffman (CU) for much assistance with the AMS, Lars Kalnajs (CU) for doing so many last minute improvements to the instruments, Craig Stroud and Sreela Nandi (NCAR) helped with the SMPS measurements, Eiko Nemitz (currently CEH) AMS and ammonia fluxes and size distributions, Thomas Karl (NCAR) PTRMS measurements of VOCs, Jose Fuentes (UVA) O_3 and NOx profiles, Chris Geron (EPA) meteorology, and the personnel at the FACTS-I site for their assistance in getting everything set up as well as the rest of the scientists involved.

Last, but not least, my family has been wonderful throughout the last five years in providing encouragement and advice, as well as listening patiently while I went on about my research. Their support has been instrumental in making me believe that I really could do this.

TABLE OF CONTENTS

LIST OF FIGURES

LIST OF TABLES

CHAPTER 1: INTRODUCTION

Aerosols can have a significant influence on air quality, visibility, health, and regional and global climate. Their study is complicated by their size and compositional variability, which depends on the nature of local sources, atmospheric conditions, and their histories. They are efficiently scavenged by precipitation or gravitational sedimentation, so the lifetimes of aerosols are relatively short, days to weeks. This means that the composition, size, and number of the aerosols will depend strongly on the local or regional conditions in which they are produced and transported.

One of the most obvious effects of high aerosol and pollutant levels is loss of visibility. Many major cities deal with persistent haze issues; for example, on many days Denver's "brown cloud" is clearly visible. Visibility is determined by the absorption and scattering of light by aerosols and gases and by the wavelength of the light and the position of the sun (i.e., a longer path early or late in the day may cause more severe visibility reduction). Scattering by particles of the same size as the wavelengths of visible light (i.e., 400 to 700 nm) is mostly responsible for visibility reduction. [Finlayson-Pitts and Pitts, 1999]

Concerns about the health effects of atmospheric particulate matter have increased in the last several years. The fine particles, those less than approximately 2.5 μm in diameter, can have especially serious effects since these particles can travel into the lungs where gas exchange occurs and they may stay there for some time. In contrast, most larger particles (>2.5 μm) are removed in the upper respiratory tract by

contact with the mucus that coats that area, followed by transportation by the small hair-like cilia to the throat where they are swallowed. [Finlayson-Pitts and Pitts, 1999] In recognition of the potential health hazards of aerosols, EPA has regulated emissions for aerosol less than 10 μm in diameter with the PM 10 and the proposed PM 2.5 standards. [EPA NAAQS; Seinfeld and Pandis, 1998]

Aerosols can affect global climate in two ways: directly, by scattering and/or absorbing light, and indirectly, by acting as cloud condensation nuclei, thereby affecting cloud microphysical properties and precipitation behavior. Very little is known about the indirect effect of aerosols on clouds, but it is believed that an increased number of aerosols will cause negative radiative forcing, i.e., a global cooling effect. [IPCC, 2001; Jacobson et al., 2000]

The direct effect of aerosols is better understood than the indirect effect, but is still highly uncertain. The effect of aerosols on light scattering and absorption is dependent on the size and composition of the aerosols. As mentioned previously, aerosols of the same size as the wavelengths of visible light scatter light most efficiently. [Finlayson-Pitts and Pitts, 1999, Jacobson et al., 2000] However, some aerosols tend to scatter or absorb more light depending on their composition. Sulfate aerosols, which often form a large proportion of the aerosols, only scatter light, while elemental carbon only absorbs light. Organic carbon can both absorb and scatter light. To further complicate the issue, aerosols may contain a mixture of several different species and it is still unclear how that may affect the optical properties of the aerosols. Figure 1.1 shows estimates from the International Panel on Climate Change (IPCC) report released in January 2001 that illustrates the estimated size of these

effects and the current level of understanding of these mechanisms, which in all cases is low. It is clear that there are still many questions about aerosols and their behavior that have not yet been answered.

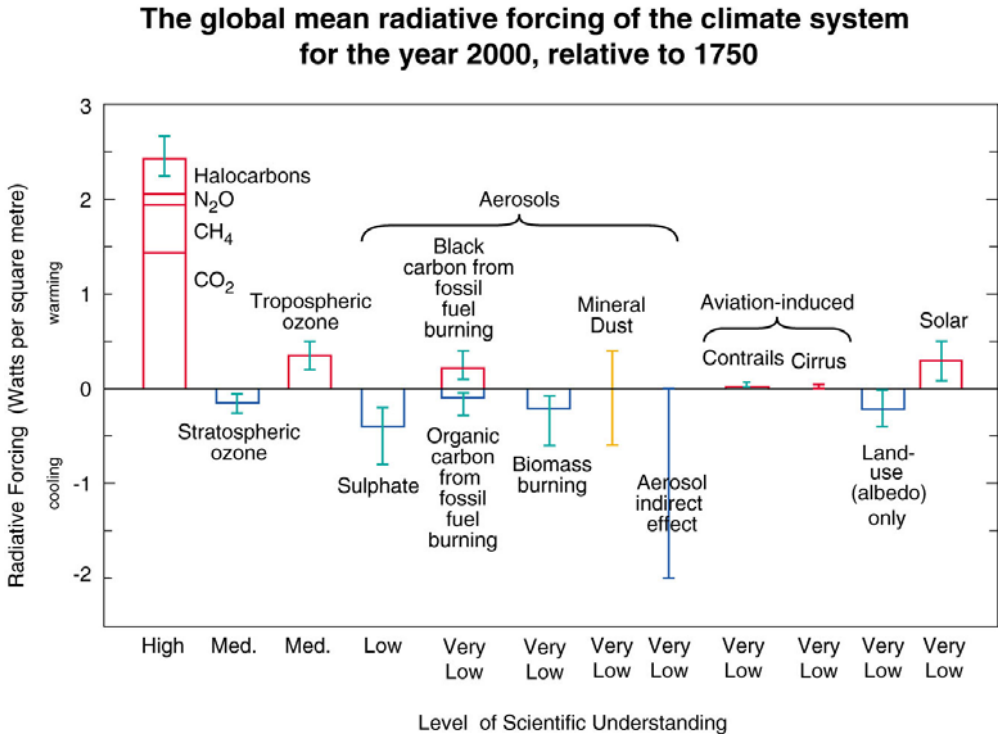

Figure 1.1: Global annual mean radiative forcings for mechanisms that impact the climate system (IPCC 2001).

1.1 Aerosol Properties and Characteristics

Particles are defined as solid or liquid objects with diameters between a few nanometers and 100 μm. Aerosols are defined as stable suspensions of solid or liquid particles in a gas. However, the terms aerosols and particles are often used interchangeably to refer to the particulate matter only. [Finlayson-Pitts and Pitts, 1999; Seinfeld and Pandis, 1998]

Aerosols can be divided into categories in several ways, as summarized in Figure 1.2. One of the primary categories is size. In general, particles below 2-2.5 μm are called fine particles and those greater than this size are termed coarse particles. This division is determined primarily by the natures of the sources. The coarse particles are generated almost exclusively by mechanical means (e.g., wind blown dust and sea spray) and often constitute a large part of the mass of the particles, although not the bulk of the number density. The fine particles are usually formed from a series of processes often involving chemical changes. Therefore, the fine particle category is further separated into ultra fine, nuclei or Aitken, and accumulation size particles. The ultra fine particles are the very smallest particles,

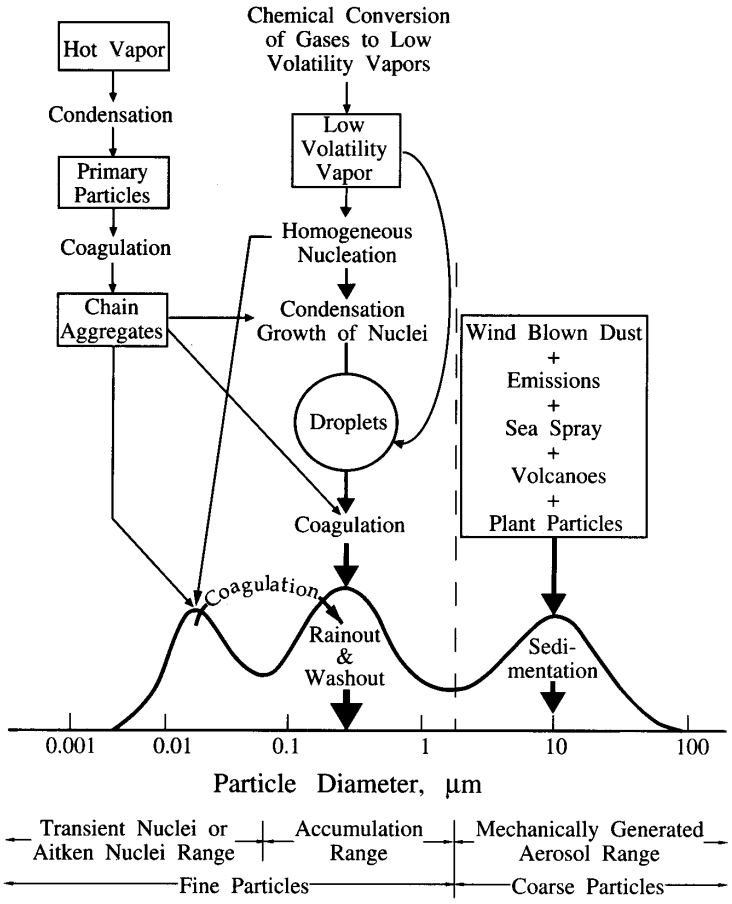

Figure 1.2: Aerosol categories and processes. Whitby and Cantrell (1976); reproduced from Seinfeld and Pandis (1998)

usually only a few nanometers in size, and are generated by gas to particle conversion of the lower volatility gases. The nuclei particles range from approximately 10 nm to 80 nm and generally form from condensation of low volatility gases. Accumulation particles, ranging between 80 nm and 1-2 μm, usually form from coagulation of smaller particles and from condensation. [Finlayson-Pitts and Pitts, 1999; Seinfeld and Pandis, 1998]

Aerosols can be classified by source also: anthropogenic and biogenic. In most urban areas, anthropogenic sources-vehicle emissions, industrial pollution, biomass burning, construction, etc., dominate aerosols. These aerosols contain primarily sulfate and nitrate, and, sometimes, significant levels of anthropogenically produced organic species. In more remote areas, biogenic sources, i.e., gas to particle conversion of plant emissions and larger particles from plant waxes, are often more significant. [Blando et al., 1998; Finlayson-Pitts and Pitts, 1999; Jacobson et al., 2000; Seinfeld and Pandis, 1998]

Tropospheric fine particles usually contain some combination of sulfate, nitrate, ammonium, carbonaceous material (both organic and elemental), trace amounts of various metals (e.g., Pb, Cd, V, Ni, Cu, Zn, Mn, Fe, etc.) and water. [Seinfeld and Pandis, 1998] These particles are often formed by combustion and gas-to-particle conversion in both urban and more remote areas. Because of their small size, fine particles have longer lifetimes than the coarse particles, sometimes lasting weeks.

In many places, especially urban areas, sulfate or sulfuric acid are the main components of the aerosol loading. Sulfuric acid (H_2SO_4) has a low vapor pressure,

so it will condense quickly onto the aerosols. However, ammonia (NH_3) is taken up preferentially by the sulfuric acid to form ammonium sulfate ($(NH_4)_2SO_4$), so if there is sufficient ammonia present, all the sulfuric acid will be converted to $(NH_4)_2SO_4$. Nitric acid (HNO_3) has a higher vapor pressure than H_2SO_4, and will not condense to form particles unless it is neutralized by ammoniua to form ammonium nitrate (NH_4NO_3). However, the ammonia will be taken up first as $(NH_4)_2SO_4$, and only after all the H_2SO_4 has been neutralized will NH_4NO_3 form. [Seinfeld and Pandis, 1998] The preferential formation of $(NH_4)_2SO_4$ before NH_4NO_3 means that there are often very low levels of NH_4NO_3 even in environments where there are high levels of gas-phase nitrates.

Many aerosol studies have focused on the effects of anthropogenic aerosols, but recently there has been increased interest in the effects of biogenic aerosols. Current estimates of gas-phase biogenic emissions range from 491 to 1150 TgC/yr, far exceeding the anthropogenic organic emissions estimates of 98 to 140 TgC/yr [Griffin et al., 1999; Glasius et al., 1999; Seinfeld and Pandis, 1998]. Most of the gas-phase biogenic hydrocarbons are alkenes or cycloalkenes and are highly reactive due to the presence of unsaturated carbon-carbon bonds. These species undergo fairly rapid reaction with oxidants, such as OH radicals and O_3 during the day and O_3 and NO_3 radicals at night to form oxygenated secondary products that typically have a lower vapor pressure than the parent molecules and therefore are more likely to partition into the aerosols. [Griffin et al., 1999; Jacobson et al., 2000]

The principal biogenic gas-phase emissions are isoprene (C_5H_8); monoterpenes ($C_{10}H_{16}$), composed of two isoprene-type units connected cyclically or

acyclically; and sesquiterpenes ($C_{15}H_{24}$), composed of three isoprene-type units. [Griffin et al., 1999] Isoprene ($CH_2=C(CH_3)CH=CH_2$) is the most abundant of these species, but it has a higher vapor pressure than the terpenes because of its smaller size. Even oxidation of isoprene to its major secondary products, methacrolein (CH2=C(CH3)CHO) and methyl vinyl ketone (CH3C(O)CH=CH2) does not lower the vapor pressure enough for significant aerosol formation. [Seinfeld and Pandis, 1998]

In contrast, the terpenes are large enough to partition into the aerosol phase. They undergo reactions similar to isoprene to form ketones, aldehydes, and acids. For example, the most common terpenes, α-pinene and β-pinene, form species such as pinonaldehyde, pinic acid, pinonic acid, and nopinone. [Finlayson-Pitts and Pitts,1999; Griffin et al., 1999; Yokouchi and Ambe, 1985]

This dissertation addresses some of the outstanding questions in aerosol science, specifically those relating to forest environments. The operation and development of the Aerodyne Research Aerosol Mass Spectrometer (AMS), a valuable instrument for measuring submicron chemical composition and size, will be discussed, as well as some details of the analysis procedures. Results from two field studies at forested sites, one remote and one urban, are also presented. Some of the issues addressed include the mixing state of aerosols (i.e., internal or external mixtures), the effect of biogenic aerosols, effect of transported aerosols, forest-aerosol interactions, and the formation and growth of aerosols.

CHAPTER 2: INSTRUMENTATION

Atmospheric aerosols have a wide range of sizes, shapes, and chemical and optical properties, making it very difficult to form a complete picture of the aerosols with only one instrument. Changes in temperature, relative humidity, and active surfaces can quickly change the aerosols themselves, making it almost impossible to sample the aerosols without changing their properties. Due to these instrument and sampling complexities, the field of aerosol measurement is changing rapidly, with new methods and issues becoming important all the time.

There are several classes of aerosol measurement: optical (real time counters and sizers using lasers to detect the particles), collection (filters and impactors where particles are collected for a relatively long time period and then removed and analyzed later by some chemical method), and in-situ mass spectrometry. The mass spectrometric methods are becoming more popular because they generally provide more information in a timely manner than many of the other methods. There are many variations in these types of instruments and my focus is on the Aerosol Mass Spectrometer (AMS) developed by Aerodyne Research, Inc.

2.1 Aerosol Mass Spectrometer

The Aerodyne AMS provides quantitative measurement of the chemical composition and size distribution of the submicron non-refractory (non-refractory generally refers to everything except black carbon and mineral particles) particle mass [Jayne et al., 2000]. The AMS consists of three, or four in the newer versions,

differentially pumped chambers maintained by either five turbomolecular pumps [Varian V-70, V-250, and/or V-301] and one hybrid turbo-drag pump [Alcatel] or six turbomolecular pumps and separate the sampling, sizing, and detection of the particles as shown in Figure 2.1.

Particles enter the instrument through a critical orifice and lens [Liu et al., 1995a, 1995b; Zhang et al., 2002] that focuses the particles into a narrow beam. At the exit of the lens, the particles expand into the lower vacuum region of the sizing chamber and separate based on their vacuum aerodynamic size. In the detection chamber, the particles impact a resistively heated surface and the non-refractory portions of the particles are flash vaporized and then ionized by electron impaction and chemically analyzed by standard quadrupole mass spectrometry.

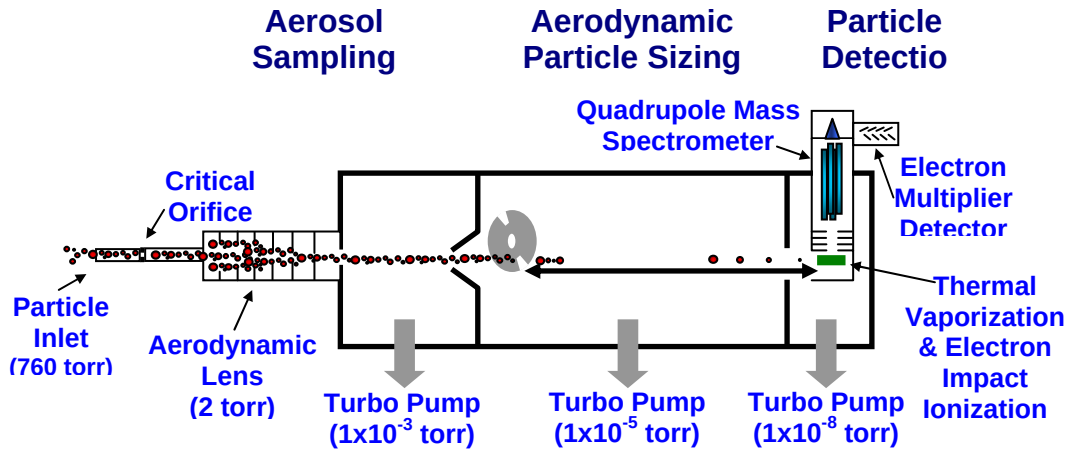

Figure 2.1: AMS diagram

The sampling chamber draws particles into the instrument through a 100 μm critical orifice that sets the inlet pressure to approximately 2 torr and gas flow rate to approximately 1.5 cm^3/s. The gas and particle stream then enters a lens consisting of six precision-machined orifices mounted in a ½ inch O.D. stainless steel tube

following the design of Liu et al. [1995a, 1995b]. This lens focuses the aerosols into a tight beam approximately 1 mm in diameter, as shown in Figure 2.2, while simultaneously concentrating the particles relative to gases by a factor of approximately 10^7. The first five apertures focus the particles onto the centerline and the final aperture controls the supersonic expansion and particle acceleration into the next chamber.

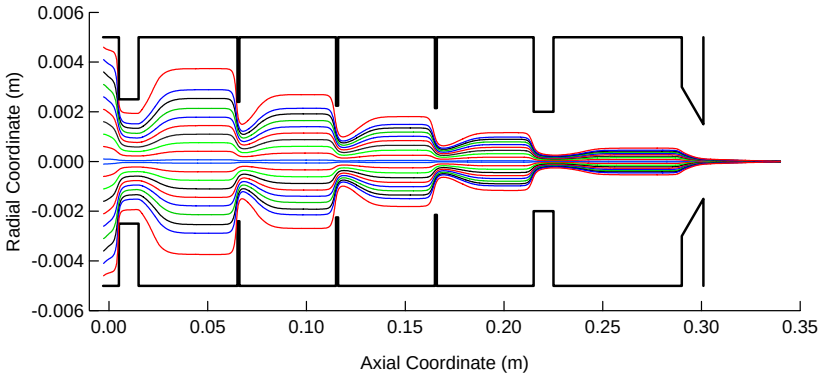

Figure 2.2: Calculated particle trajectories for 100 nm diameter unit density spheres through the aerodynamic lens. Pressure is 2.4 torr at inlet, $1x10^{-3}$ torr at exit. [Jayne, et al., 2000]

2.1.2 Aerosol Sizing

As described in the previous section, as the aerosols exit the lens they are accelerated in a supersonic expansion that gives different velocities to aerosols based on their particle inertia. Smaller particles are accelerated to higher velocities than larger particles and therefore require less time to reach the detector. However, size is not the only factor in determining the particle flight time, the density and shape of the particle are also important.

The vacuum aerodynamic diameter is a function of the density and a shape factor that indicates the level of non-sphericity as shown in the following equation [Jimenez et al, 2003].

$$D_{va} = \frac{\rho_p D_v}{\rho_o \chi_v} = \frac{\rho_p}{\rho_o} \chi_{v,inv} D_v = \frac{\rho_p}{\rho_o} S D_m \qquad (1)$$

D_{va} – vacuum aerodynamic diameter
D_v – volume equivalent diameter
D_m – mobility diameter
ρ_p – particle material density
ρ_o – unit density (1 g cm^{-1})
χ_v – dynamic shape factor in free molecular regime
$\chi_{v,inv}$ – 1 / χ_v
S – 'Jayne' shape factor [Jayne et al., 2000], similar to but not the same as χ_v

Similar model results show that this initial lens system allows 100 percent transmission efficiency for particles between 60 and 400 nm in diameter and partial transmission down to 20 nm and up to 2000 nm as shown in Figure 2.3. Differences

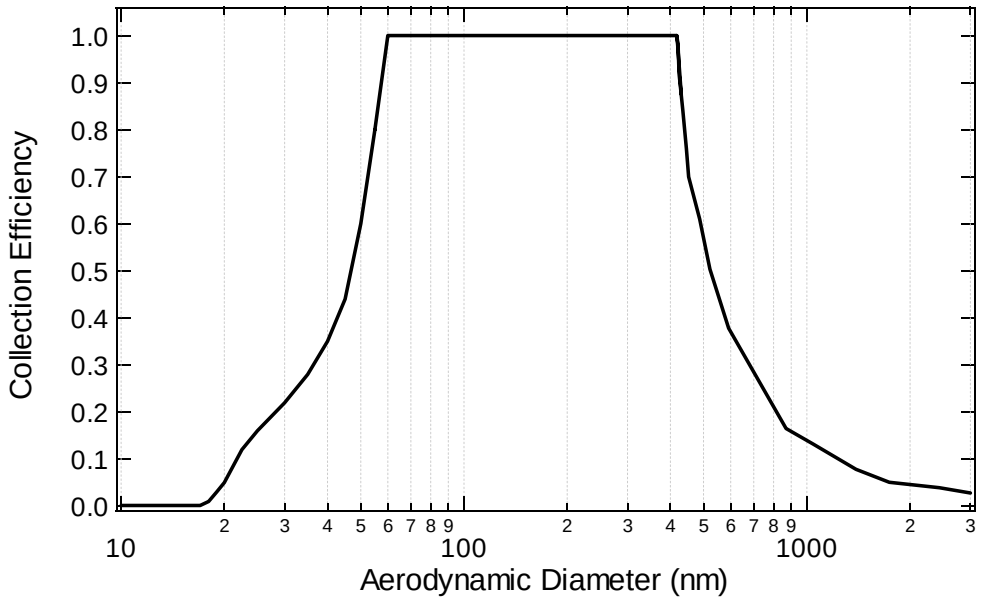

Figure 2.3: Particle transmission for 2001 lens, predicted by FLUENT (1995). Courtesy of J. Jayne.

in the diameter and spacing of the apertures can shift the transmission range. There are now several different lens configurations available, generally intended to provide better transmission to the smaller particle sizes. The lens can easily be changed to reflect the sampling needs of a particular application.

The loss of particles at the small end of the size range is a result of less efficient focusing in the aerodynamic lens, causing the particles to have a wide angular dispersion as they exit the lens, similar to gases, and consequently they do not follow the straight path across the typical 39 cm sizing chamber that allows them to pass into the particle detection chamber. The particles greater than approximately 600 nm in vacuum aerodynamic diameter suffer from impaction losses, so that only those particles that are already close to the centerline pass through the lens. [Jayne, et al., 2000]

Shortly after entering the sizing chamber, the particles encounter a rotating chopper wheel that has two radial slits located 180˚ apart. The chopper can be placed in any of three positions relative to the particle beam: completely blocking the beam so that no particles pass through (beam closed), not blocking the beam so that all the particles pass through (beam open), and partially blocking the beam so particles pass through the radial slits only (beam chopped). The specific applications for each of these chopper positions will be discussed in detail in section 2.1.3.

2.1.3 Aerosol Detection

Particles are detected as the particle beam reaches a resistively heated surface and the volatile and semi-volatile (non-refractory) portions of the aerosols are flash

vaporized and then immediately ionized by electron impaction in a custom-built closed source election impact ionizer/heater assembly as shown in Figure 2.4. A standard quadrupole mass spectrometer (QMS) detects the positive ion fragments (*m/z*) generated by the electron impact ionization. The positive ions are extracted from the ionization region and focused through the QMS so that each *m/z* is measured in turn. Upon exiting the QMS, the selected ions (i.e., one *m/z* at a time) are then deflected to an electron multiplier detector [ETP AF140, Scientific Instrument, Inc.]. This detector operates by amplifying the signal so that an easily measurable current can be detected. Each ion that impacts the initial plate produces an electron that impacts the second plate, releasing several electrons for each impact, and each of these electrons impacts a third plate that releases several electrons, etc., as shown below.

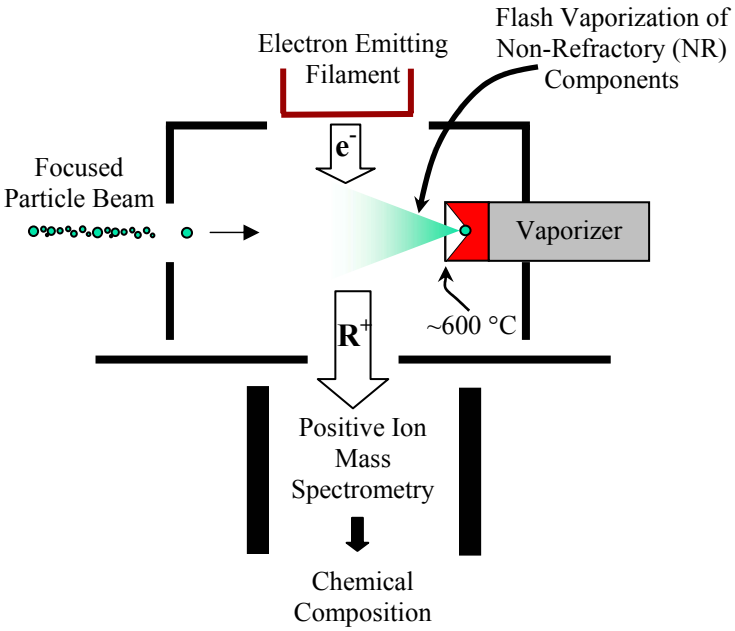

Figure 2.4: Diagram of vaporizer/ionizer assembly.

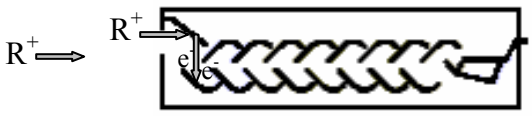

Figure 2.5: ETP AF140 electron multiplier detector.

Quick bursts of ions (tens of microseconds in length compared to the milliseconds required to traverse the particle sizing chamber) classify single particle

events of sufficient size. For a pure NH_4NO_3 particle, only a particle containing approximately $5x10^7$ molecules (approximately $7x10^{-15}$ g) or 200 nm will rise above the background levels to be counted as a single particle. Regardless of the presence of single particles, the signal at each m/z is summed over the entire sampling period to give a bulk mass concentration. [Jayne et al., 2000]

2.1.4 Data Products

A complete mass spectrum (*m/z* 1-300) can be measured by moving the entire chopper wheel in and out of the particle beam to measure both the background of the chamber (beam closed) and the total signal (beam open). This is called mass spectrum (MS) mode. The difference of these two signals gives the particulate signal at each *m/z*. Because of the particle amplification with respect to gases in the lens, only the most abundant atmospheric gases (nitrogen, oxygen, argon, water, and carbon dioxide) are detected. However, no size data can be collected in this mode because all particles are passed through and there is no timing information to determine sizes. Mass distributions can be determined only with the Time of Flight mode as described below. In addition to the standard MS mode, the AMS can also operate in Jump Mass Spectrum (JMS) mode, where a small number of masses, typically 10-15, can be sampled in MS mode instead of the full range to provide better signal-to-noise ratio for those masses of greatest interest. This is especially useful for applications where a long sampling interval is not possible or preferable, e.g., airplane operations.

When the chopper wheel is in the chopped position, the QMS is set to measure only one mass fragment at a time so that the complete size distribution for that fragment can be measured. This is called time-of-flight (TOF) mode. The size distribution for, at most, about 25 masses can be monitored in this mode with a cycle of 3.3 masses per second, so that 25 the masses can be measured in less than eight seconds. Often, the masses selected for TOF mode are those with the largest concentration as determined from the mass spectrum.

The particle beam is blocked most of the time in the chopped position and passes particles only through the slits, usually between 1 and 3.5 percent of the time depending on the width of the slits. The chopper slit width, along with the chopper speed, determines the size resolution, the smaller the slit width the better the resolution. However, a small slit width also limits the number of particles that pass through, so an optimal balance must be determined between size resolution and signal strength.

An IR reflective sensor detects the position of the chopper slits, defining the start of each TOF cycle. As the particles travel on a straight path through the sizing chamber, they spread out according to their size as a result of the supersonic expansion through the final aperture of the lens, with the smaller particles traveling faster than the larger particles. When the particles reach the detection chamber, the time to travel across the sizing chamber is determined, and from this the particle velocity and vacuum aerodynamic diameter are calculated following calibration, which will be discussed in section 2.2.3.

2.1.5 Quantification

The AMS measures the number of ions produced through the ionization of the molecules released by vaporization of the particles. By itself, this is not a quantitative measure of the aerosol mass, or concentration, of a particular species. However, by measuring the ionization efficiency of the species (IE_s, measured as ions detected/molecule vaporized) and calibrating the gain of the electron multiplier detector the particulate mass loading can be determined quantitatively.

The method for the conversion from ions to mass concentration is adapted from Bley [1988]. The molecular flux M_i (molecules/s) of species s entering the AMS detection region per unit time is calculated from the signal at a single m/z as:

$$M_s = \frac{I_{sf}}{X_{sf}\ IE_s} \tag{1}$$

I_{sf} - number of ions detected per unit time at the f^{th} fragment (m/z) of species s

X_{sf} - fraction of ions formed from species s detected at its f^{th} fragment

IE_s - ionization efficiency (ions detected / molecule vaporized) for species s.

IE_s is calculated by sampling monodisperse particles of a particular species, which are generated with a collison atomizer, diffusion dryer, and electrostatic classifier (TSI, St. Paul, Minnesota), and counting them with the AMS and/or with a Condensation Particle Counter (CPC 3010/3022/3025, TSI, St. Paul, MN). The gain, also known as the detection efficiency, of the electron multiplier detector and the transmission efficiency of the quadrupole are a function of the m/z in the range of interest and must be accounted for before using equation (1) by:

$$I_{sf}^{corrected} = \frac{I_{sf}^{measured}}{T_{m/z}\ G_{m/z}} \tag{2}$$

where $T_{m/z}$ and $G_{m/z}$ are the relative quadrupole transmission and the relative response (gain and detection efficiency) of the electron multiplier detector. [Jimenez et al, 2002]

The mass concentration of species s in the aerosol can then be calculated as:

$$C_s = \frac{M_s \, MW_s}{Q \, N_{AV}} = \frac{I_{sf}^{corr}}{Q \, N_{AV} \, X_{sf}} \frac{MW_s}{IE_s} \tag{3}$$

where MW_s is the molecular weight of species s, and Q is the air volume sampling rate into the AMS. This procedure assumes that only one species contributes to the signal at that particular m/z.

The IE_s, and X_{sf} are measured during the calibration procedure, described in more detail in section 2.2.1, using the known molecular weight of the calibration species ammonium nitrate (NH_4NO_3). For unknown species, the values for IE_s, MW_s, and X_{sf} are estimated from the available data. Given no indication of the species, IE_s/MW_s is assumed to be equal to IE_{NO3}/MW_{NO3}, as determined during calibration. If the chemical nature of the molecule (or group of molecules) is known, e.g., a hydrocarbon, or an oxygenated organic, or an inorganic salt, by the methods described by McLafferty and Turecek [1996], IE_{NO3} is multiplied by a relative response factor obtained for that type of molecule (R_t).

$$\frac{IE_s}{MW_s} = R_t \frac{IE_{NO_3}}{MW_{NO_3}} \tag{4}$$

The electron impact ionization cross-sections (σ) with 70 eV electrons are related to the number of electrons in the molecule [Flaim and Ownby, 1971; Irikura, 2000; NIST, 2000; Summers, 1969] as shown in Figure 2.6. This illustrates that the ionization efficiency of a molecule is directly proportional to σ, the ionization

efficiency on a molecular basis. The number of electrons in a molecule is highly correlated with the molecular weight of the molecule, especially for the volatile and semi-volatile molecules present in aerosols. Therefore, since IE_s is directly proportional to the electon impact cross section (σ) and the number of electrons in the molecule (N_e) is approximately proportional to MW_s, IE_s/MW_s will be proportional to σ/N_e. [Jimenez et al., 2002]

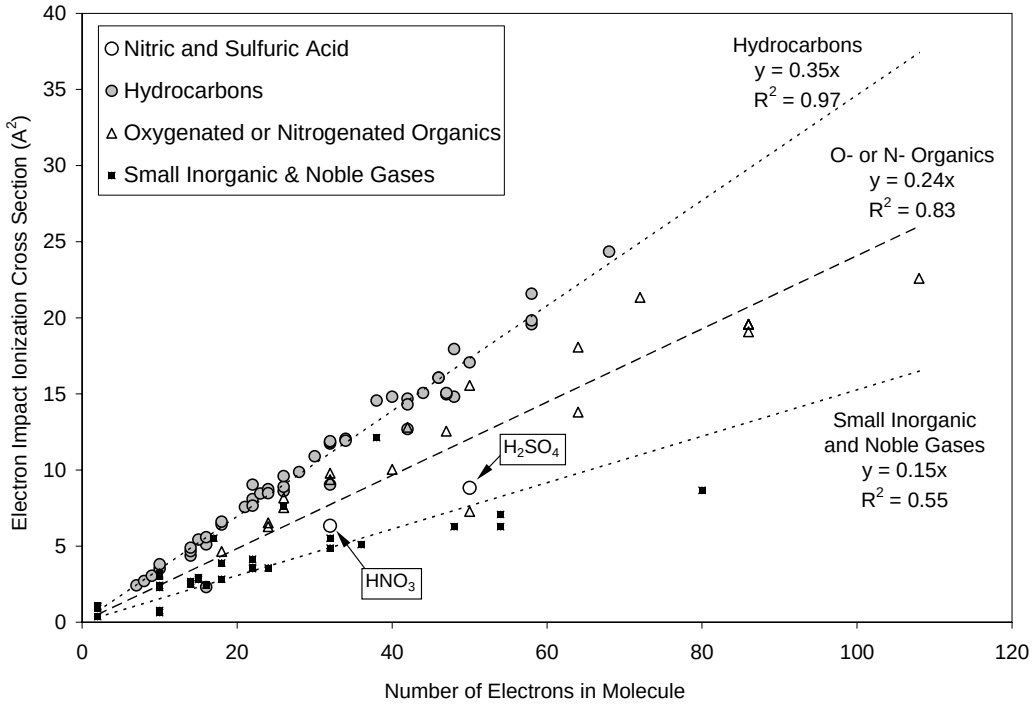

Figure 2.6: Relation between Ionization Cross Section and number of electrons. Each type generally falls on the same line. [Jimenez et al., 2003]

For small molecules of a given type, σ /N_e is approximately constant. From the data and regressions in Figure 2.6 R_t is estimated at 0.57 for hydrocarbons, 0.83 for oxygenated hydrocarbons, and 1.12 for sulfuric acid. Experimental verification of this relative response with individual aerosol species is ongoing in several laboratories.

2.2 Instrument Issues and Calibration Procedures

In order to maintain high quality measurements there are a large number of factors that must be checked and calibrated. Some of these are necessary for the determination of aerosol mass and others ensure proper instrument function. Most of this information is also available in the AMS Operating Manual version 3.2, first drafted in 2001 following extensive training at Aerodyne Research, Inc.

2.2.1 Ionization Efficiency Calibration

The ionization efficiency (IE) calibration, also called the mass or nitrate calibration, determines the ionization and ion transmission efficiency of ammonium nitrate. This is one of the most important calibrations since it is critical to the calculation of particulate mass. Ionization efficiency can be defined as the ratio of the number of ions produced to the total number of available parent molecules for that ion species (e.g., if the ionization efficiency is 1e-6, then 1 molecule out of every 1 million molecules is ionized). Transmission efficiency is the ratio of number of ions reaching the multiplier to the number of ions produced in the detection region. In the IE calibration the product of ionization efficiency and ion transmission efficiency is determined for NH_4NO_3.

Ammonium nitrate is used as the primary mass calibration species because the ionization efficiency, density, and shape are well known and ammonium nitrate does not leave much residue to interfere with subsequent measurements. Ammonium nitrate vaporizes with close to 100% efficiency, so the ionization efficiency of NO_3^+

can be quantitatively measured and it is well-focused by the aerodynamic lens so that all the particles can be detected.

The ionization efficiency for nitrate (IE_{NO3}) is calculated by determining the number of ions produced per particle of a select size as shown in the following equation.

$$\frac{IonsPerParticle}{\pi/6 \times D_m{}^3(nm) \times \rho(1.72g/cm^3) \times (1e-7cm/nm)^3 \times S(0.8) \times f_{NO3}(0.775)} \times \frac{MW_{NO3}(62g/mole)}{N_{AV}(6.02e23molec/mole)} \quad (5)$$

where the number of ions per particle is determined from the calibration (usually several hundred), D_m is the mobility diameter of the calibration particles (typically 350 nm), ρ is the density of ammonium nitrate, S is the Jayne shape factor (<1 for

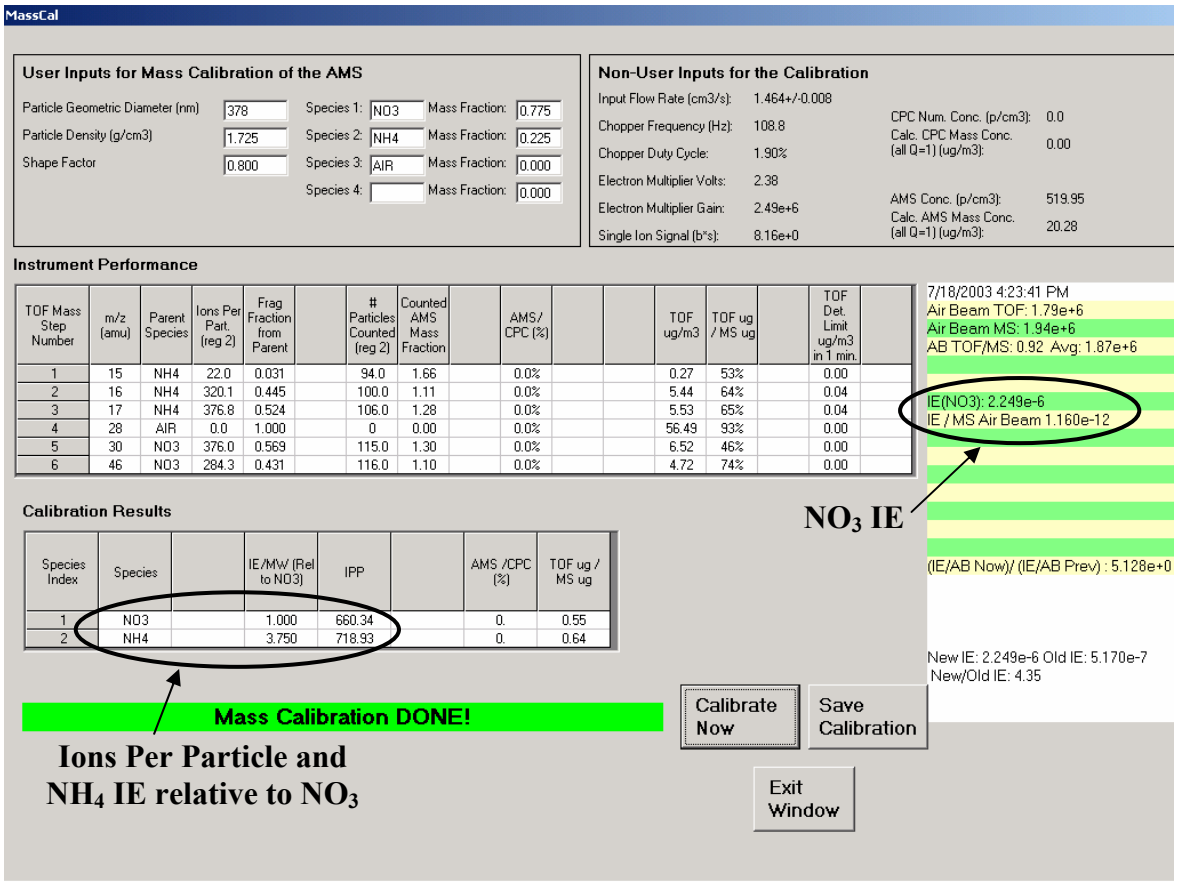

Figure 2.7: Ionization efficiency calibration results from CELTIC field campaign on July 18, 2003.

non-spherical particles), f_{NO3} is the fraction of NO_3 in NH_4NO_3 (MW_{NO3} / (MW_{NO3} + MW_{NH4})) and N_{AV} is Avogadro's number.

Ammonium nitrate particles, typically 350nm as determined by a differential mobility analyzer (DMA), are generated, sized, dried, and then passed into the AMS. The relevant mass fragments: *m/z* 15=NH^+, *m/z* 16=NH_2^+, *m/z* 17=NH_3^+, *m/z* 28=N_2^+, *m/z* 30=NO^+, and *m/z* 46=NO_2^+ are set in TOF mode and the AMS is set to alternate between MS and TOF mode. After sufficient signal is accumulated, the automated calibration procedure determines the number of ions produced per particle and calculates the ionization efficiency as described in equation 5 as shown in Figure 2.7.

2.2.2 Electron Multiplier Calibration

The electron multiplier calibration determines the gain of the multiplier and tracks and compensates for its decrease over time. The gain is calculated by comparing the observed area of a single ion (in contrast to the burst of ions produced by a particle) with the expected area of the single ion. The area of the single ion is measured in bitsteps (basically, the voltage multiplied by time in a 10 μs step).

Inside the multiplier every positive ion that impacts the first stage produces one

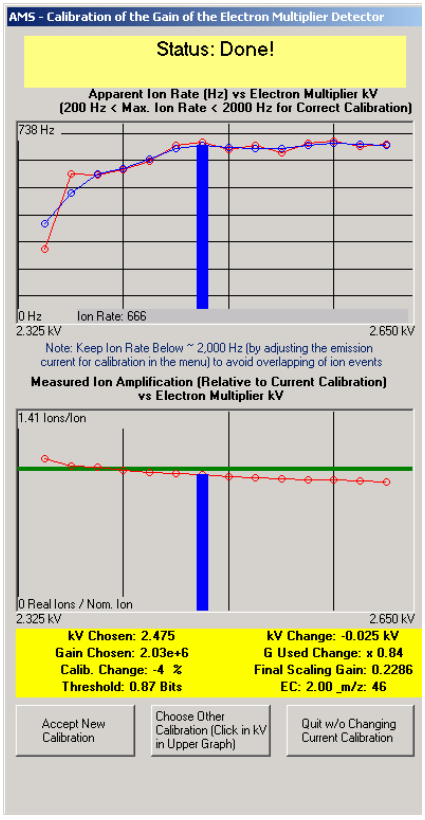

Figure 2.8: Electon multiplier calibration during the CELTIC campaign, July 21, 2003.

electron (e^-), which is increased by the value of the gain as it impacts the stages of the multiplier. This produces the current measured at the output of the multiplier.

$$V = I*R = q*R / t \tag{6}$$

$$V*t \text{ (bitsteps)} = q*R = G*q/ e^-*R \tag{7}$$

where R is the preamp resistance (1e6 Ω), I is the current, q is the charge, q/e^- is the charge per electron (1.6e-19 C), t is the time, and G is the gain of the multiplier. Since q/e^- and R are not changing over time, the area of the single ion (V*t) depends only on the gain of the multiplier.

The multiplier gain is described by the gain curve (i.e., the gain of the multiplier vs. the multiplier voltage) as shown in Figure 2.8. For low voltages the multiplier gain increases proportionally to the voltage. The gain increase levels off for higher voltages, resulting in a "plateau." In this flat region of the gain curve, higher voltages do not increase the gain further. The edge of this plateau is the best setting for the multiplier, where the highest gain at the lowest voltage setting is used, giving the best possible signal while extending the lifetime of the multiplier. However, it is also important to maintain a consistent gain to avoid large changes to the corrections of the mass concentration, so sometimes it is necessary to compromise between the optimal voltage and gain.

The gain curve is described by the following equation:

$$\text{Gain} = \text{scaling factor} * 10^{(C_1 + C_2*U_{mult} + C_3*U_{mult}^2)} \tag{8}$$

where U_{mult} is the voltage of the multiplier in kV and C_1, C_2, and C_3 are constant coefficients. The coefficients are determined when a new multiplier is first installed by determining the multiplier signal of single ion events for different multiplier

voltages and fitting the results to the curve described by this equation. These constants do not usually change very much between multipliers of the same type. This equation is stored in the software and used for all subsequent multiplier gain calculations. This procedure is similar to performing the multiplier gain calibration. Except for the first calibration of a new multiplier, the automated calibration procedure can be used to calculate the gain.

2.2.3 Time of Flight Calibration

As described in Section 2.1, particles are accelerated through the supersonic expansion at the end of the lens and are separated as a function of their vacuum aerodynamic diameter. The relationship between the particle velocity and vacuum aerodynamic diameter is dependent primarily on the outside pressure, but is also affected by the lens position.

The time of flight, or size, calibration determines how the aerosol aerodynamic diameter is calculated by the AMS acquisition software and should be performed whenever the AMS is moved or at the beginning and end of a field or laboratory study, but should stay constant, assuming there are no major hardware issues or changes. Polystyrene latex spheres (PSLs) of various sizes are the most reliable method of performing the size calibration, but NH_4NO_3 particles sized by a Differential Mobility Analyzer (3080L, TSI, St. Paul MN) can also be used if the performance of the DMA is first checked with PSLs.

A few drops of the PSLs of a particular size [Duke Scientific] are placed in deionized water and then generated as particles in a collision atomizer [TSI, St. Paul MN], dried, and then passed into the AMS. The AMS in TOF mode is set to a *m/z*

with strong signal, typically *m/z* 104 and the vaporizer temperature increased to approximately 1000°C to ensure the PSLs are vaporized quickly, thereby giving a sharp signal as shown in Figure 2.9. After sufficient mass is accumulated to give a clear indication of that particular PSL size, the file is saved and the process repeated with additional sizes. As wide a range of sizes as possible is necessary to get an accurate calibration. Typically, 5 sizes between 100 and 1000 nm provides a reasonable range. It is desirable to extend this to sizes smaller and larger than this, but PSLs less than 100 nm diameter have a tendency to clump so NH_4NO_3 or oleic acid can be used with a DMA to determine the smaller sizes. The small size range often has the greatest uncertainty in the calibration, making measurements in this range critical, but since the AMS measures the mass of particles and small particles have very little mass it can be difficult to accumulate sufficient signal to clearly determine the time of flight. Extending the size calibration above 1000 nm is also

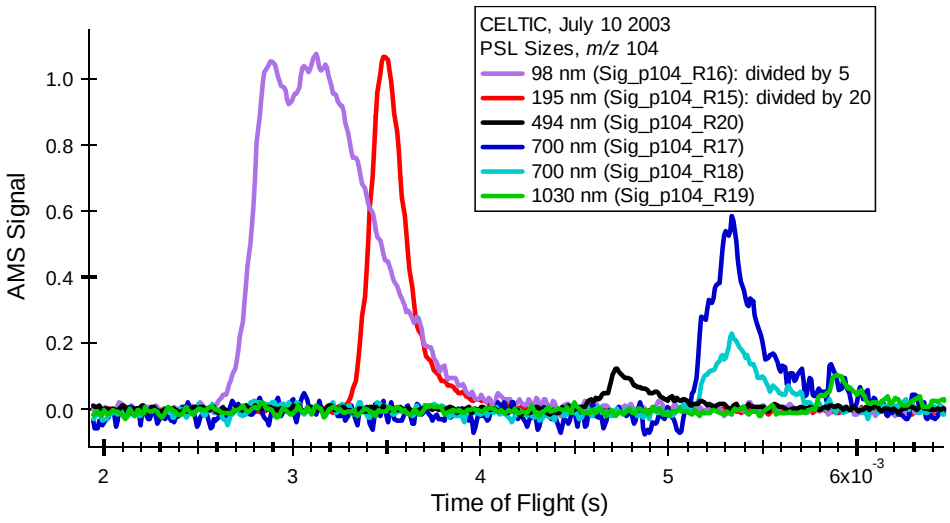

Figure 2.9: TOF calibration, raw PSL signals. CELTIC July 10 2003.

difficult because impaction of particles at the critical orifice and lens restricts the number of large particles to those already close to the centerline of the sampling system.

After determining the particle time of flight in seconds for each size, the particle velocity and vacuum aerodynamic diameter are determined by the following equations.

$$v_p = \text{flight distance (typically 0.39 m)} / \text{time of flight (s)} \quad (9)$$

$$D_{va} = D_m \text{ or } D_{PSL} * \rho * S \quad (10)$$

Where v_p = particle velocity
D_{va} = vacuum aerodynamic diameter
D_m and D_{PSL} = mobility and PSL diameters respectively
ρ = density of NH_4NO_3 (1.72 g/cm^3) or PSLs (1.04 g/cm^3)
S = Jayne shape factor: 0.8 for NH_4NO_3 and 1 for PSLs

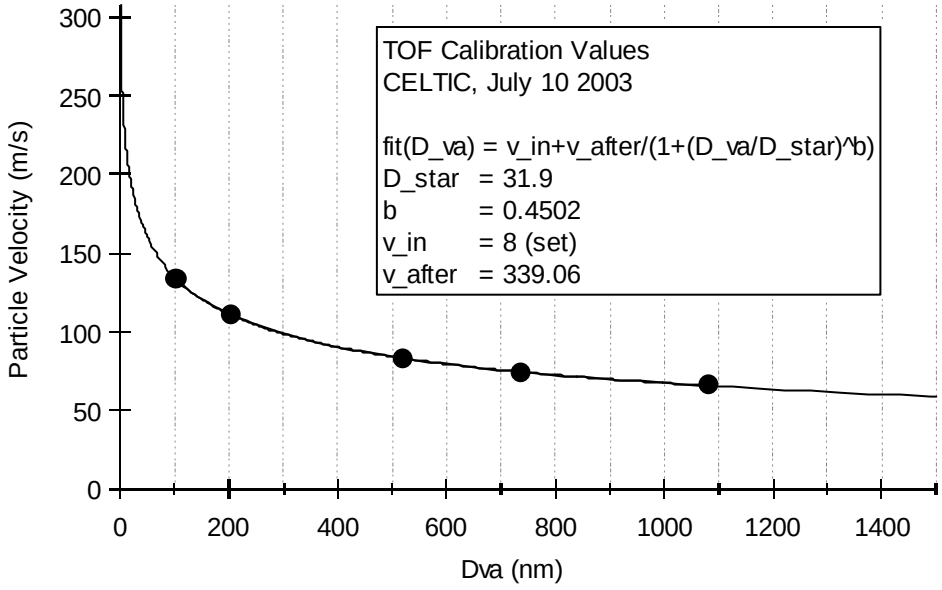

Figure 2.10: TOF calibration curve. CELTIC, July 10 2003.

The velocity dependence of the particle vacuum aerodynamic diameter is described by the expression below adapted from Jayne et al [2000]:

$$v = \frac{v_l + (v_g - v_l)}{(1 + \frac{D_{va}}{D^*})^b} \qquad (11)$$

where v is the particle velocity of particles with vacuum aerodynamic diameter D_{va}, v_g is the gas velocity (typically ~550 m/s), v_l is the velocity within the lens (typically ~8 m/s), D^* and b are fitted coefficients. A graph of the particle velocity vs. particle vacuum aerodynamic diameter is used to fit this equation as shown in Figure 2.10.

2.2.4 Quadrupole Mass Spectrometer Tuning

Quadrupole mass spectrometers (QMS) employ several voltages to extract the ions from the ionization region and guide them through the QMS to the detector. Many of these voltages can be changed, or tuned, to optimize the QMS performance. Generally, the QMS should not be tuned often since it can change the

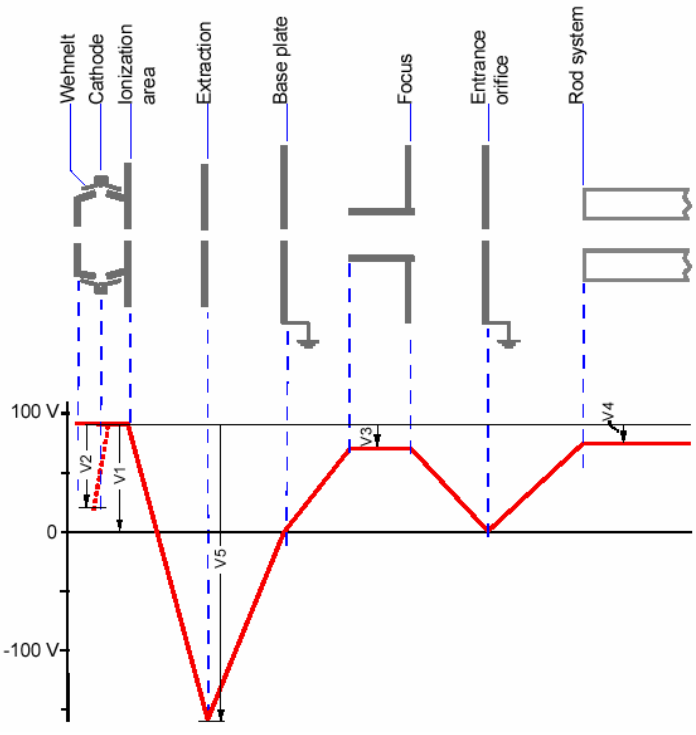

Figure 2.11: QMS Voltages as depicted in the Balzers Operating Manual.

transmission efficiency of the QMS, potentially changing the calculation of particulate mass. However, after any major change in the hardware configuration, especially exposure of the vacuum chamber to ambient air (e.g., to change of the ionization filaments or electron multiplier detector), the QMS voltages must be tuned.

The QMS voltages are shown in Figure 2.11 (Balzers QMA-430 Manual) and described in Table 2.1. There are seven QMS voltages, all except the ion reference and cathode are varied during the tuning procedure, and there is another potential called the heater bias that is associated with the custom vaporizer, not the standard QMS, which is also varied to produce the best signal. These voltages are all set in relation to the ion reference, so the ion reference is generally not changed. The cathode is also a standard value and most electron impact mass spectra are produced at 70eV. Reducing the cathode can produce a softer ionization, resulting in less fragmentation but smaller signals, which may be desirable in identifying organic species.

Table 2.1: QMS Voltages

Voltage	Description	Value (V)
Ion Reference	Nominal potential at which ions are formed and reference potential for all other potentials. Not varied.	90 V
Cathode	Determines the acceleration voltage of the electrons and therefore the nominal ionization energy. Not varied.	70 eV
Focus	Affects peak level, related to extraction voltage.	~12 V
Field Axis	Nominal voltage of ions in the rod system: decelerating voltage, causes ions to remain in the rod system long enough to be resolved	~14 V
Extraction	Accelerates ions from ionization area towards the rod system	150-250 V
Inner Deflection	Direct ions through the 90° turn to reach electron multiplier.	~15 V
Outer Deflection	Direct ions through the 90° turn to reach electron	~30 V

	multiplier.	

The AMS acquisition software has an automated tuning procedure where the signal strength is measured at one *m/z*, typically *m/z* 28 (N_2), as the focus, field axis, extraction, and deflection voltages are varied in turn. In addition, there is one voltage not part of the QMS, the heater bias, which is also determined in the tuning process. The voltage at the greatest signal is set as the 'tuned' value and the process is repeated until the strongest signal is determined. The tuning process should be repeated until only small changes in the signal are evident. The voltages can also be changed manually in the parameter menu of the AMS acquisition software.

2.2.5 Peak Position and Shape Calibration

The shape and position of mass spectral peaks must be calibrated to ensure the optimum resolution because signal can be artificially lost or gained if it is set incorrectly. The resolution of the QMS determines the peak shape and spacing between peaks.

The quadrupole mass spectrometer is a mass filter, which can be passed by ions of a mass range depending on the voltage settings of the mass spectrometer electrodes. This range, for which the mass filter is 'open', defines the resolution of the mass spectrum. To distinguish ions of different mass number, the mass resolution ($m/\Delta m$) at the mass of the ion has to be at least the value of this mass in amu ($m/\Delta m = 100$ for resolution of mass 99 and 100).

At high resolution the mass is a peak of asymmetric shape. It has a sharp tail on the right side (the high mass side) and a longer, less sharp tail on the left side (the

low mass side). Decreasing the mass resolution of the QMS makes the peak wider. It does not change the shape of the peak and the position of its right tail. The peak shape can be changed by changing the value of the field axis. The ideal peak shape would be a "top hat" or a "flat top" shape so that the signal intensity for each amu can be determined by averaging over the flat section of the top hat. To maximize the ion transmission through the QMS the resolution setting should be as low as possible. With too low resolution the left tail of the peak ends in the peak of the next lower mass, which changes the intensity of this peak. The AMS should be operated with a 1 amu resolution throughout the entire mass scan range. So for optimization of ion transmission the resolution must be set as low as possible (to maximize the transmission) and as high as necessary (to get correct ion signals of the different masses).

In the **MS Mode** of the AMS program the ion intensity at the single masses (also referred to as stick intensities in the mass spectrum) is measured as averaged ion signal, averaged over a window region (adjustable in parameter window) in the center of the peak. The averaging width should be as large as possible to maximize signal to noise ratio. On the other hand it should not be wider than the flat top part of the peak to maximize signal intensity. Typically a window width of 0.4 amu centered about 0.5 amu to the left of the right hand edge of the peak is ideal for obtaining peak

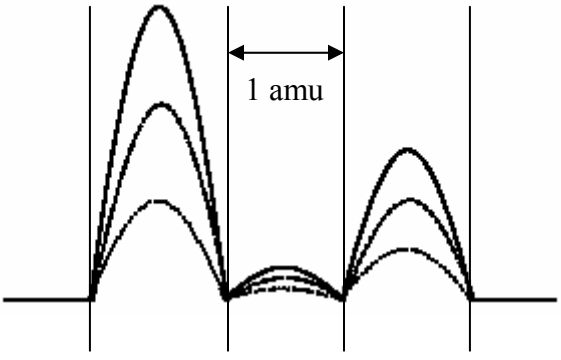

Figure 2.12: Proper peak resolution to avoid signals leaking over into the next peak.

signal intensity. In the MS window this averaged ion signal is displayed as a box with height equal to the averaged intensity and width equal to the averaging window. The resolution of the mass spectra may be as low that the left tail of the peaks reaches the next peak on the low-mass side and alters the right tail of this peak. For correct ion signal calculation, the right tail should not extend into the averaging window of the next mass as shown in Figure 2.12.

2.2.6 Lens Alignment

A critical issue in the sampling process is the alignment of the particle beam. Slight differences in the orientation of the lens, the lens holder, and the heater in the ionizing region of the quadrupole mass spectrometer can cause the particle beam to shift so that it only partially intersects the heater or misses it entirely, leading to a decrease in particles detected and sometimes a compositional and/or size bias depending on the focusing properties of the particles.

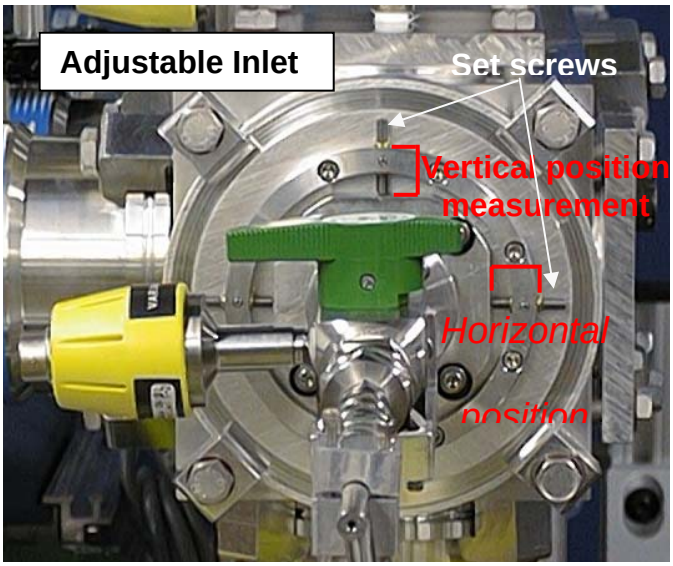

Figure 2.13: Adjustable lens system. Picture by J. Jayne, ARI.

The lens is adjusted by set screws set into the lens plate, as shown in Figure 2.13. Measurement of the number of ions detected per laboratory-generated NH_4NO_3 particle and the percentage of particles detected by the AMS compared to a CPC are used to determine the best lens alignment. The lens is adjusted in small increments measured by calipers so that the beam moves across the vaporizer. Toward the edges the percentage of particles transmitted is small and in the center it is close to 100%. After moving the lens both horizontally and vertically, the values at each position are plotted and the lens is set in the center of the region of full transmission as shown in Figure 2.14 and the lens plate is tightened against the front flange of the AMS to lock the lens in place.

Although this procedure is straightforward, it can be difficult because the measurement of the horizontal and vertical distance by the calipers can actually move the lens slightly, making the exact position difficult to determine. The first version of the movable lens used an x-y translation tilt stage with micrometer adjustment knobs, which allowed for much easier and more accurate position measurements. This system was not used in the commercial instruments because the lens position was not intended to be a frequent adjustment and the problems with the position measurement

were not at first apparent, but the micrometer adjustment knobs may be implemented in new instruments.

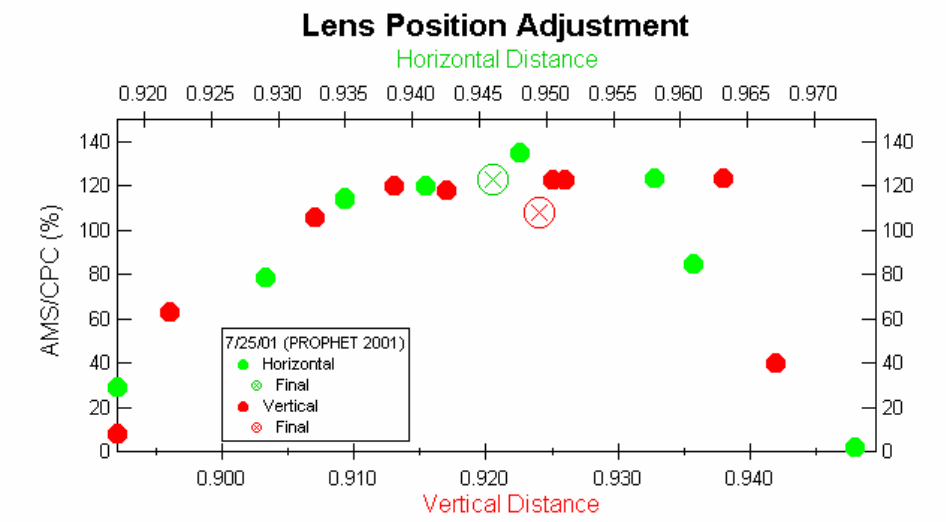

Figure 2.14: Lens alignment, open circles represent location chosen as center. PROPHET 2001.

2.2.7 Collection Efficiency

The signal received by the multiplier does not always perfectly reflect the amount of material entering the system. Therefore, it is important to characterize what is actually being measured by determining the collection efficiency of the instrument. There are two different types of collection efficiency crucial to the AMS.

The ***particle collection efficiency*** is a measure of the transmission of particles through the lens and body of the AMS. It is simply the ratio, translated to a percentage, of the number of particles measured by the AMS to the number of particles measured by a Condensation Particle Counter [TSI, St. Paul MN]. This value is determined by the lens transmission, shape of the beam, and aerosol chemical characteristics. For NH_4NO_3, the collection efficiency approaches 100%. However,

for $(NH_4)_2SO_4$, the collection efficiency is closer to 15% in the laboratory, probably due to the small amount of water on these particles because of the drying process. This means that only 15% of the particles measured by a CPC are reaching the heater. This is a significant issue, since $(NH_4)_2SO_4$ often constitutes a major portion of the aerosol mass. However, field studies indicate that the collection efficiency for $(NH_4)_2SO_4$ is much higher for ambient than for laboratory particles, again probably because ambient particles have a much larger amount of water.

The ***ion collection efficiency*** is a measure of the number of ions that are actually measured by the electron multiplier out of the total number of ions produced. This is determined by taking the ratio of the electron multiplier signal to the faraday cup signal for nitrogen (N_2 = *m/z* 28). The faraday cup can be used as an alternate detector; it is not often used because the signal is so much smaller than the electron multiplier. It is a plate with a negative potential directly above the QMS rods that attracts the positively charged ions created in the ionization region. The faraday cup is the default detector if the deflection voltages are set to zero. Both signals should be measured with the AMS software to ensure the same values are being measured.

2.3 Hardware Development

The AMS is a relatively new instrument and has only been commercially available for about three years. During that time there have been a number of improvements and additions to the initial system. The ISAACC instrument was one of the first purchased, serial number 4, and several upgrades were required to

maintain the highest quality measurements. Most of the hardware improvements were performed in the summer of 2003.

2.3.1 Lens

Continuing improvements in the understanding of the sizing system has resulted in several versions of the focusing lens. Based on modeling activities at ARI, the relative diameters of the lens apertures have been changed several times and thus have shifted the diameter range [ARI]. The original lens received in 2001 transmitted 100% of the 40-600 nm vacuum aerodynamic diameter particles with partial transmission 20-40 nm and 600-2000 nm. Several additional lenses have been developed more recently and in May 2003 a new lens was installed, with better transmission of smaller particles.

As described in section 2.2.6, the lens is mounted on an adjustable plate that floats on an o-ring so that the particle beam can be moved to intersect the center of the vaporizer and minimize particle loss. However, early versions of the AMS did not have an adjustable lens and the particle beam alignment was a critical issue, leading to large uncertainty in the measurement. With the fixed lens, the particle beam was aligned by making a 'spot.' This is a tedious and inaccurate process where the instrument is vented to atmosphere and a clear piece of tape is placed on the outside of the aperture to the detection chamber with the outline of the aperture marked in pen. Ammonium nitrate particles of a standard size, typically 350 nm, are generated and pumped into the AMS for a few minutes. Neither the ionizer nor the heater is on for this procedure since all the particles are collected on the tape at the

entrance to the detection chamber, leaving a white 'spot' on the tape. The AMS is vented to atmosphere again and the tape removed. Examination of the relative positions of the aperture outline and the 'spot' gives an indication of the alignment. The lens is rotated and the procedure repeated until the 'spot' is as close to the center of the aperture outline as possible.

2.3.2 Ionizer

One of the most significant changes to the system was the replacement of the ionizer with a smaller, more enclosed version. The reduced ionizer volume increased the ionization efficiency by almost a factor of two.

2.3.3 Pumping System

Another important change was the addition of a fourth differential pumping stage in the detector region. In the previous system, the area between the heater/ionizer at the base of the quadrupole mass spectrometer and the electron multiplier at the top of the quadrupole mass spectrometer was open, allowing unrestricted movement of all ions through this area. With the addition of the extra pumping stage, this chamber was divided into two chambers by a vacuum baffle, or collar, just above the heater/ionizer region of the quadrupole mass spectrometer and a Varian V-70 turbo pump was added to the section containing the electron multiplier. This reduced the number of stray ions reaching the detector and therefore reduced the background signal, lowering the detection limit and allowing smaller signals to be detected.

The addition of the turbo pump required a new coupling flange connecting the AMS chamber body and the QMS housing. Because of small differences in the length of both the coupling flange and the QMS housing, a thin spacer flange is used to ensure that the vaporizer/ionizer at the base of the QMS is aligned with the particle beam. The distances involved were carefully measured, as shown in Figure 2.15, to determine the exact height required for the spacer flange, which was then machined out of aluminum.

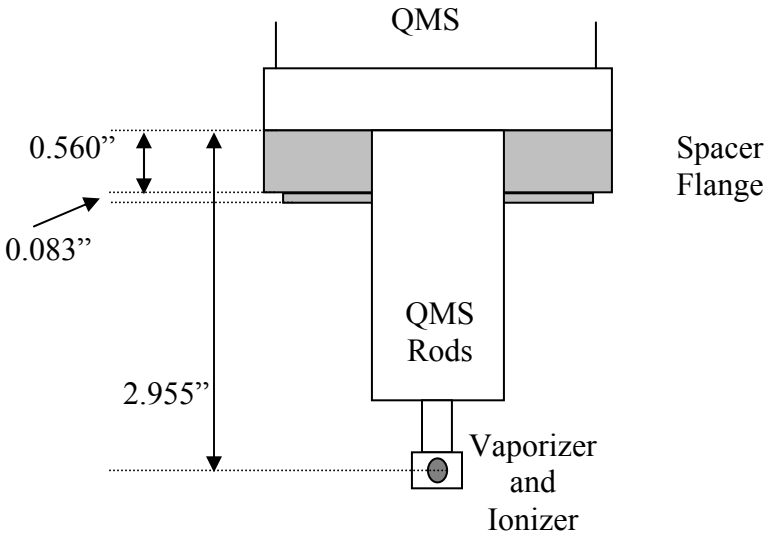

Figure 2.15: Diagram and dimensions of new spacer flange.

The vacuum baffle separating the vaporizer/ionizer from the rest of the detection region also required exact measurement and machining. A generic vacuum baffle, basically a ring through which the QMS rods extended, purchased from ARI needed to be modified to fit as tightly as possible around the QMS mass filter. However, there are four pieces that had to fit between the baffle and the mass filter: three plastic pieces running the length of the mass filter and the controls for the vaporizer. The position, width and height of each of these had to be measured and the

smallest possible opening in the baffle machined for minimal gas and ion transfer outside the QMS mass filter as shown in Figure 2.16.

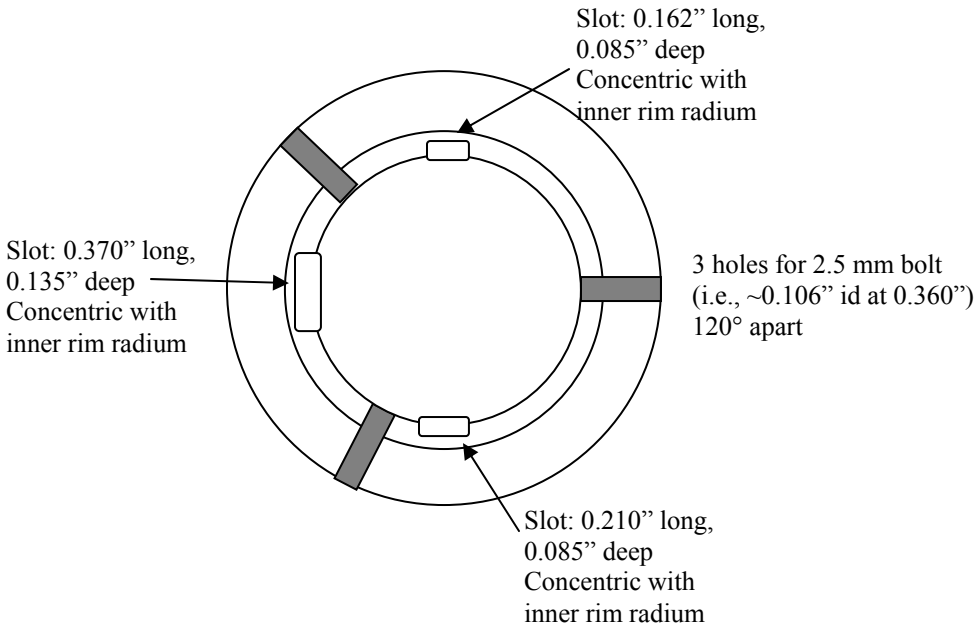

Figure 2.16: Diagram and dimensions required for modification of the vacuum baffle to allow extension of QMS rods.

2.3.4 QMS Control

Another improvement is the modification of the QMS IS420 circuit boards. These boards control the filaments in the ionizer and all the voltages used to create, extract and direct the ions through the QMS. The modifications affect the deflection voltages and the emission current of the ionizer filaments. Two voltages are used to deflect the ions into the electron multiplier for detection. The resolution of these voltages is relatively coarse since the typical QMS operation uses only one voltage at a much higher potential. However, empirical evidence shows that finer resolution of

these voltages can increase the efficiency with which ions reach the electron multiplier detector, thus increasing the signal through increased ion collection efficiency. The second modification to these boards is an increase in the ionizer current. With the existing tungsten ionizer filaments the higher current merely burns the filaments out much more quickly. However, new filaments made of thoriated tungsten or iridium may be available soon and the higher ionizer current will be very valuable at that time in increasing the ionization efficiency.

2.3.5 Beam width measurement

One of the most persistent issues with the AMS has been the uncertainty of how well the particle beam is being focused onto the vaporizer. In early experiments, this had to be estimated from the comparison to other measurements, which is inherently difficult to do quantitatively since the number of variables increases considerably with the addition of all the uncertainties of a second measurement and sometimes this is not possible if a comparable instrument is not available. The beam width measurement has substantially reduced the uncertainties in this area and initial results have shown that the focusing of the particle beam is primarily determined by the relative humidity, or water content, of the particles entering the critical orifice and lens of the AMS.

The beam width module is located just upstream of the aperture leading into the detection chamber. It employs a thin (0.2-0.7 mm diameter) wire that moves across the aperture in controlled increments, allowing for 3-7 positions as shown in Figure 2.17. The attenuation of the signal at each position compared to the unblocked

signal when the wire is at the edge of the aperture determines the focusing of the particle beam. For example, if there is close to 100% attenuation when the wire is in the center of the aperture, then the beam is very well focused and there is no particle loss. However, if the attenuation at the center is only 20% and there is still sizeable signal at the off-center positions, then the beam is very broad and there may be significant particle loss. For broad beams, additional wire positions between the center and the edge are critical for determining the extent of particle loss.

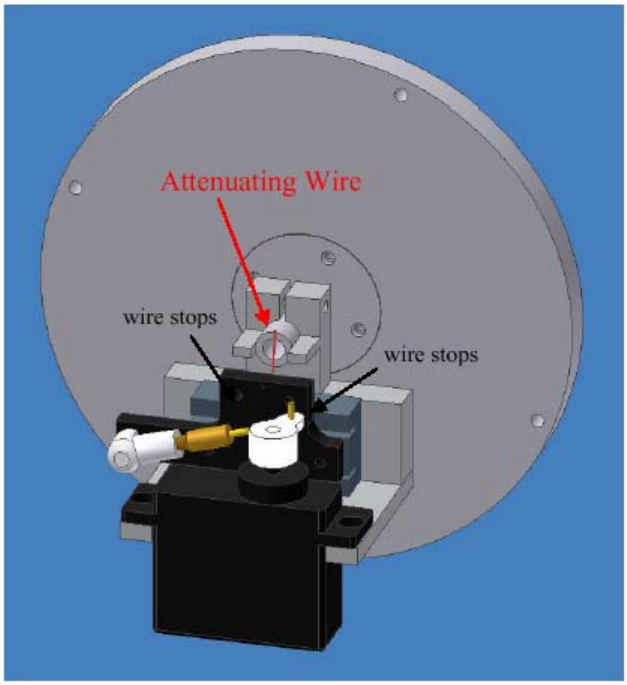

Figure 2.17: Beam width probe assembly. J. Jayne (ARI)

2.4 AMS Analysis

The AMS generates an incredible amount of data, making the processing and interpretation of the data one of the most challenging aspects of this instrument. The early analysis procedures were labor-intensive and clumsy, and it was difficult to compare measurements by different instruments because of variations in the processing. The development of reliable software for analyzing the data has taken several years and the efforts of many AMS users. However, James Allan, formerly a graduate student at the University of Manchester Institute of Science and Technology,

has done the majority of the development, consolidation, and refinements of the basic software into a user-friendly and robust package available to all AMS users that allow rapid production of high quality preliminary data and easy comparison of data sets.

2.4.1 Initial Analysis Procedure

The software James Allan has developed uses a powerful data analysis and graphing package called IgorPro from Wavemetrics (www.wavemetrics.com). The details are described in Allan et al. [2003a], but in general the software first loads the individual data files and, in the more recent versions, creates a matrix of these values for both the mass spectrum and time of flight data. Placing the data in a matrix format is essential for large data sets to reduce processing time and file size. The raw signals in the matrices are then converted into particulate mass according to the equations described in section 2.1.5.

After loading the data, a diagnostics graph is generated that displays all of the important instrument parameters: multiplier voltage, multiplier gain, heater bias, ionization efficiency, computer duty cycle, flowrate, TOF airbeam, and MS airbeam. An interval shortly after an ionization efficiency calibration is chosen as the reference airbeam value and this is used to correct for the drift in multiplier gain over time, since the signal from the air does not change. Other corrections can also be applied, including corrections for changes in flowrate (due to blockage of the critical orifice) and averaging of the airbeam to reduce noise, recalculation of the 'stick' value in case of a shift in the mass scale calibration, calculation of error, recalculation of the baseline in case of signals in those regions set as MS 'zero' that could shift the

baseline, recalculation of the TOF calibration, and recalculation of the TOF 'zero' in case of very large particles. After these corrections have been applied, calculation of the mass concentrations over time, averaged mass spectra, size over time for those mass fragments set in TOF mode, and averaged size distributions can be calculated. The data diagnostics graphs, described in section 2.4.3, are especially useful in the initial stages of data analysis to display the overall trends in a dataset and highlight any periods of atypical behavior that may warrant additional investigation.

In order to calculate the mass concentrations for each species, the contributions from all mass fragments must be included. However, electron impact ionization typically causes considerable fragmentation, sometimes making it very difficult to account for all the contributions. There are often contributions from several different species at one *m/z*, as well as interferences from gas phase species (N_2, O_2, Argon, CO_2, and H_2O). The major inorganic species, sulfate (SO_4^{2+}), nitrate (NO_3^+), and ammonium (NH_4^+), have well known fragmentation patterns and comparisons of the patterns in the NIST database [NIST Chemistry Webbook, http://webbook.nist.gov] and empirical AMS measurements show fairly close agreement. The differences can be attributed to the heating of the molecules prior to ionization by the vaporizer. The main fragments of sulfate and nitrate have relatively little interference, and can therefore be determined accurately. Ammonium is more difficult because of the interferences at all of the fragments, which will be discussed in more detail in Chapter 3.

2.4.2 Organic Analysis

The organic species are much more difficult to identify both because of their much more complicated fragmentation patterns and because of the large number of species that may be present. However, it is possible to determine general classes of organics using a method called ion series or delta analysis suggested by McLafferty and Tureček [1993]. This method is based on one of the most common ion fragments, CH_2. In molecules with long chains, any of the equivalent C-C bonds can be broken; therefore, a clear pattern of CH_2 units (14 mass units) is observed as shown in Figure 2.18.

The R backbone (or classes of R backbones) can be determined by shifts in the starting point of the CH_2 units, which is called the delta value. Therefore, the R class can be determined using this formula:

$$\Delta = \text{Peak mass} - 14n + 1 \qquad (12)$$

where n is the number of CH_2 units. The scale of the delta values ranges from –7 to +6. In general, alkane and alkene species have delta values between –2 and +2, the larger delta values indicate the presence of more oxygenated species, i.e., ketones, alcohols, acids, etc., and the negative values tend to be aromatic species. In addition to the class of organic species, this analysis also gives an indication of the size of the molecule by looking

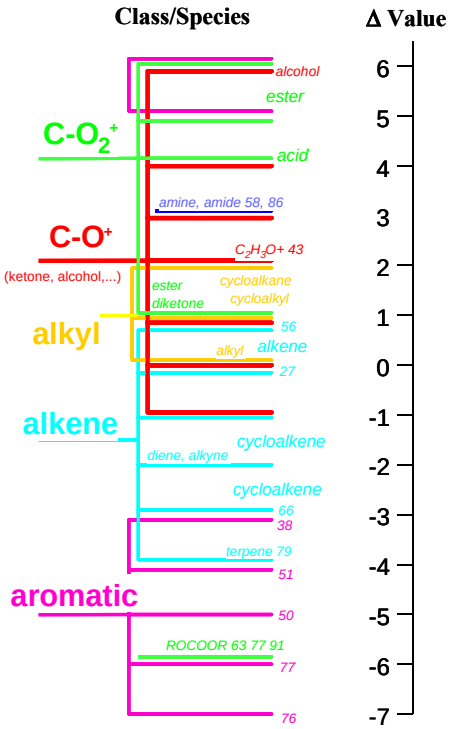

Figure 2.18: Ion series analysis summary. Adapted by D. Worsnop from McLafferty and Tureček [1993].

at the length of the series, i.e., the number of carbons in the molecule.

2.4.3 Data Diagnostics

After the initial processing, it is useful to perform some basic diagnostic procedures to get an overall picture of the dataset as a whole. This is most helpful for large field data sets, but can also be useful for laboratory data. I developed a set of useful graphs that demonstrate these basic properties for each major species: sulfate, nitrate, ammonium, and total non-refractive organics. The sulfate and nitrate diagnostics show the time trends of the species and the fragmentation ratios of the different ions (SO^+, SO_2^+, SO_3^+, HSO_3^+, and $H_2SO_4^+$ for sulfate and NO^+ and NO_2^+ for nitrate) as shown in Figure 2.19.

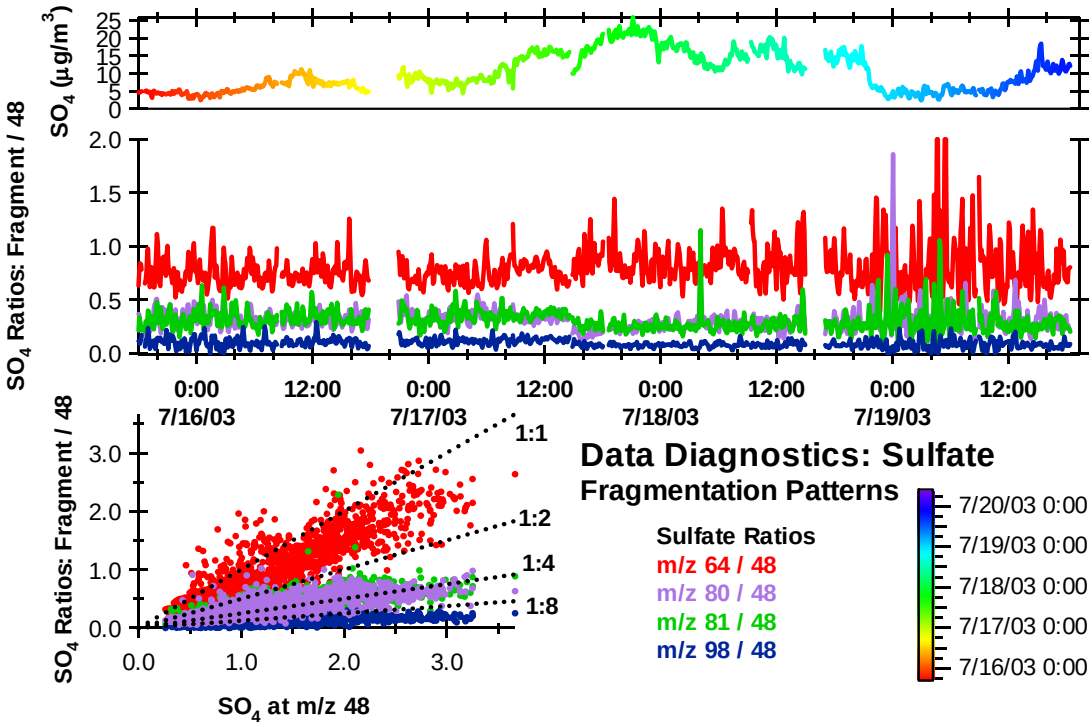

Figure 2.19a: Sulfate diagnostic plot. Top: species concentration over time. Middle: ratio of each fragment to m/z 48 over time. Bottom: Ratio of each fragment to m/z 48 as scatter plot.

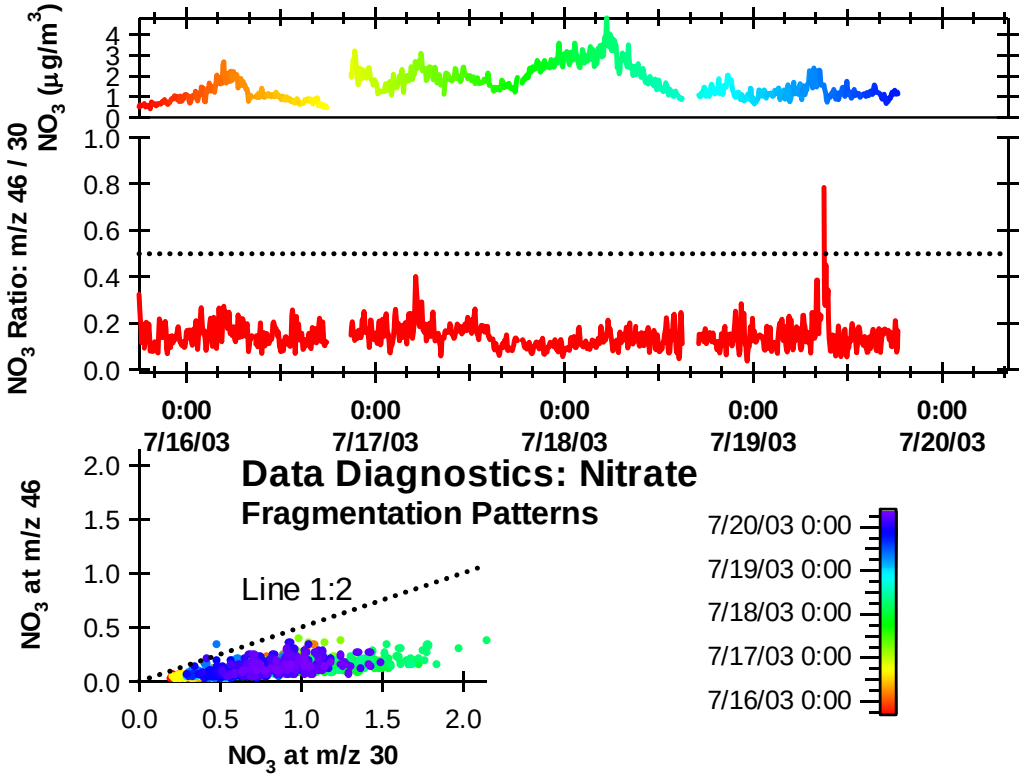

Figure 2.19b: Nitrate diagnostic plot. Same as above.

The ammonium diagnostics plots are more complex because the calculation of ammonium is more complicated than sulfate and nitrate as described in more detail in Chapter 3. First is a graph that shows the main fragments of ammonium, NH^+ and NH2+, similar to that for the sulfate and nitrate and the time trends. This is very important because the relative proportions of these ions change with variations of the ionization and extraction process. This diagnostic can be used to set this ratio and ensure a proper ammonium calculation. The second ammonium diagnostic calculates the predicted ammonium based on the assumption that all aerosols are neutralized in sulfate, nitrate, and chloride:

$$\text{Predicted } NH_4 = (36/98)*SO_4 + (18/63)*NO_3 + (18/35)*Cl \qquad (13)$$

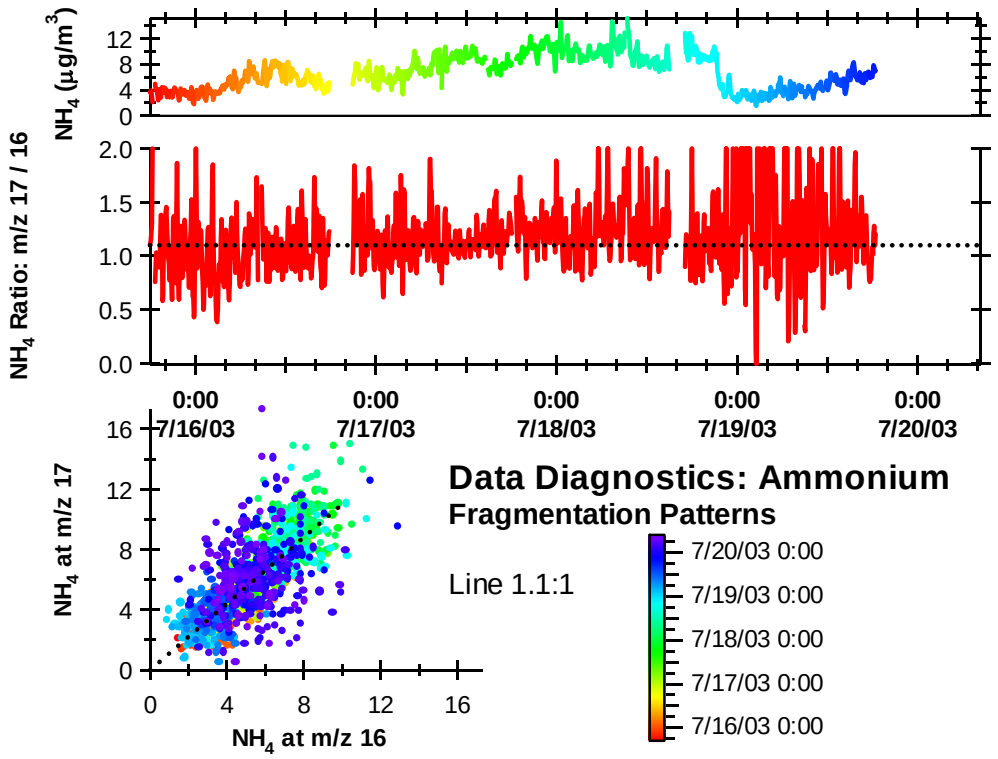

Figure 2.20: Ammonium diagnostic plot. Same format as Figures 2.20a and b. The bottom panel shows the two main fragments, corrections must be made to the relative fractions to account for differences in the ionization of air.

The level of neutralization is very important because it gives an indication of the age of the aerosols and sometimes the source.

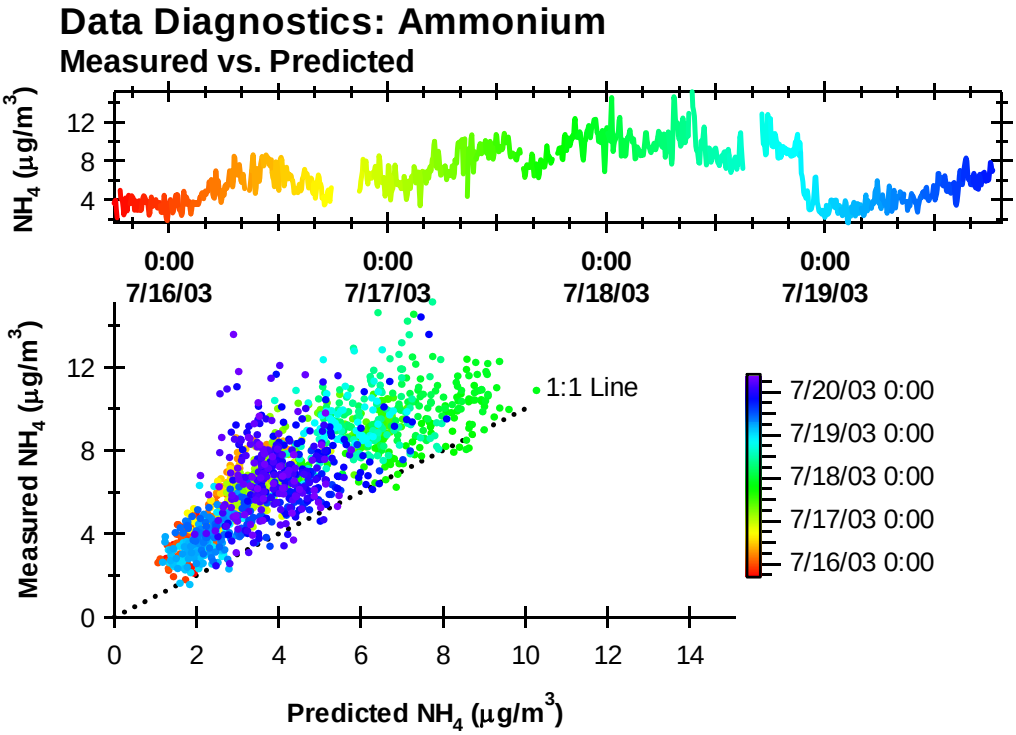

Figure 2.21: Ammonium diagnostic plot. Top: species concentration over time. Bottom: ratio of measured and predicted ammonium according to equation 13. In this case there appears to be a slight excess of ammonium

Finally, the organics diagnostic displays some of the common fragments and gives an indication of the oxidation level of the aerosols. The AMS generally produces too many fragments for identification of specific organic species, but it can identify general classes of compounds as described in section 2.4.2. Both *m/z* 43 ($C_2H_3O^+$) and *m/z* 44 (CO_2^+) are typical of oxidized aerosols, but *m/z* 43 can also contain the straight hydrocarbon fragment, $C_3H_7^+$. Therefore, the relationship between *m/z* 44 and the sum of the rest of the organics indicates the overall level of oxidation and the ratio of *m/z* 43 to *m/z* 57, which is purely hydrocarbon, is another indication of the relative contribution of oxidized and non-oxidized organics.

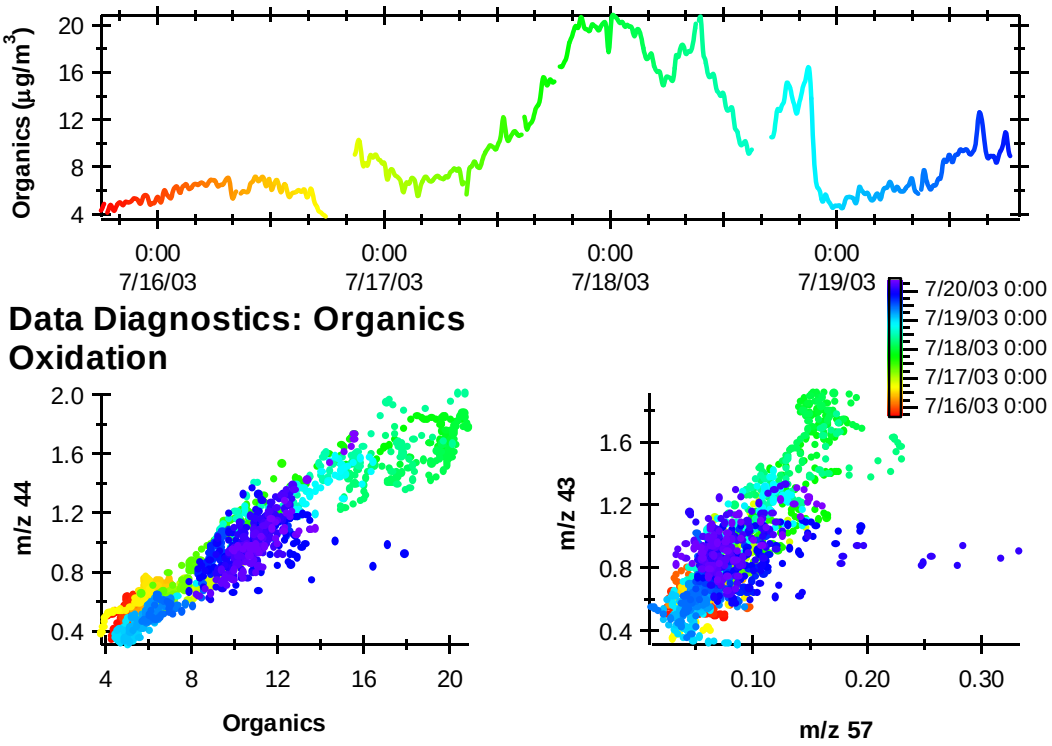

Figure 2.22: Organics diagnostic plot. Top: species over time. Left: indicates level of oxidation. Right: indicates oxidative influence at m/z 43.

2.5 Other Measurement Techniques

There are many instruments that are complementary to the AMS, such as particle sizing instruments (electrical mobility and optical), filters, impactors, and other types of mass spectrometers. Since it is impossible to measure all aspects of aerosols with one instrument, it is useful to have a suite of measurements that can cover a wide range of properties so that a more representative picture of the aerosols can be developed.

2.5.1 Condensation Particle Counter

Particles are enlarged by butanol condensation so that they can be easily detected and counted by a laser-diode light source. The CPC can count particles between 0.007 and 9.99×10^6 particles/cm^3. The CPC can be used by itself, in conjunction with the AMS to provide an independent particle count and with a DMA to size particles as described below. [TSI Product Information, 2001]

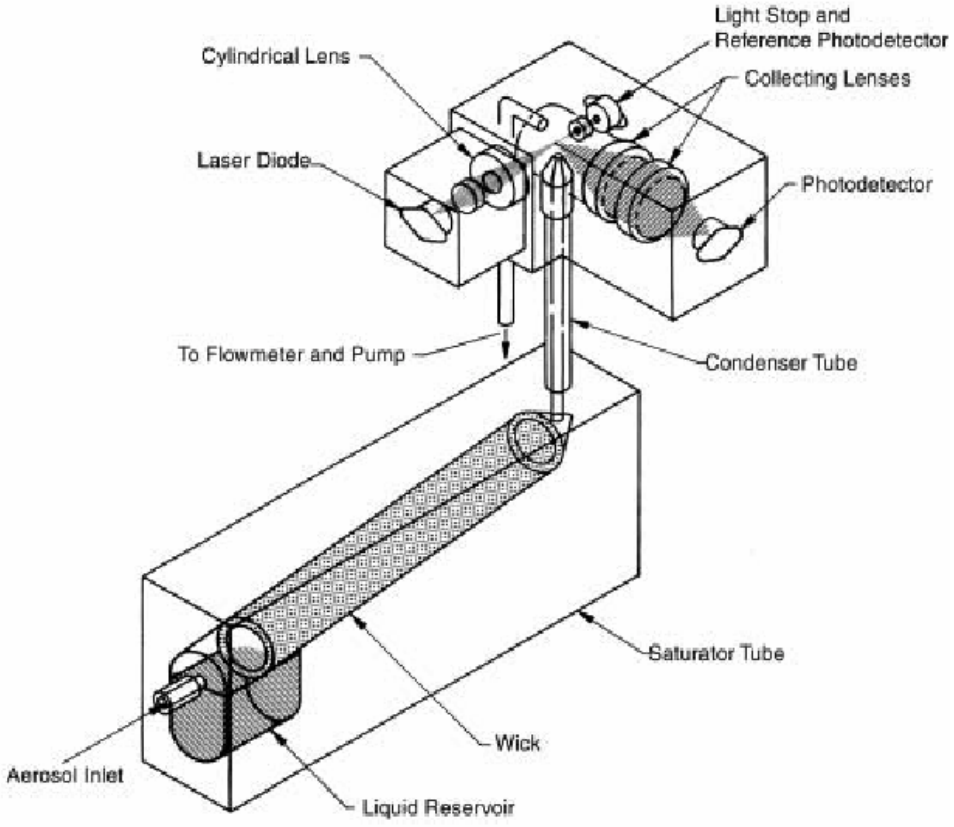

Figure 2.23: Diagram of a CPC (TSI Product Information, 2001)

2.5.2 Electrostatic Classifier and Differential Mobility Analyzer

Polydisperse particles are given a known (+1) charge with a Kr-85 neutralizer shortly after entering the instrument and then pass through a DMA where they are separated according to their electrical mobility so that only one size particle is

allowed to pass through as shown in Figure 2.25. In these experiments a long DMA was used, which has a sizing range of approximately 15 to 650 nm in mobility diameter (this is not the same as the vacuum aerodynamic diameter that the AMS measures). The DMA can be used to select only one size particle or it can scan through the range of particle sizes. [TSI Product Information, 2001]

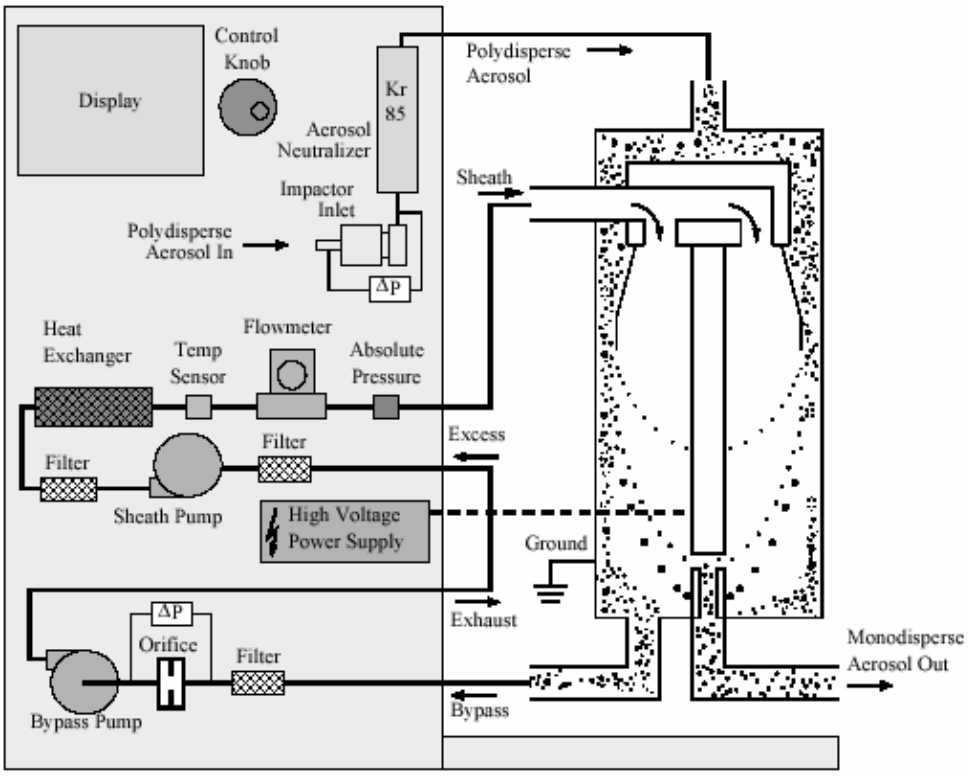

Figure 2.24: Diagram of electrostatic classifier and DMA (TSI Product Information, 2001)

2.5.3 Scanning Mobility Particle Sizing (SMPS)

The SMPS is a common aerosol sizing system. The SMPS was used to monitor the AMS performance, to determine number and size distributions, particularly for the smaller particles that were below the detection limit of the AMS, and to provide information on the bulk density of the aerosol population. Typically, we used a TSI 3936L22 SMPS, which consisted of a TSI 3081 electrostatic classifier

to separate particles according to their electrical mobility and a TSI 3022A condensation particle counter that counted the particles size-selected by the electrostatic classifier. The electrostatic classifier scanned through the mobility size bins to give the complete size distribution for particles between 16 nm and 640 nm in diameter in concentrations of 2 to $1x10^8$ particles/cm^3 every five minutes, which was set to correspond to the AMS saving interval for ease of comparison of the measurements. [TSI Product Information, 2001]

2.6 Summary

The AMS provides real-time in situ measurement of the size and chemical composition of submicron non-refractory particles. The particles are focused by a critical orifice and lens at the entrance to the instrument and then pass through a chopper to cross a sizing chamber and finally reach the vaporizer and ionizer where the particles are evaporated and then ionized by electron impaction. The fragments generated by the ionization are then analyzed by a quadrupole mass spectrometer. The AMS usually alternates between the mass spectrum mode, where a complete mass spectrum 0-300 amu is generated, and the time of flight mode, which provides the size distribution for a small number of mass fragments.

There were also a number of hardware improvements over the past several years, including several lenses that extended the transmission of small particles, a more compact ionizer that increased the ionization efficiency, a new vacuum chamber in the detection region with an additional pump to decrease stray ions, more refined

control of the QMS deflection voltages, and a beam width probe to measure the particle focusing.

There have also been a number of improvements to the various software routines, including development of several diagnostic graphs that provide an overall view of the basic characteristics of any data set. These include the fragmentation patterns for the major species, the calculation of ammonium from the nitrate, sulfate, and chloride to compare with the measured concentration, and an estimate of the level of oxidation of the organics.

CHAPTER 3: AMMONIUM DETERMINATION

Ammonia is the primary basic gas in the atmosphere and one of the most abundant nitrogen-containing species. Sources of ammonia include animal waste, ammonification of humus, emission from soils (including fertilizer sources), and industrial emissions. Ammonia is readily absorbed by surfaces, including soils and water, so its residence time in the atmosphere is only about 10 days. The main removal mechanisms for ammonia are wet and dry deposition. The ammonium ion (NH_4^+) is one of the principal components of tropospheric aerosols and is the primary neutralizing agent of acidic species such as sulfuric and nitric acid. [Andersen et al., 1999] Measurement of this species is therefore critical to an accurate understanding of aerosol behavior.

Initially, the ammonium calculation from AMS data appeared too difficult. The complexity of the contributions from different species and the lower sensitivity of the earlier instruments made a meaningful ammonium calculation seem impractical. However, during the PROPHET 2001 field campaign the issue of the level of neutralization became important during a particle growth event. It appeared that a plume of sulfur dioxide that converted to sulfuric acid caused the growth, but it was unclear if the sulfuric acid underwent further conversion to ammonium sulfate. This event is discussed in more detail in Chapter 5, but the need to determine the state of neutralization motivated this chapter.

3.1 Fragmentation Patterns

As described in Chapter 2, the ionization process of quadrupole mass spectrometry fragments the molecules in patterns characteristic of specific chemical species. While these distinctive patterns can be used to identify the major chemical components of aerosols, the mixture of species typical of ambient aerosols sometimes makes this difficult. Frequently, more than one species will have a contribution at a particular *m/z*. If the fragmentation patterns are well known, the various contributions of several species at a particular *m/z* can be determined from ratios of the signal at less congested *m/z*. The current procedure is described in Allan et al. [2004], but was first developed while studying the results from the PROPHET 2001 field campaign.

The determination of the ammonium ion concentration is one of the more difficult calculations for the AMS because of the large interferences at all the relevant masses. The ionization of ammonia can be described by:

$$NH_3 \text{ (vapor)} + e^- \rightarrow N^+ + NH^+ + NH_2^+ + NH_3^+ \quad (1)$$

This gives fragments at *m/z* 14, 15, 16, and 17, although the AMS fragmentation does not give a measurable signal at *m/z* 14. As shown in Table 3.1, all of these masses include species other than ammonia. The main interferences are water (both gas phase and particulate) and air (gas phase nitrogen and oxygen), but other species can also contribute, such as particulate organics (the CH_3^+ ion), particulate sulfate (from fragmentation into SO_3^+ and H_2O^+) and particulate nitrate (N^+). In addition to the varying contributions from these species, the ionization of O^+ (*m/z* 16) can change based on the voltage settings of the QMS and must be accounted for every time the settings change.

Table 3.1: Contributions to the masses relevant to the particulate ammonium determination.

	m/z 14	*m/z* 15	*m/z* 16	*m/z* 17	*m/z* 18
Air	N^+	$^{15}N^+$	O^+	$^{17}O^+$ ♦	$^{18}O^+$ ♦
Water			O^+ ♦	OH^+	H_2O^+
Organic		CH_3^+			H_2O^+
Sulfate					H_2O^+
Nitrate	N^+ ♦				
Ammonium		NH^+	NH_2^+	NH_3^+	

♦Minor contribution

3.1.1 Air Interference

Although most of the gases that enter the AMS are pumped away, the most abundant gases (i.e., nitrogen, oxygen, argon, carbon dioxide, and water vapor) still have a significant signal, especially nitrogen and oxygen. The largest air signals are in the diatomic form (N_2^+ and O_2^+), but there are still significant signals at the monatomic masses (N^+ and O^+) and at the largest isotopic signals that are so much larger than the contribution from the ammonium fragments that careful corrections are required. Although *m/z* 14 is not one of the ammonium fragments, it is almost entirely free of anything other than N^+ from air. There is a small contribution from nitrate, but the air N^+ is so much greater that it is usually insignificant. All the other contributions from air can be related to the air N^+ signal at *m/z* 14.

Table 3.2: Corrections due to air interferences [Allan et al., 2004]

	Correction	Source
***m/z* 15**	0.00368 * (air N^+ signal at *m/z* 14)	Coplen et al. and De Laeter et al.
***m/z* 16**	0.353 * (air N^+ signal at *m/z* 14)	Empirical-must be determined for every experiment
***m/z* 17**	0.000391 * [0.353 * (air N^+ signal at *m/z* 14)]	Coplen et al. and De Laeter et al.

As shown in Table 3.2, most of the air interferences are easily calculated based on isotopic ratios. However, as mentioned earlier, the exact correction to *m/z*

16 (O^+) is dependent on the specific ionization conditions and therefore must be measured, both to determine the exact value and to ensure it remains constant.

3.1.2 Water Interference

There are many sources for water; including sulfate, organics, gas phase, and particulate; sometimes making it difficult to account for all contributions. Although speciation of the water is complex, the ammonium calculation uses only the total *m/z* 18 signal, regardless of the contributions of the individual species. However, the specific fragmentation pattern of water is important for the determination of the contribution at each mass.

The thermal decomposition and ionization of ammonium sulfate leads to the formation of water.

$$(NH_4)_2SO_4 + \text{heat} \rightarrow NH_3(g) + H_2SO_4(g) \quad (2)$$

$$H_2SO_4(g) \rightarrow SO_3 + H_2O \quad (3)$$

Based on empirical laboratory data gathered primarily by Jay Slowik (ARI), the signal at *m/z* 18 due to sulfuric acid decomposition is 0.67 of the primary fragments SO^+ (*m/z* 48) and SO_2^+ (*m/z* 64).

A similar fragmentation of dicarboxylic acids leads to a contribution to the *m/z* 18 signal from organics.

$$RCOOH + NaHCO_3 \rightarrow RCOONa + CO_2 + H_2O \quad (4)$$

The current system assumes that one H_2O^+ ion is produced for every CO_2^+ ion, although this has not been conclusively proven due to the complexity of the organic species fragmentation patterns.

There can also be a contribution from gas phase water. This is currently set based on an assumption that water vapor constitutes 1% of the atmosphere. While this is sufficient for a rough estimate, actual measurement of the water vapor content is far more accurate, especially as the amount of water vapor can change significantly over the course of a day.

Finally, the remainder of the water signal at *m/z* 18 is assumed to be particulate water. This is not an absolute measurement since approximately half of the particulate water content is lost in freeze drying as a result of the supersonic expansion following the critical orifice and lens in the AMS sampling chamber. In several field studies, it is apparent that only in humid environments does a measurable amount of particulate water survive to be measured.

The water fragmentation is similar to the standard NIST 70eV pattern, but there are slight differences in the relative ratios of the masses due to the heating of the particles for vaporization. In general, the AMS fragmentation patterns, determined empirically, tend to have larger signals at the smaller mass fragments than the NIST pattern as shown below.

Table 3.3: Relative abundances of NIST (NIST Chemistry WebBook (http://webbook.nist.gov/chemistry) and empirically determined AMS water fragments.

	NIST (% Relative Abundance)	AMS (% Relative Abundance)
***m/z* 16**	1	4
***m/z* 17**	21	25
***m/z* 18**	100	100

3.1.3 Ammonium Calculation

After all of the contributions to the ammonium masses are measured or calculated, they are combined to provide the ammonium concentration. As

mentioned above, the signal at *m/z* 14 due to ammonium is very small (approximately 1%) and therefore immeasurable in the AMS due to the large nitrogen signal at that mass. Similarly, the ammonium signal at *m/z* 15 is also small (approximately 10% of the ammonium signal at *m/z* 16) and the variability of the organic contribution (CH_3^+), and the subsequent difficulty in accurately accounting for it, makes it almost impossible to use this mass except when the organic mass loading is very low. Therefore, only *m/z* 16 and 17 are routinely used to calculate the ammonium concentration. This is accomplished simply by taking the full signal at these masses and subtracting the contributions from air, water, sulfate, nitrate, and organics as shown in Figure 3.1.

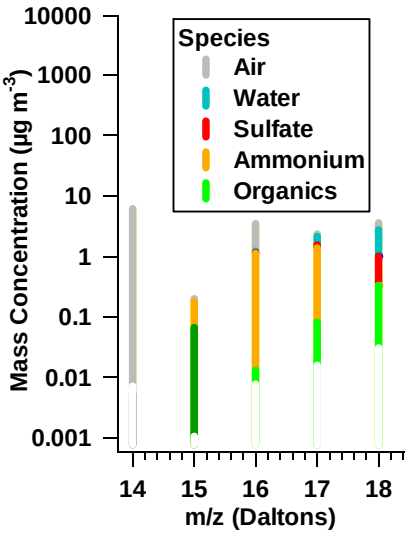

Figure 3.1: Separation of species for ammonium determination. Data from PROPHET 2001, a moderately polluted period (8/6/01 0630 – 8/7/01 0640.

3.2 Experimental Determination

There are several ways to determine the correction factors for the ammonium calculation. At first, the relationships between the interferences were unclear. After plotting each of the relevant masses against each other, some patterns began to emerge. One of the most interesting graphs was *m/z* 16 vs. *m/z* 32 in concentration units of $\mu g/m^3$ as shown in Figure 3.2. It was not a single cluster, as the graphs of *m/z* 14 vs. *m/z* 28 or *m/z* 28 vs. *m/z* 32 showed. There was a concentration of points and then a spread of other points along the *m/z* 16 axis, indicating both the 'nominal'

correction for air and the presence of something else. Taking an average value of the concentrated cluster gave a correction for the air contribution at this study to *m/z* 16 of 2.3 μg/m^3. This value did not change much during this study because there were no alterations to the QMS voltages. A similar procedure provided a correction for ^{15}N as well, although that became less important when it was decided that using *m/z* 15 for the ammonium calculation was too difficult.

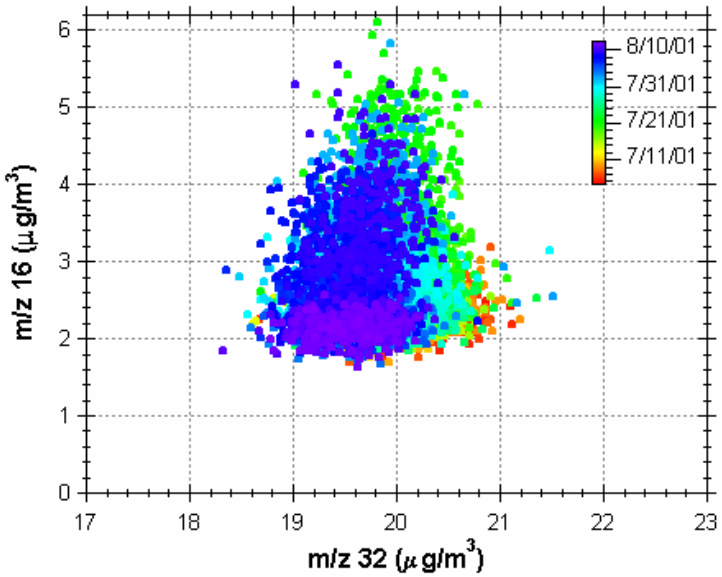

Figure 3.2: Relationship between m/z 16 and m/z 32 without corrections. The spread in m/z 16 above ~2 mg/m3 represents the presence of species other than air. Data from PROPHET 2001.

The water interference was evident in any of the masses plotted against *m/z* 18 and, to a lesser extent, *m/z* 17 as shown in Figure 3.3 (16 vs. 18 and 17 vs. 18?). There were two distinct sets of points, one during the clean periods when it was generally dry (red and blue points) and the other during the more polluted periods when it was more humid (green points). There was no offset for *m/z* 17 and 18, but it was clear that *m/z* 17 could not be used for the ammonium calculation in this case because of the variability and size of the water contribution. Therefore, ammonium

was determined from the *m/z* 16 offset and the contributions to ammonium from *m/z* 15 and 17 were calculated based on the fragmentation pattern.

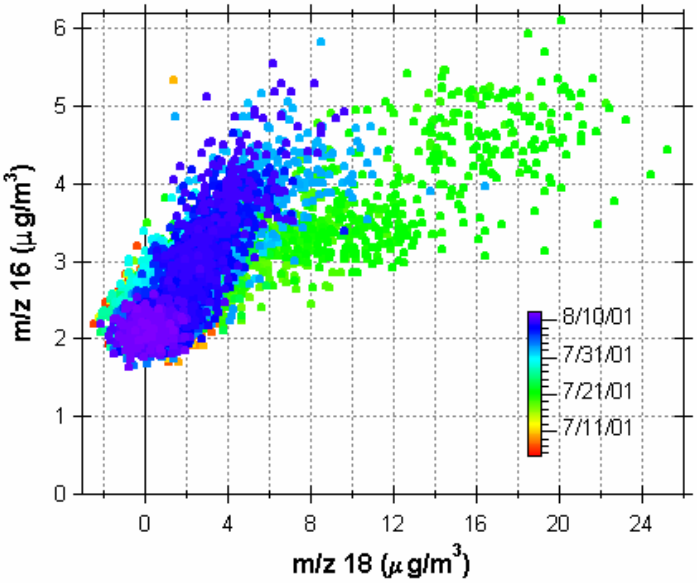

Figure 3.3: Relationship between m/z 16 and m/z 18 without corrections. The period represented by the green points had exceptionally high water content. Data from PROPHET 2001.

While this procedure worked reasonably well to give an approximate ammonium value, it was not accurate enough to determine the extent of neutralization for the particle growth event that motivated these calculations. A more quantitative method was developed in conjunction with James Allan's work in developing fragmentation tables that set the contributions from all species for every mass [Allan et al., in press]. In these tables (see Table 3.4), the fragmentation patterns are set and only the contribution of air to *m/z* 16 needs to be determined.

Table 3.4: Fragmentation tables (5/21/2003) for the masses relevant to the ammonium calculation.

	Frag_air	Frag_RH	Frag_O16	Frag_water	Frag_SO3
14	14,-frag_nitrate[14]				
15	0.00368*frag_air[14]				
16	frag_O16[16],frag_RH[16]	0.04*frag_RH[18]	0.353*frag_air[14]	0.04*frag_water[18]	0.04*frag_SO3[18]
17	0.000391*frag_O16[	0.25*frag_RH[		0.25*frag_water[	0.25*frag_SO3[

	16],frag_RH[17]	18]		18]	18]
18	0.002*frag_O16[16], frag_RH[18]	0.01*frag_air[28]		18,-frag_air[18],-frag_sulphate[18],-frag_organic[18]	0.67*frag_SO3[64],0.67*frag_SO3[48]

	Frag_NH4	**Frag_NH4_17**	**Frag_nitrate**	**Frag_organic**
14			0.04*frag_nitrate[30], 0.04*frag_nitrate[46]	
15	0.1*frag_NH4[16]			15,-frag_NH4[15],-frag_air[15]
16	16,-frag_water[16],-frag_air[16],-frag_sulphate[16],-frag_organic[16]			0.04*frag_organic[18]
17	0*1.1*frag_NH4[16],1*frag_NH4_17[17]	17,-frag_water[17],-frag_air[17],-frag_sulphate[17],-frag_organic[17]		0.25*frag_organic[18]
18				1*frag_organic[44]

There are two ways to ascertain the air contribution. The simplest method is to set a particle filter at the inlet of the AMS and measure the air alone. This will provide the gas phase values, which are the only variables. If a filter is unavailable, a clean period can also be used to make a reasonable estimate. From an averaged mass

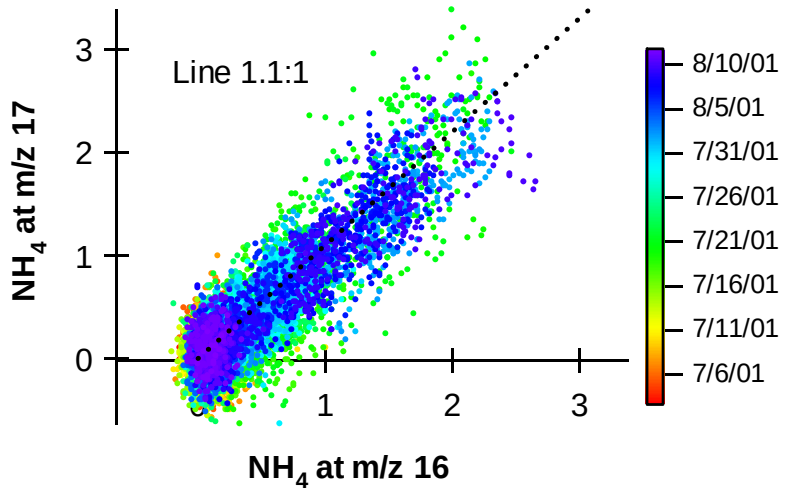

Figure 3.4: Relationship between the m/z 17 and m/z 16 ammonium contributions. The points fall closely on the 1.1:1 line, so the correction to m/z 16 for air is correct. Data from PROPHET 2001.

spectrum of this clean period, the ratios are clear and the 'frag_O16' value can be changed until the ammonium contribution from *m/z* 17 is 10% higher than the contribution form *m/z* 16. The *m/z* 16 air correction can be checked by plotting the ammonium determined from *m/z* 17 vs. the ammonium from *m/z* 16. When the correction is set properly, all the points in this plot will fall on a 1.1:1 line, as shown in Figure 3.4.

3.3 Laboratory Confirmation

The procedure for applying corrections to *m/z* 16 and 17 in order to get accurate ammonium concentrations was developed using field data, but can be verified using laboratory-generated particles that have known proportions. Ammonium nitrate particles were used to test this procedure for a wide range of particle sizes and concentrations. Figure 3.5 shows ammonium m/z 17 vs. m/z 16. In this experiment, the m/z 17 is slightly too high at the higher mass concentration and

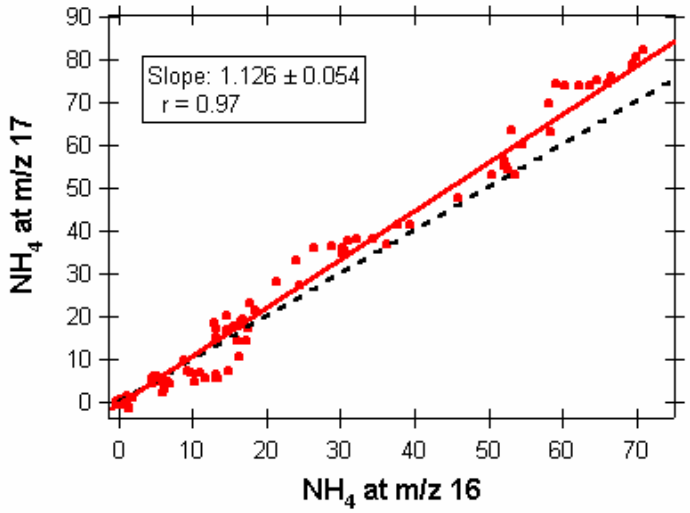

Figure 3.5: Relationship between the m/z 17 and m/z 16 ammonium contributions from laboratory-generated ammonium nitrate. There is an increase in the m/z 17 contribution at high mass concentration.

no change in the 'frag_O16' value removes this discrepancy. It may be that at very high mass concentrations, higher than could be expected for ambient data, the fragmentation changes slightly.

This discrepancy at high mass concentrations translates into what appears to be underneutralization of the ammonium nitrate when comparing the measured ammonium concentration to that calculated based on the nitrate concentration as shown in Figure 3.6.

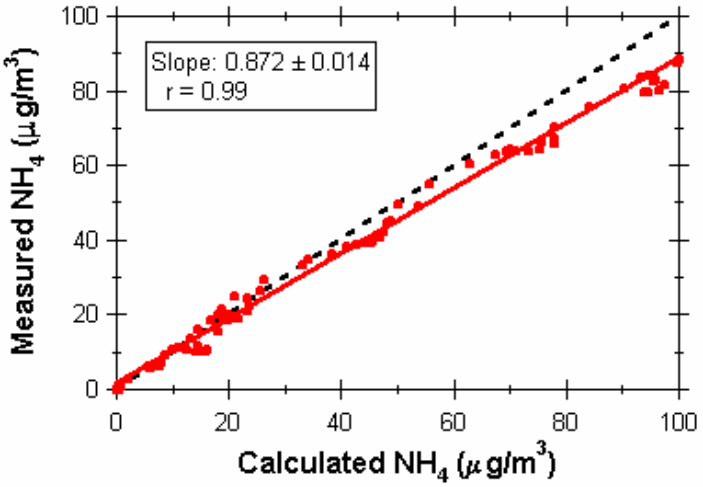

Figure 3.6: Relationship between the measured ammonium and calculated based on the nitrate concentration. Corresponding decrease in the ammonium concentration at the upper mass concentration.

3.4 Summary

The procedure for determining the ammonium concentration is complicated by the presence of so many interfering species, especially gas-phase species, like nitrogen and oxygen, which have much higher concentrations than the particulate species. Essentially, the ammonium concentration is determined by subtracting very large air concentrations, which is an inherently difficult procedure. Despite the

obstacles involved, this procedure has been proven to be effective for most situations, including both laboratory and ambient conditions.

CHAPTER 4: FIELD SAMPLING

The sampling system is one of the most important aspects of any measurement, but especially of aerosol measurements. Aerosols exhibit a wide range of sizes, chemical compositions, and characteristics that make it difficult to sample the particles without changing them in some way. While it is almost impossible to avoid altering the particles, potential interferences must be minimized in order to obtain a measurement that is representative of ambient conditions.

This chapter describes the sampling conditions of the two field campaigns that comprise the majority of the scientific results discussed in subsequent chapters. Also included are the calculated and measured losses for this system, which is a critical component in evaluation of the data.

4.1 General Sampling Issues

There are two components to sampling: the inlet, which extracts the aerosol sample from the air, and the transport system, which carries the aerosol sample to the measuring instrument. The primary purpose of the inlet is to determine the size of particles allowed into the system. There is a large range of particle sizes, from a few nanometers to hundreds of microns and it is very difficult to design either a sampling system or an instrument that can measure accurately over such a large dynamic range. Therefore, most systems are optimized for small size ranges and must take into account diffusive losses from small particles and inertial and gravitational losses from larger particles. The transport system then carries the particles from the inlet to the

instrument with the smallest impact on the particles possible. In general, it is desirable to make the transport system as short as possible to minimize any interference.

There are several issues that are of concern in sampling particles at any location. The first is that the tubing must be electrically conducting so that static build-up does not prevent charged particles from traveling through the tubing. Typically, this means using copper or stainless steel tubing. There is also electrically conducting plastic tubing that can be used, but unpublished tests performed by Rami Alfarra at the University of Manchester show that the particles can be contaminated by polyethylene, apparent in the signal at *m/z* 149, and possibly by other organic species. Copper and stainless steel tubing can also affect the particle composition through interactions with the walls. Copper can be especially reactive, even after flowing ambient air through the tubing for several days to 'passivate' the walls. However, long lengths of stainless steel can be difficult to manipulate and are very heavy, so large diameter copper tubing (to minimize wall interaction; i.e., minimize surface area to volume ratio) is often used for the main portion of the sampling line and stainless steel is used only for the more precisely machined sections that connect the main sampling line with the instruments.

The loss of material to the walls and the re-entrainment of material deposited on the walls can be significant issues. Both of these concerns can be addressed by using sample tubing of sufficient diameter that the main flow through the tubing will have little contact with the walls and by limiting the time the particles are in the tubing, thus decreasing the probability that they will interact with the walls. The

actual sample flow through most particle instruments, and especially the AMS, is small and the flow through the sampling tube is large, so only a small amount of the flow is actually sampled. The majority of the flow is discarded, particularly that portion that has had the most interaction with the wall.

Another issue is the physical environment of the sample tubing. Some species, such as ammonium nitrate, are semi-volatile and can evaporate when the tubing is heated (e.g., heating through sunlight). Conversely, gas-phase species may also condense onto the particles in the tubing when the temperature is low, which can often happen at night. This issue can be addressed by somehow insulating the sampling tubing to minimize temperature differences, increasing the air flow to minimize the amount of time spent in the sample tubing, and/or accounting for losses with another measurement. A related issue is the interaction of the particles with water. Some species are hydrophilic and may adhere to the walls more than hydrophobic species when the relative humidity is high. There is not a solution for this issue other than to measure both the water vapor concentration and temperature and be aware of those periods when this issue may affect the particle composition.

Finally, the inertial, gravitational and diffusive losses must be considered. The inertial and gravitational conditions are somewhat conflicting, since minimizing inertial losses requires that the sampling velocity be low enough that the particles can adjust to the gas flow and minimizing gravitational losses requires that the sampling velocity be high enough that the particles do not settle appreciably during sampling. The inertial and gravitational losses primarily affect the larger particles, typically

those larger than 1 or 2 μm, so they should not be a large factor for the instruments described here, which are primarily submicron measurements.

Analytic expressions to evaluate transport efficiency against these various types of loss processes are given here, and an example of their application is shown in section 4.1.2. Transport efficiency for inertial losses [Baron and Willeke, 2001]:

$$\eta_{inert} = \exp\left[\frac{-\pi d L V_t}{Q}\right] \tag{1}$$

d = inside tube diameter
L = tube length
V_t = turbulent inertial deposition velocity
Q = volumetric flow rate

Transport efficiency for gravitational losses [Baron and Willeke, 2001]:

$$\eta_{grav} = 1 - \frac{2}{\pi}\left[2\kappa\sqrt{1-\kappa^{2/3}} - \kappa^{1/3}\sqrt{1-\kappa^{2/3}} + \arcsin\left(\kappa^{1/3}\right)\right] \tag{2}$$

$$\kappa = \frac{3}{4}\frac{L}{d}\frac{V_{ts}}{U}\cos\theta \tag{3}$$

V_{ts} = terminal settling velocity
U = mean gas velocity
θ = angle of inclination from the horizontal

Diffusion refers to the random movement of gas molecules and particles. Large particles diffuse more slowly than small particles because of the increase in inertia with particle mass and bombardment by gas molecules averaged over the larger surface area. Therefore, diffusive losses usually affect only the smallest particles, those with diameters less than 100 nm. [Baron and Willeke, 2001]
Transport efficiency for diffusion losses [Baron and Willeke, 2001]:

$$\eta_{diff} = \exp\left[\frac{-\pi d L V_{diff}}{Q}\right] \quad (4)$$

V_{diff} = diffusive deposition velocity, also called mass transfer coefficient

There is one other key consideration in designing a sampling system – the type of flow regime. The flow pattern is governed by the ratio of the inertial force of the gas to the friction force of the gas moving over the surface, called the Reynolds number (Re_f). At low Reynolds numbers, less than about 2000, frictional forces dominate the gas flow and the flow is smooth, or laminar, meaning none of the streamlines loop back on themselves. At high Reynolds numbers, greater than about 4000, inertial forces dominate and the flow becomes chaotic, or turbulent.

$$\mathrm{Re}_f = \frac{\rho_g U d}{\eta} \quad (5)$$

τ = particle relaxation time (time to reach 1/e of final velocity subject to gravity)

$\tau = \rho_p d_p^2 Cc / 18\eta$

g = gravitational acceleration

d = characteristic system dimension

ρ_g = gas density

η = gas absolute viscosity

4.2 PROPHET Sampling Setup

The scientific goals at PROPHET; primarily, to determine the bulk particle characteristics of the area and the difference, if any, between the particles above the forest canopy and those within the canopy; determined the sampling setup. It was necessary to sample the particles at several heights to investigate the interaction with the forest canopy and the long lengths of sample tubing determined the tubing size

and flow rates. It was decided to sample at three heights, one below the canopy to measure contributions from the ground and human influences, one at the top of the canopy to measure contributions from the forest and one several meters above the forest canopy to measure the regional contribution.

Figure 4.1: Picture of the PROPHET laboratory building (left) with the base of the tower visible on the right side of the building and the tower (right) with the two lowest aerosol sampling inlets visible protruding from the right side of the tower.

The site consists of a 31m scaffolding tower with an internal stair next to a 6 m by 9 m laboratory building with a separate room for large pumps and blowers that is exhausted several hundred meters away near the access road. There is a permanent manifold for gas-phase measurements, but nothing in place for aerosols. Therefore, the aerosol sampling system had to be added to the tower. Copper tubing (½ in O.D.) was attached to the outside of the tower on the west side, with one inlet placed at the top of the tower (30 m), one at the top of the forest canopy at 18 m and one just above the ground at 5 m. Initially, the plan was to have only one sampling line and install valves that would switch between the different heights, but that would mean that the upper portions of the sampling line would not have air flow when the lower inlets were being sampled, which could lead to differences in the measured particles caused

by disruption in the air flow or deposition of gas-phase material to the walls while there was no air flow.

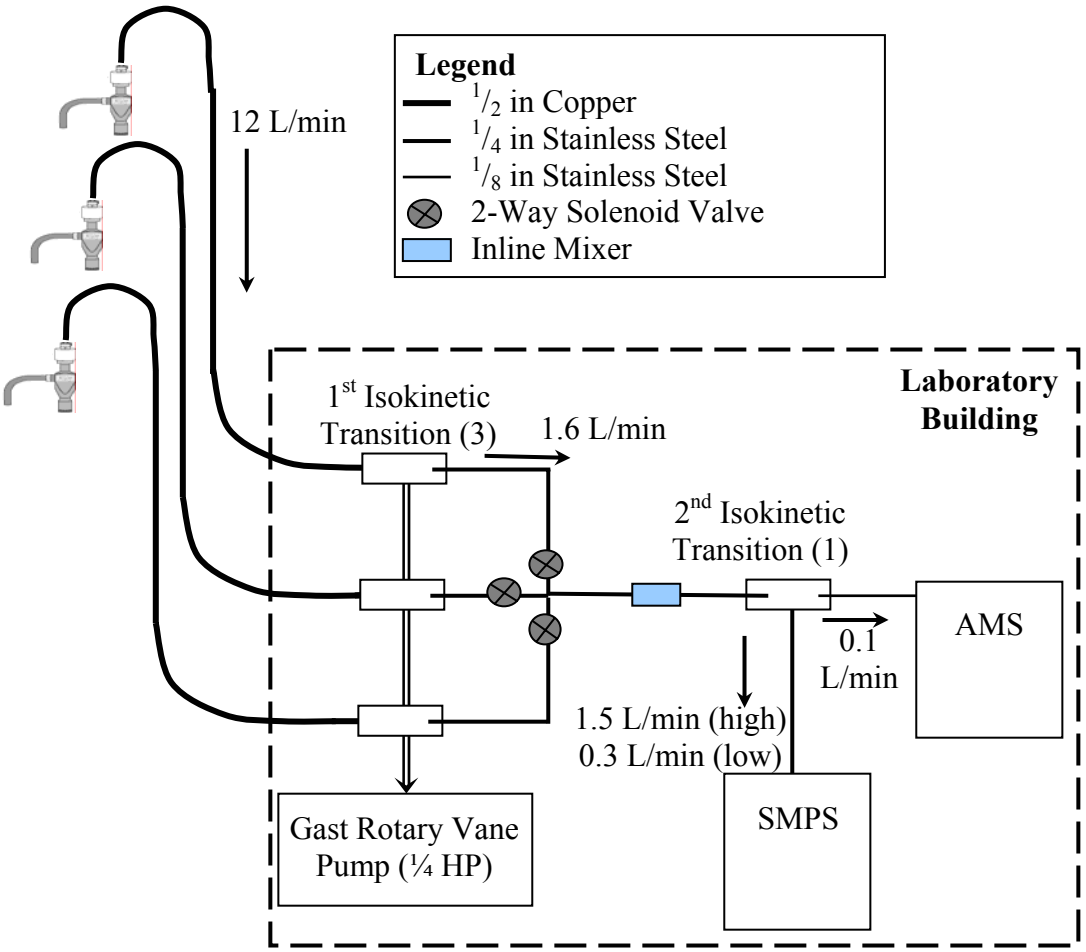

Figure 4.2: Diagram of PROPHET sampling setup (not to scale). The components within the dashed box were inside the laboratory building.

Figure 4.2 shows a diagram of the sampling situation at the PROPHET tower. Each sample line had a cyclone at the end (URG 2000-30EN) that removed larger particles and small insects by drawing the ambient air into a small chamber where it swirled around and the larger material gravitationally settled to the bottom. The

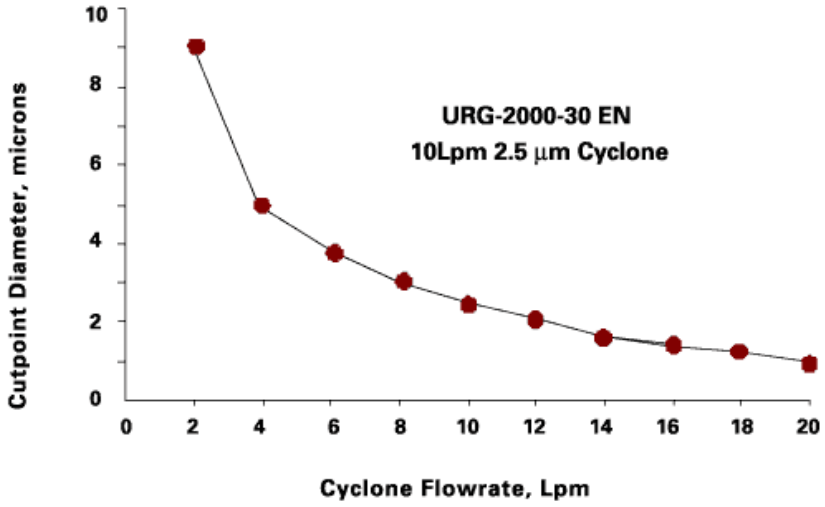

Figure 4.3: Cutpoint diameter as a function of flowrate. http://www.urgcorp.com.

flowrate could be adjusted to provide a different cutpoint, which is defined as 50% transmission for the stated particle size, based on sampling requirements, shown in Figure 4.3. The PROPHET study was focused on submicron particles, so the flowrate was set to 12 L/min to set the cutpoint to 2 μm. The main sampling lines were ½ inch O.D. copper tubing and extended from the inlet on the tower to the point where the majority of the air was exhausted through the main pump. At this point an isokinetic transition, shown in Figure 4.4, was used to extract a sample of the air from the center of the copper tubing. Sampling is considered isokinetic when it is laminar, isoaxial, i.e., all on the same plane, and the mean sample flow velocity upstream of the inlet or transition is equal to the downstream gas flow velocity. Because the velocity in the center of the flow is twice that of the mean flow, this means that the downstream velocity must be twice that of the upstream velocity. The isokinetic transition allows a reduction in the flow to accommodate the much lower flow rate of the instruments while limiting the disruption in the gas flow that might in turn perturb the particles.

All three lines were pumped continuously by a Gast rotary vane pump (0.25 HP 0523-101QG588DX), and each line had a 2-way normally closed NResearch solenoid valve (P/N 648T012) that blocked the flow when closed and allowed sampling when open. Only one valve was open at any time. These valves were controlled by a simple program (Digiline, M. Canagaratna, ARI) that synched the switching of these valves to the AMS computer clock and were set so that they would switch each time the AMS saved a data file. The sample then passed through an inline mixer (Omega Engineering, FMX8451S) consisting of six curved plates that mixed up the air sample to remove any inhomogeneities in the sample, and then a second isokinetic transition (Figure 4.4) to reduce the airflow to the 0.1 L/min required by the AMS. The remainder of the sample from the second isokinetic transition was sent to a scanning mobility particle sizing system (3080L SMPS, TSI Inc. St. Paul, MN) to measure the particle number distribution.

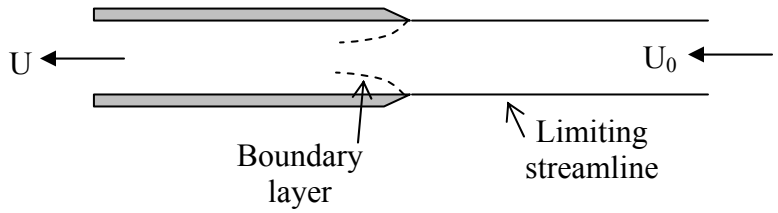

Figure 4.4: Diagram of isokinetic transition. The first transition (½ in to ¼ in) has U_0=1.86m/s and U=3.75m/s. The second transition (¼ in to $^1/_8$ in) has U_0=3.75m/s and U=4.05m/s and is therefore slightly superisokinetic. Adapted from Baron and Willeke, 2001.

In addition to the AMS and SMPS set up by the Toohey group, a similar system was used by a group from Arizona State University (Jonathan Allen and Umar Siddiqui) to measure aerosol concentration and fluxes at the top of the tower. The only difference in the measurement setup of these two groups was the absence of the solenoid valves used to switch between sample lines. The ASU group measured only

from an inlet at the top of the tower, separate from the inlet used by the Toohey group.

The flow rates, lengths, and diameters of the tubing used in the sampling system were designed to minimize the amount of time particles spent in the sampling system, thus limiting interactions with the tubing walls and other particles, and sampling losses.

Table 4.1: Sampling parameters for each section of tubing.

	½ in	¼ in	1/8 in
Inner diameter (m)	0.0117	0.003	0.000675
Avg velocity (m/s)	1.86	3.75	4.05
Length (m)	30	0.8	0.1
Re_f (<2000→laminar)	1450	750	182
Residence time (s)	8	0.2	0.025

The types of losses described in section 4.1.1 can be calculated for the inlet used at PROPHET. These are shown in Figure 4.5, indicating that minimal particle losses – on the order of 10% were expected for this sampling system. An experiment was conducted during the sampling campaign to determine the actual losses. During

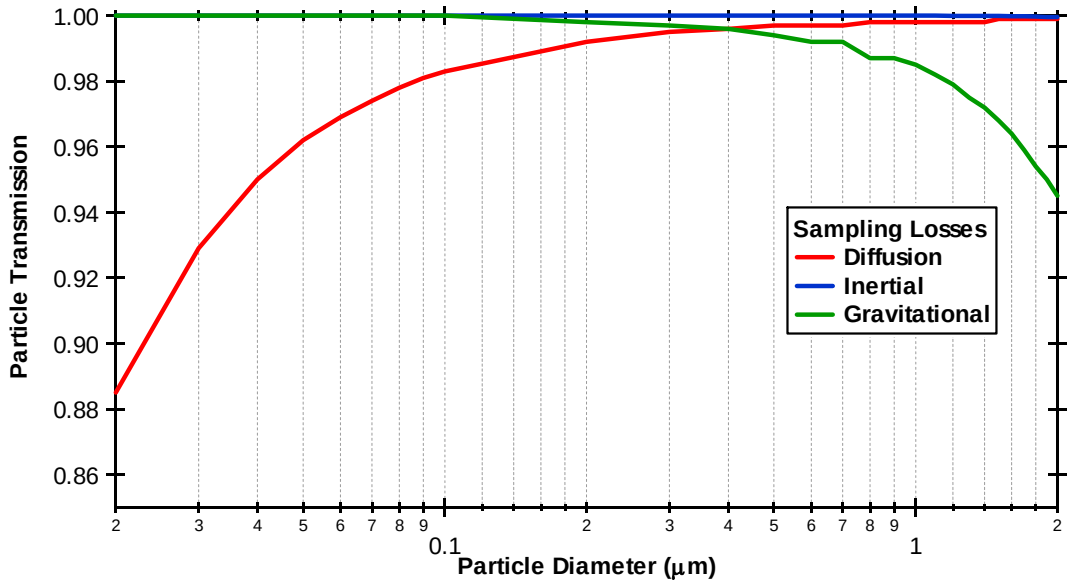

Figure 4.5: Calculated sampling losses. Equations from Baron and Willeke, 2001.

this experiment ammonium nitrate particles of various sizes, as set by a DMA, were generated in the laboratory building at the base of the tower. These particles were pumped to the top of the tower through ¼“ copper tubing and directed into the inlet of the URG 2000-30EN cyclone and the rest of the sampling apparatus and into a 3022A Condensation Particle Counter (TSI, St. Paul, MN) placed at the top of the tower to count the number of particles that reached the inlet.

Comparison of the number of particles counted at the top of the tower and by the AMS and SMPS measurements in the laboratory building showed losses of approximately 60% for those particle sizes in the 100% transmission region of the AMS and considerably higher losses outside that region, as shown in Figure 4.6. However, the number concentration is not an effective measure because the AMS does not count particles less than approximately 200 nm individually, but rather

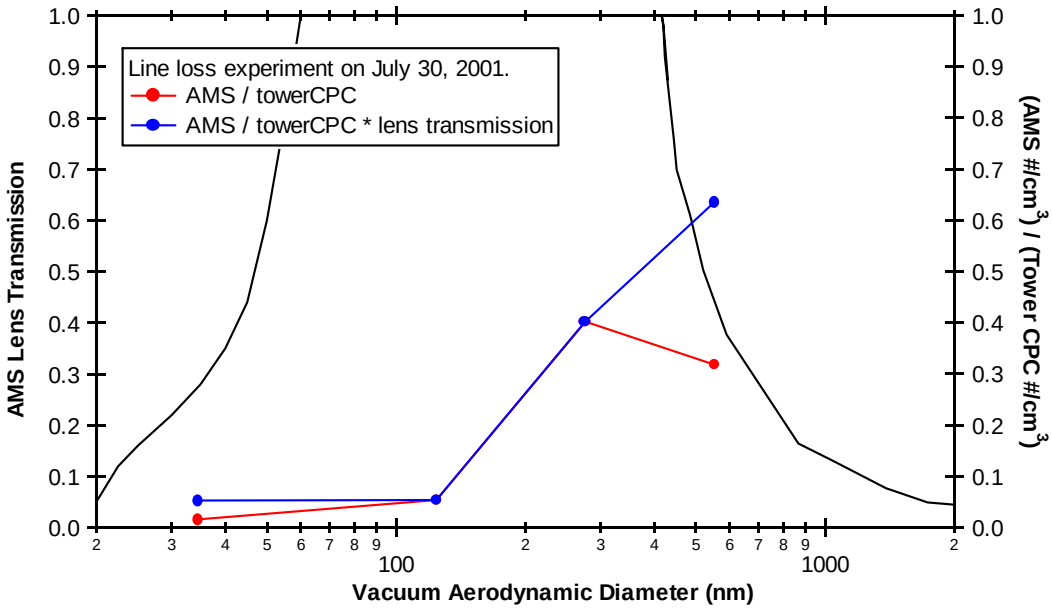

Figure 4.6: Experimental sampling losses measured at PROPHET 2001. Comparison of particles counted by the AMS and the CPC on the tower with the calculated AMS lens transmission efficiency [FLUENT] in black.

determines the aggregate mass of the particles. Unfortunately, it is impossible to determine the mass distribution at the top of the tower because only the absolute particle number (with no size information) was measured by the CPC at the top of the tower. An examination of the mass distribution as measured by the AMS and the SMPS at the end of the sampling line illustrates another issue. The three sizes of ammonium nitrate test particles for which there is comparable data (90, 200, and 400 nm) shows that the distributions are multimodal (see Table 4.2 and Figure 4.7) and therefore the calculation of particle mass from the CPC at the top of the tower based on the assumption that the particle size did not change significantly as it was pumped to the top of the tower is faulty. Only the 400 nm particles exhibited mostly monomodal behavior and the discrepancy between the SMPS and AMS measurements cannot be explained solely by the decrease in the AMS lens transmission (approximately 50% for 550 nm particles).

Table 4.2: Summary of line loss experiment. The number in parentheses refers to the particle mode observed from smallest (1) to largest (3) and the percentage refers to the particle transmission based on the CPC mass. This is only possible for the 400 nm particles because the others are multimodal and there is no accurate way to determine the CPC mass without assuming a particle diameter.

	90 nm	**200 nm**	**400 nm**
AMS Mass (μg/m^3)	(1) 0.09 (2) 0.4 (3) 1.1	(1) 2.5 (2) 4.3	3.0 (25%)
SMPS Mass (μg/m^3)	(1) 0.03 (2) 1.2 (3) 5.5	(1) 10.0 (2) 10.8	10.7 (90%)
Tower CPC Mass (μg/m^3)	2.5	12.0	11.9

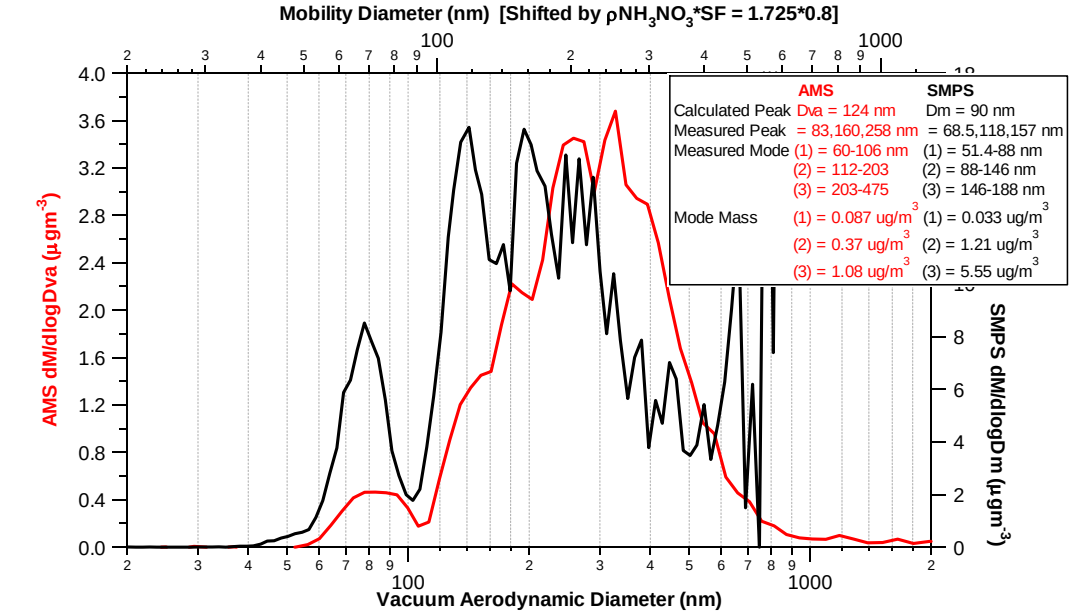
Mobility Diameter (nm) [Shifted by ρNH4NO3*SF = 1.725*0.8]
AMS
SMPS
Calculated Peak Dva = 124 nm
Dm = 90 nm
Measured Peak = 83,160,258 nm
= 68.5,118,157 nm
Measured Mode (1) = 60-106 nm
(1) = 51.4-88 nm
(2) = 112-203
(2) = 88-146 nm
(3) = 203-475
(3) = 146-188 nm
Mode Mass
(1) = 0.087 ug/m3
(1) = 0.033 ug/m3
(2) = 0.37 ug/m3
(2) = 1.21 ug/m3
(3) = 1.08 ug/m3
(3) = 5.55 ug/m3
AMS dM/dlogDva (µgm-3)
SMPS dM/dlogDm (µgm-3)
Vacuum Aerodynamic Diameter (nm)

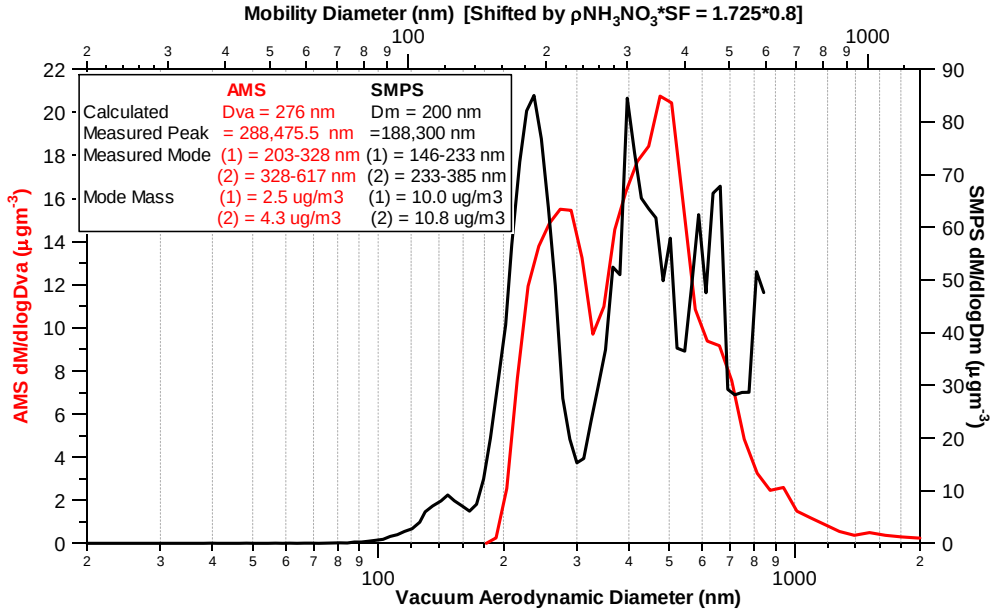
Mobility Diameter (nm) [Shifted by ρNH4NO3*SF = 1.725*0.8]
AMS
SMPS
Calculated Dva = 276 nm
Dm = 200 nm
Measured Peak = 288,475.5 nm
=188,300 nm
Measured Mode (1) = 203-328 nm
(1) = 146-233 nm
(2) = 328-617 nm
(2) = 233-385 nm
Mode Mass
(1) = 2.5 ug/m3
(1) = 10.0 ug/m3
(2) = 4.3 ug/m3
(2) = 10.8 ug/m3
AMS dM/dlogDva (µgm-3)
SMPS dM/dlogDm (µgm-3)
Vacuum Aerodynamic Diameter (nm)

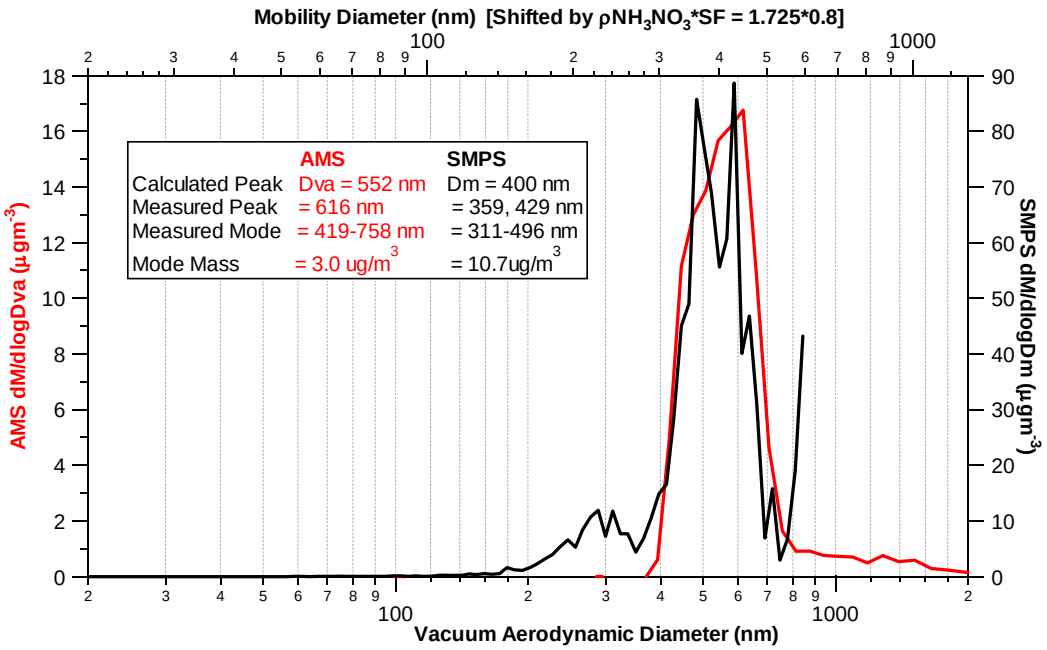

Figure 4.7: Experimental sampling losses. Comparison of AMS and SMPS mass distributions for 90 nm (top), 200 nm (middle), and 400 nm (bottom) ammonium nitrate test particles.

After examining the results from this experiment it became clear that there were several flaws that made these results potentially unreliable. Ammonium nitrate was chosen as the test species because it is well focused and has high transmission through the AMS. Therefore, any losses could be attributed to the sampling line and not the AMS. However, ammonium nitrate is semi-volatile, as described earlier, and it is very possible that losses could be attributed to interactions with the tube walls or to temperature changes rather than simple particle loss because of inertia or diffusion. Also, as shown above, simply counting the number of particles at the top of the tower rather than measuring their size distribution did not account for any changes to the particle size on the way up to the top of the tower.

4.3 Laboratory Line Loss Experiment

The potential problems with the sampling line loss experiment on the PROPHET tower made another experiment under more controlled laboratory conditions essential. It was also clear that the AMS was not an instrument that could provide representative results for this type of experiment; there are evidently other issues involved in AMS sampling as demonstrated by the large discrepancy between the AMS and SMPS measurements during the PROPHET line loss experiment.

An experiment was formulated to measure line losses for a similar sampling system as employed at PROPHET with the AMS and an Ultra High Sensitivity Aerosol Spectrometer (UHSAS, Particle Measuring Systems), which is an optical particle counter/sizer with a sampling range of approximately 0.05 to 1 μm. The advantage of using an instrument like the UHSAS is that there are almost no calibrations or corrections required, so the data are more reliable for an experiment of this type.

The sampling system used at PROPHET was replicated in the laboratory, with a cyclone, 100 ft of ½" O.D. copper tubing, and two isokinetic transitions. The flow through the ½" O.D. tubing was 11.5 L/min, reduced to 1.6 L/min after the first isokinetic transition. The UHSAS sampled just upstream of the AMS critical orifice to reduce any differences caused by tubing.

Particles were introduced into the sampling system at three locations in order to test the transmission of various components of the system: through the cyclone at the end of the sample tubing to examine the full transmission (denoted high flow long, HFL); just upstream of the first isokinetic transmission to test the 100 ft of tubing while maintaining the same flowrate and avoid the issue of dilution (denoted high flow short, HFS); and just upstream of the AMS inlet to provide an upper limit on the transmission (denoted low flow, LF).

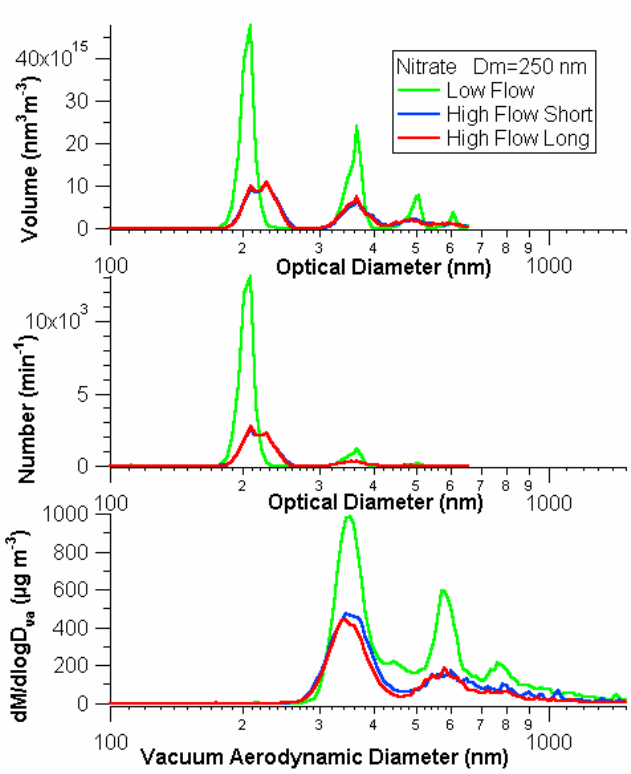

Figure 4.8: Example of results from line loss experimentswith the PMS UHSAS (top two panels) and the AMS (bottom panel)

Several types of test particles of various sizes; 98, 300, and 494 nm polystyrene latex spheres (PSLs), 100, 250, 500, and 650 nm ammonium nitrate, 200 and 400 nm oleic acid, and 400 nm ammonium sulfate; were used to determine the composition and size dependence of the sampling system.

An example of one of these runs is shown in Figure 4.8 for 250 nm ammonium nitrate particles. The dilution of the higher flow results in comparison to the low flow results gives the appearance of higher transmission, but that is not necessarily the case. Therefore, only the high flow results have been used to determine the sampling transmission.

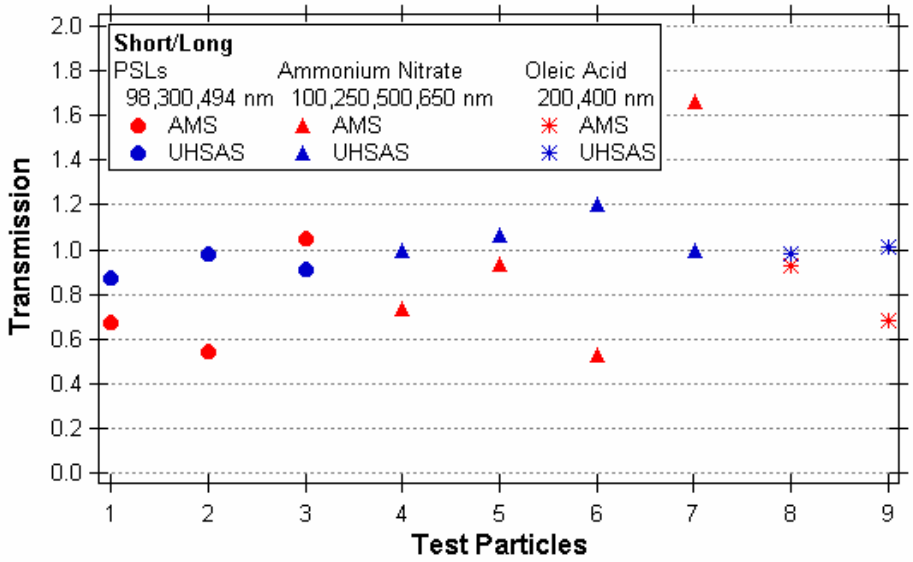

Figure 4.9: Summary of line loss experiment. Particle types displayed in order as described in legend. AMS values in red and UHSAS values in blue.

Figure 4.9 summarizes the results from this experiment. The results from the high flow short runs were viewed as complete transmission, so the ratio of the high flow long to short determines loss as a result of traveling through the tubing. The UHSAS results are fairly consistent in showing that the losses are typically less than 10%. However, the AMS results are much more varied, ranging from 0.53 to 1.67. There is at least one value greater than 10% for each type of test particle and there does not appear to be a relationship with size of particle. The reason for this discrepancy is not yet clear and further experiments are required to explore this issue.

4.4 CELTIC Sampling Setup

The sampling goals at CELTIC were very similar to those at PROPHET: to determine the bulk particle characteristics of the area and to assess any difference between the particles above the forest canopy and those within the canopy. Based on the low calculated losses for the system used at PROPHET, a similar system was used for CELTIC. The only significant difference to the sampling hardware was the absence of the inline mixer. However, the environment and facilities at the two sites were quite different. Whereas the PROPHET site was designed solely for measurements, the CELTIC study was based at the Duke Forest FACTS-1 Research Site. This facility is designed to study the effects of carbon dioxide enrichment and consists of several scaffolding walk-up towers similar to the PROPHET tower surrounded by small triangular towers that are used to release large amounts of carbon dioxide or air for the control towers. Trailers were brought in both for transportation and as laboratory facilities. Ring 6 housed most of the aerosol measurements and ring 5 most of the gas phase measurements. Due to lack of space adjacent to the scaffolding tower, the trailers were placed just outside the ring of smaller towers. Since the ideal sampling situation

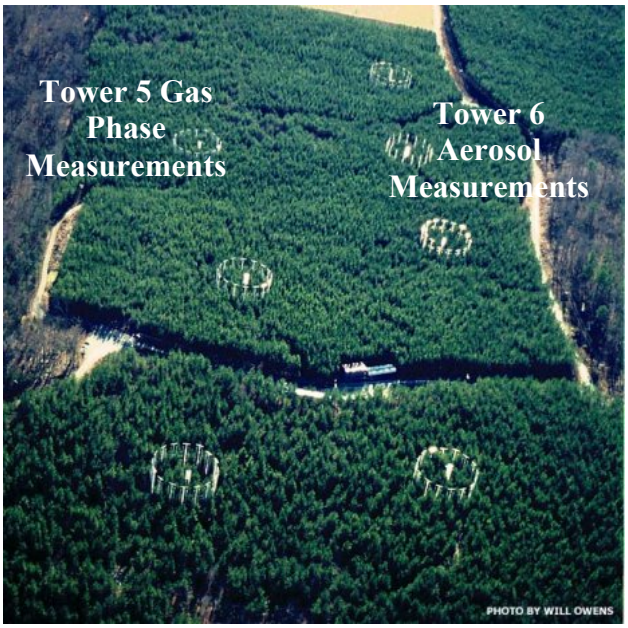

Figure 4.10: Picture of Duke Forest rings.

for the aerosol measurements included using the shortest length of sampling tubing possible, the small towers were employed for the aerosol sampling system and the trace gas measurement sample lines were also placed on the same small tower to facilitate comparison with the aerosol measurements.

As a result of the difficulties with temperature differences between the ambient air and that inside the research facility, the sampling lines and instruments were positioned so that only a short length of sampling tubing was inside the trailer. No insulation was used to minimize temperature differences in the sampling lines since it was not considered effective during PROPHET.

A second AMS at ring 6 was operated by the CIRES group (Jose Jimenez and Alex Huffman, Chemistry Department, University of Colorado). The purpose of this instrument was to determine fluxes using the eddy covariance method, so the flowrate was much larger, causing turbulent flow, and the cyclone was placed just outside the measurement trailer rather than at the top of the tower to minimize interference in the air flow. This AMS alternated between concentration and flux measurements, so that it would have a reference for the flux measurements.

The gas phase measurements at ring 6 (CO_2, H_2O, O_3, NO, and NO_x) were made from the same small triangular tower as the aerosol measurements. Teflon tubing (¼ in O.D.) was used for the O_3 (TEI 49C) and NO/NO_x (TEI 42C-TL/32) measurements and Dekoron (polyethylene over aluminum) for the CO_2/H_2O (LI-7000 CO_2/H_2O Analyzer) measurement. The O_3 and NO/NO_x data were saved every minute and the CO_2/H_2O data every second.

4.5 Summary

The same basic sampling system of three inlets at different heights on a tower was used for both the PROPHET and CELTIC field campaigns. The tubing and flow rates were chosen to optimize the sampling so that the particles spent a minimum amount of time in the tubing, but the flow was low enough to maintain laminar flow, thus reducing interaction with the walls. In addition, several gas-phase measurements were added for the CELTIC campaign that were useful for describing the general conditions at the site.

The calculated line losses were dependent on size, but were less than 12% for the most extreme case and generally much less than that. A line loss experiment conducted during PROPHET showed much higher losses, approximately 60% for the AMS, which seemed unreasonable. Therefore, an additional experiment was conducted in the laboratory with both the AMS and a newly developed optical scattering instrument (UHSAS, Particle Metrics, Inc.) that confirmed much lower losses – on the order of 10% for several different chemical species and sizes as measured by the UHSAS. The AMS measured losses were much larger and more variable, without a clear pattern to explain the discrepancy. It is apparent that there are additional issues with the AMS that cause it to be unreliable for this type of experiment.

CHAPTER 5: PROPHET 2001 FIELD CAMPAIGN

There are few good comprehensive remote or long-range aerosol measurements due to the difficulties in measuring aerosols and their spatial and temporal variability. Therefore, aerosol measurements at a wide variety of sites and conditions are necessary to develop a general aerosol climatology that includes non-urban locations and processes. Since the field of aerosol measurements is still fairly young in comparison to gas-phase measurements, the emphasis has been on urban environments. However, biogenic aerosols can make up a significant fraction of the aerosol mass in some locations [Blando et al., 1998; Finlayson-Pitts and Pitts, 1999; Jacobson et al., 2000; Seinfeld and Pandis, 1998] and transported aerosols can affect communities hundreds of miles away.

For the past several years, ambient data has been collected at a remote site in northern Michigan as part of a program called PROPHET (**P**rogram for **R**esearch on **O**xidants: **PH**otochemistry, Emissions and **T**ransport). PROPHET is a collaborative research effort designed to improve understanding of gas phase and heterogenous oxidant chemistry, the exchange of gases and particulate matter between the biosphere and the atmosphere, and how forest-atmosphere interactions influence the composition of the atmosphere.

The purpose of the aerosol measurements at this site for the 2001 field intensive were to gain an understanding of the bulk aerosol population, study the effect of transported aerosols on local conditions, and determine what, if any, effect biogenic aerosols may have.

5.1 Site description

The program is part of the research activities at the University of Michigan Biological Station facilities in northern Michigan, which are located approximately three kilometers northeast of the PROPHET site. The site is located in a relatively undisturbed and well-characterized mixed, or transition, forest, comprised of northern hardwood (maple, beech, birch, basswood), mixed aspen (native, bigtooth, trembling, representing new or re-growth), bog conifers in lower, wet areas (white and black spruce and balsam fir), pine and red oak in the drier upland regions, and grass-covered sand dunes along the coast. [Carroll et al., 2001; PROPHET website, 2001] The immediate vicinity of the site consists of forests, lakes, and small communities. The nearest city with a population greater than 10,000 is Alpena, more than 100 km

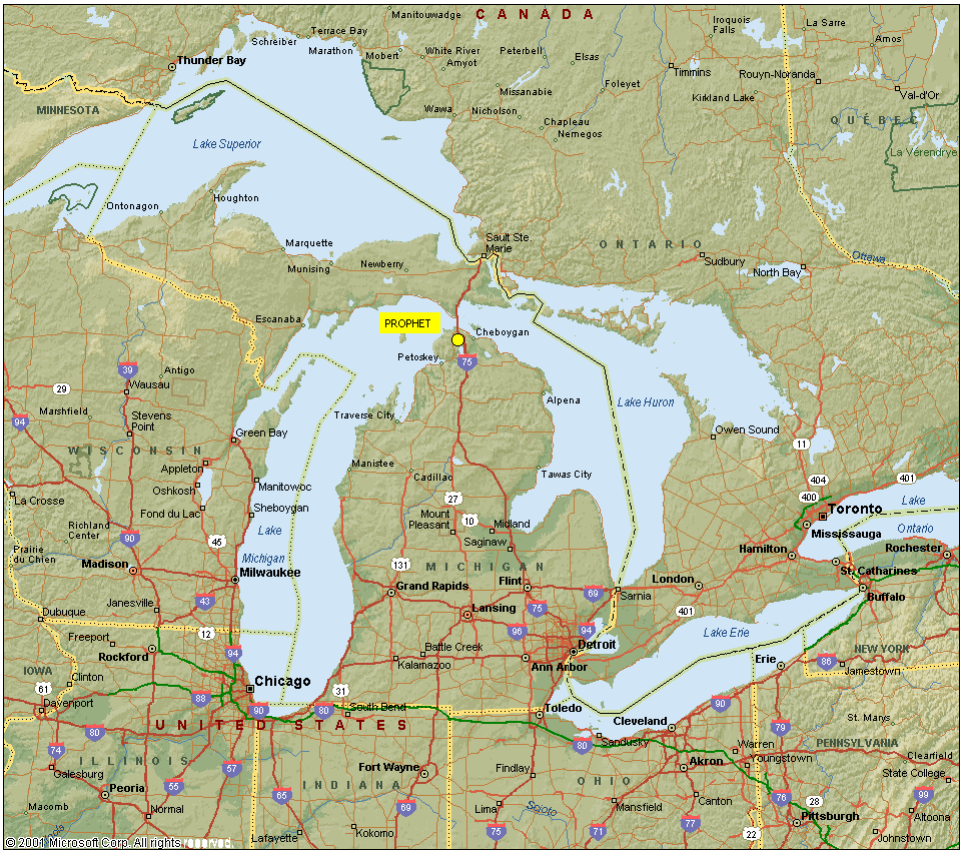

Figure 5.1: PROPHET site and the surrounding area. Created by Microsoft Streets & Trips.

to the southeast (see Figure 5.1).

The laboratory, a 6.1 m by 9.1 m pole barn, is positioned at the base of a 31-meter scaffolding tower. Most gas phase instruments were located within the laboratory and sampled through a 5 cm Pyrex manifold with a flow rate of approximately 3300 liters per minute, but those measuring more reactive species were mounted on the tower itself. [Carroll et al., 2001; PROPHET website, 2001] The aerosol measurements did not employ the manifold, but had a separate sampling system as described in Chapter 4.

Most of the data collected at PROPHET were gas-phase measurements; including CO, O_3, NO_x, PANs, HONO, light hydrocarbons, isoprene, H_2SO_4, OH, HNO_3, and peroxides. Also measured at the site were standard meteorological parameters, such as wind speed, wind direction, temperature, and relative humidity; UV radiation and photolysis rates; air mass trajectories; and vertical wind profiles. PROHET 2001 was the fourth intensive field campaign at this location. The dominant gas phase biogenic species at this location is isoprene, a five carbon unsaturated hydrocarbon. The double bond makes this species extremely reactive and its interaction with NO_x, as one of the major species involved in photooxidant chemistry, has been the focus of these studies. However, isoprene and its oxidation products have relatively high vapor pressures and, therefore, do not usually condense onto particles.

Aerosol measurements have been made during previous intensives, but none of these results have been released. The AMS measurements made during PROPHET

2001 are the first real-time in situ measurements of aerosol chemical composition at this site.

5.2 Measurements Overview

All of the measurements at the PROPHET site showed that the air quality at the site is highly direction dependent. In general, northerly airflow brought clean air with low aerosol mass loadings and southerly airflow brought more polluted air with higher mass loadings, as shown in Figure 4.2 and 4.3. There seemed to be fairly low

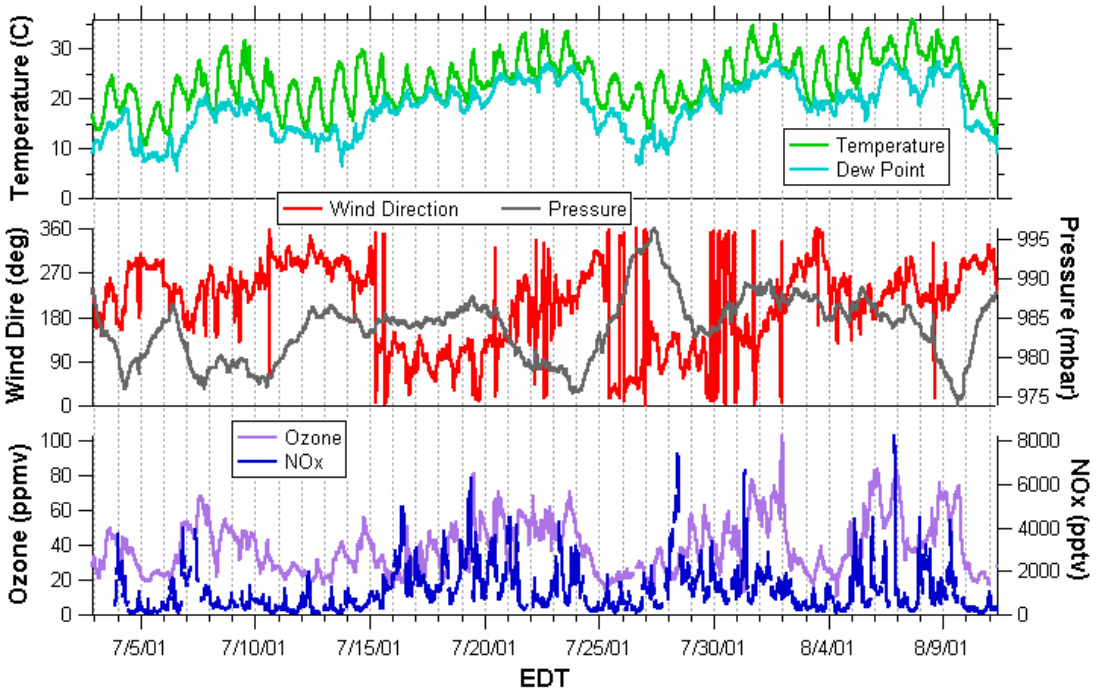

Figure 5.2: Overall conditions during PROPHET 2001.

mass loadings of locally produced aerosols, i.e., even on clean days there are very low aerosol levels, less than 1 $\mu g/m^3$ on average, indicating that the background, or local, aerosol amounts were low. In general, the mass loading on days with southerly or southwesterly flow was dominated by sulfates, with levels reaching approximately 6

$\mu g/m^3$ during the most polluted periods. There was also a strong contribution of organic species during the pollution episodes, approximately 3.5 $\mu g/m^3$ at the peak of the largest events. However, there were universally low levels of nitrates, less than 0.5 $\mu g/m^3$ even on the most polluted days. This is not unexpected, given the distance

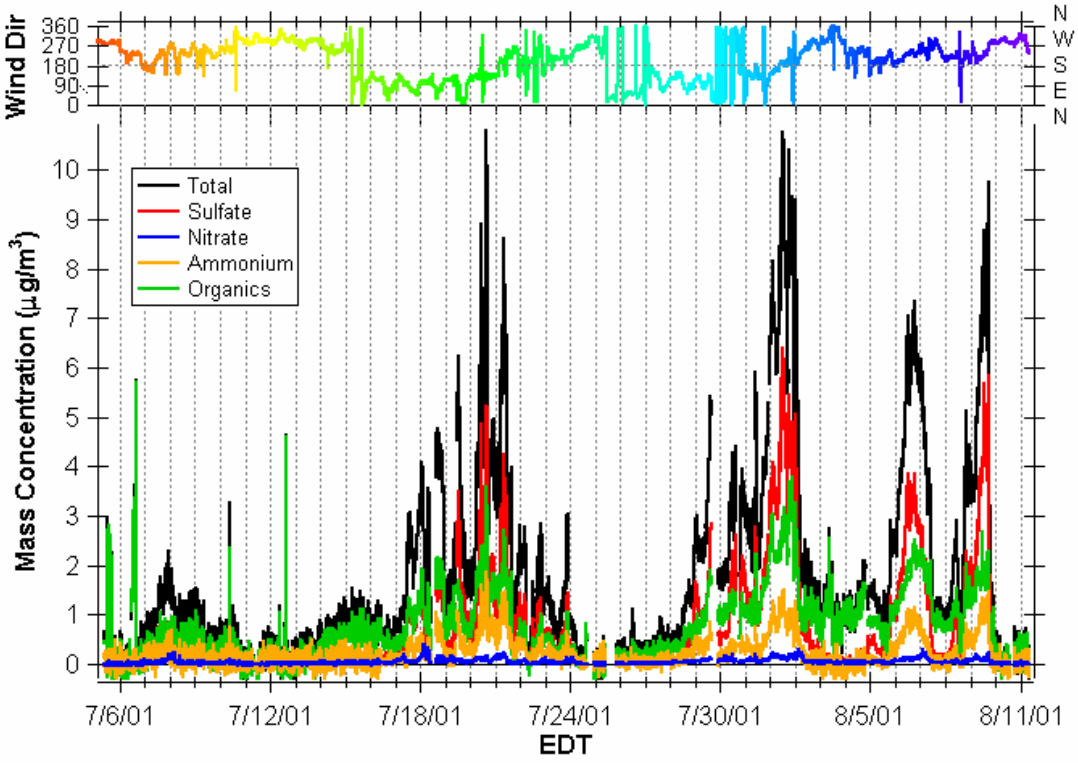

Figure 5.3: Wind direction (top) and AMS mass concentrations of major species (bottom) for entire PROPHET 2001 field campaign.

from any major urban areas. During the cleaner periods, dominated by northerly flow, the aerosol mass loading of the organic species often had the largest contribution to the aerosol loading. There were also several episodes of small particle growth during periods of low aerosol mass loading, with the most distinct event on 26 July.

5.3 Southerly Flow

The PROPHET site is remote enough that any significant pollution from large cities has to travel several hundred kilometers. Most of the large cities are located to the south and west, therefore, southerly or southwesterly flow was characterized by more polluted air as shown in Figure 5.3, with levels of sulfate approximately three to four times higher than organic levels at the peak of the pollution episodes.

These pollution episodes exhibited no diurnal pattern, as is typical closer to large urban areas. There was almost no contribution from nitrate during these episodes, which is also expected for a site far from the influences of vehicular traffic. The organic loading generally follows the pattern of the sulfate, probably indicating that the organics and sulfate are internally mixed. Figure 5.4, a correlation plot of sulfate and organics, shows this strong relationship with approximately twice as much sulfate as organic. The sulfate and organics size distributions, shown in Figure 5.5,

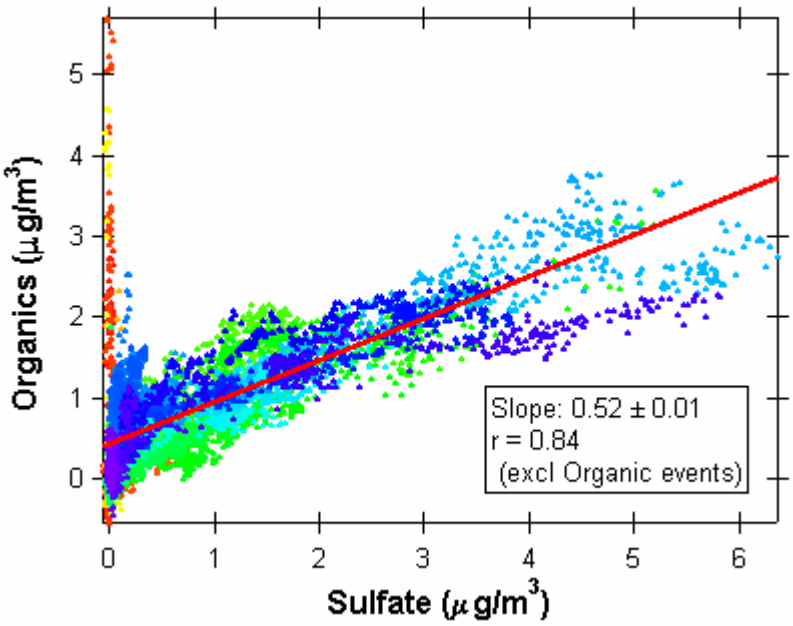

Figure 5.4: Relationship between total organics and sulfate for the entire study.

shows that the species always share the accumulation mode of approximately 400 nm vacuum aerodynamic diameter during the more polluted periods. Although this is not definitive proof that the sulfate and organics are internally mixed, it is a strong indicator.

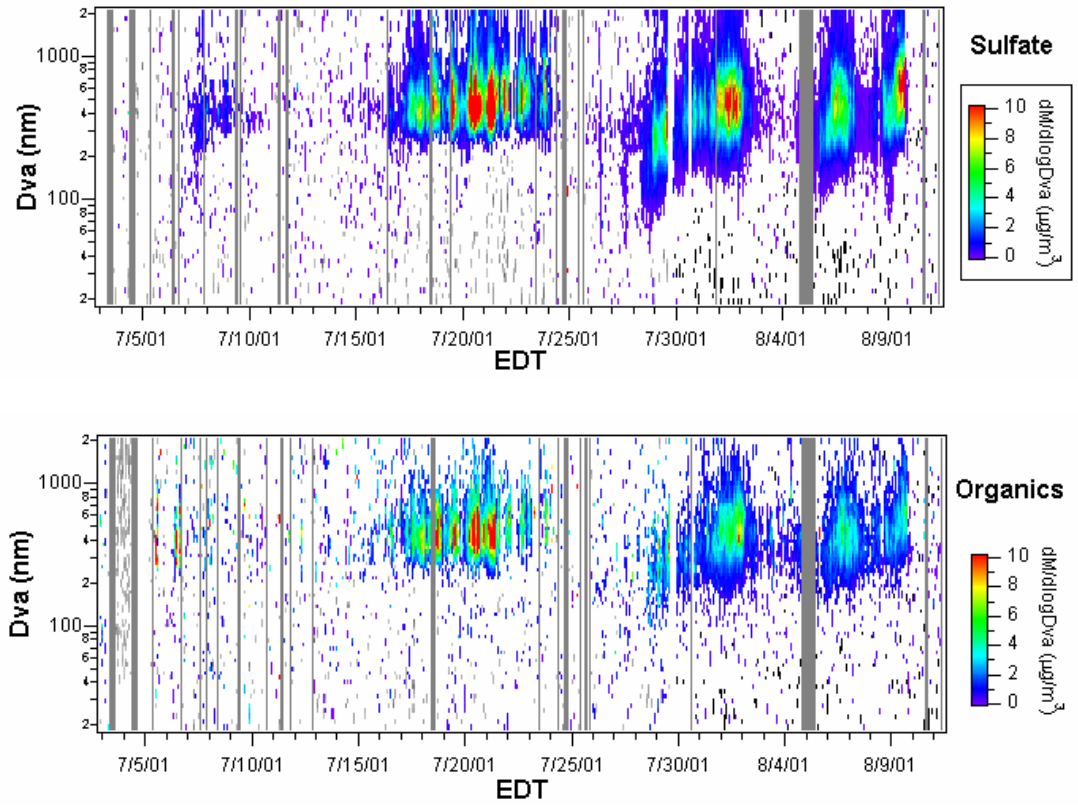

Figure 5.5: Size distributions for the entire PROPHET 2001 campaign for sulfate (top) and organics (bottom).

There were four major pollution episodes during the sampling period. The first began on the afternoon of July 16 and continued until about midnight of July 23. This was the longest period of southerly airflow, although not the greatest concentrations, and was characterized by high temperatures and dew points, O_3, CO, and NO_x, as would be expected for a polluted air mass as shown in Figure 4.2. The

peak of this event occurred on the afternoon of July 20 when the total aerosol mass loading reached approximately 11 μg/m^3.

The composition of the aerosols during this episode does not vary much. A typical mass spectrum, shown in Figure 4.6 from July 20 averaged from 1410 to 1645 local time, shows large amounts of sulfate and organics. The organics exhibit the typical delta pattern described in Chapter 2. Delta, or ion series, numbers 0 and 2 are dominant, indicating the presence of mostly unsaturated hydrocarbons.

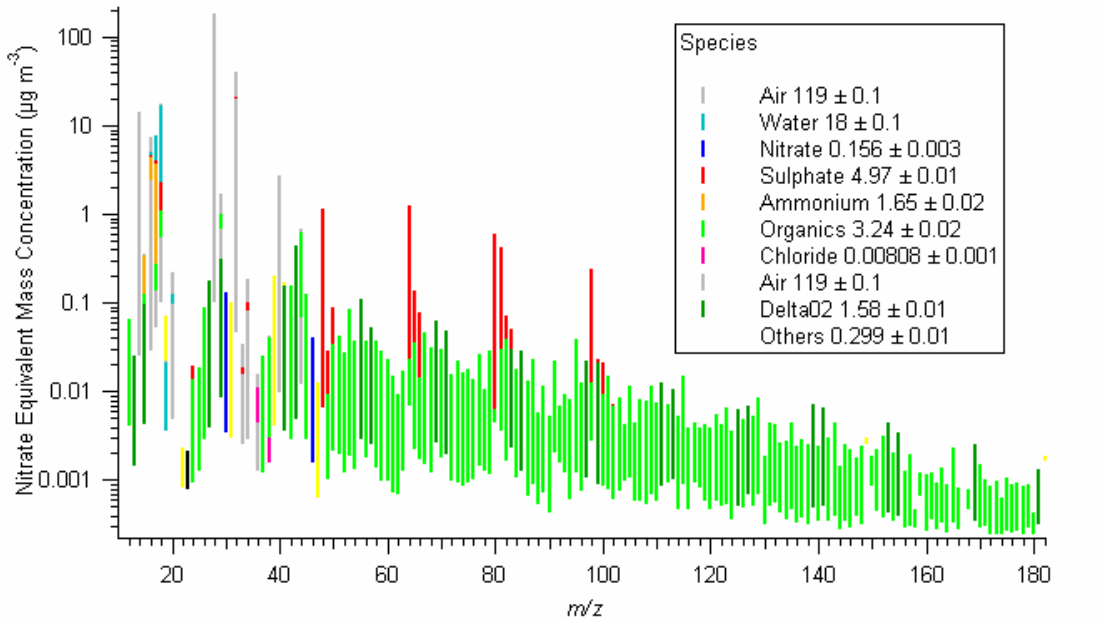

Figure 5.6: Averaged mass spectrum (20 July 1410-1645) showing dominance of sulfate (red) and organics (green). The ion series 0 and 2, indicating unsaturated hydrocarbons, are shown in dark green.

An averaged size distribution during this same period, shown in Figure 5.7, illustrates the homogeneity of the particles. All species have a mode maximum of about 450 nm and there are no smaller particles that would indicate a less well-mixed population.

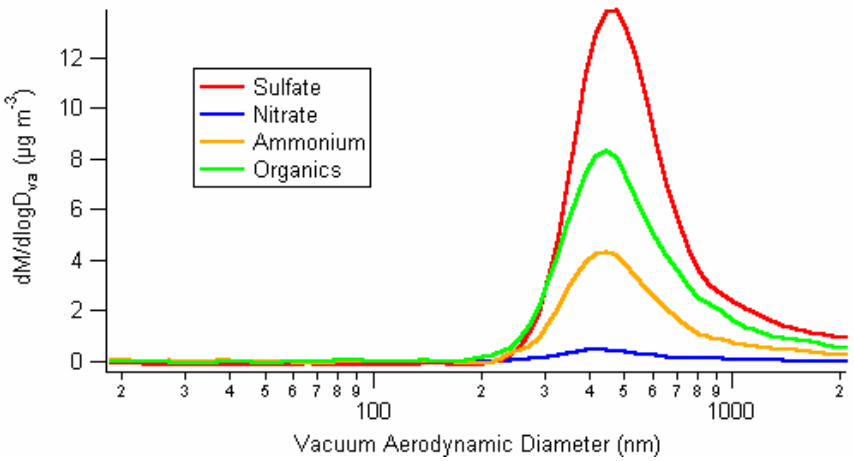

Figure 5.7: Averaged size distribution for the same period as the averaged mass spectrum in Figure 5.6 showing a mode diameter of 450 nm.

One of the more telling indicators of aged pollution is the presence of *m/z* 44, the CO_2^+ fragment. This is a general marker of oxidation. Although it is not quantitative in the sense of providing the concentration of oxidized organics, it does indicate the level of oxidation when compared to the total organics as shown in Figure 5.8, with slopes ranging from 0.03, little oxidation, to 0.15, highly oxidized. The slope from this figure for the PROPHET 2001 campaign is very tight (r = 0.91) at 0.12, which indicates a rather high oxidation level.

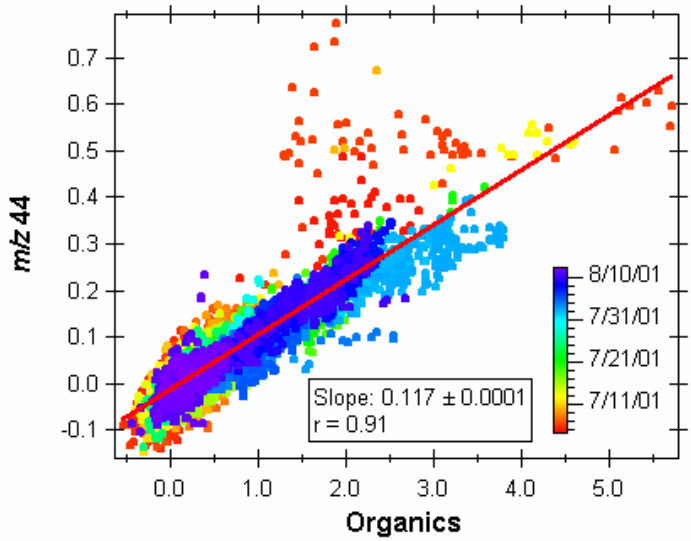

Figure 5.8: Relationship between m/z 44 and total organics indicates the level of oxidation of the bulk aerosol population.

The determination of the absolute mass loading during this event was complicated by the large gradient in temperature from outside to inside the laboratory building, approximately 10°C during the most extreme period, and the high water vapor content in the ambient air. These factors combined to cause water condensation in that portion of the sampling tubing inside the laboratory building, approximately 7.5 m. The condensation caused the particles to swell with the addition of water, giving them a larger geometric size. However, since vacuum aerodynamic diameter is a function of density as well as geometric size, the lower density of water compared to the dominant sulfate reduced this effect to a minor consideration. Of much more importance, the addition of water caused the particles to become more spherical, and thus better focused through the AMS lens system, so that more particles reached the vaporizer/ionizer and the concentration of all species increased disproportionately to the actual concentration as shown in Figure 5.9. To

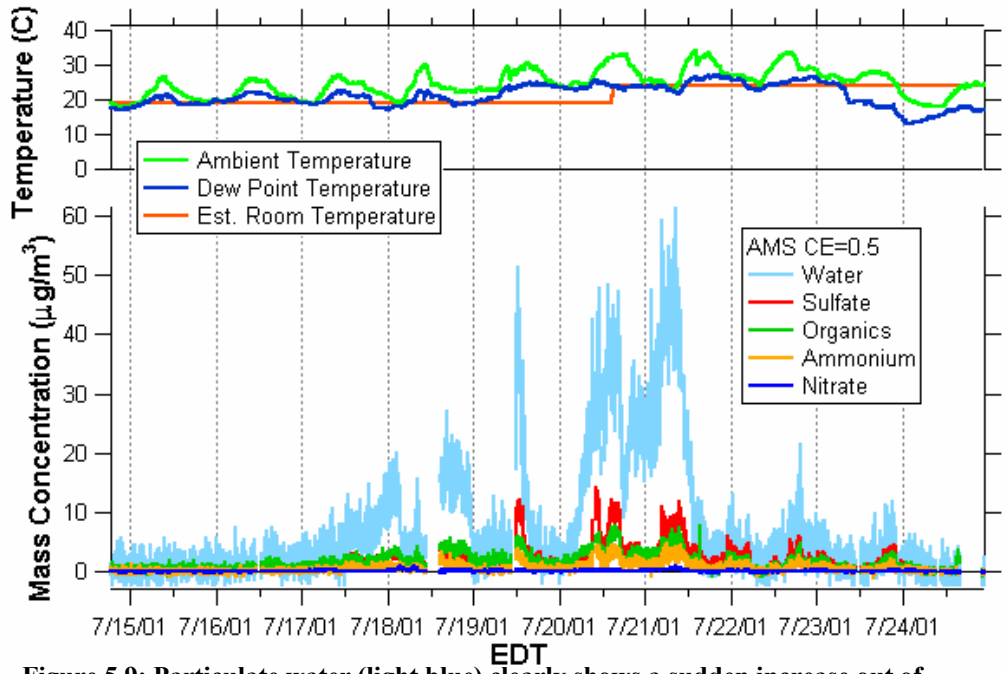

Figure 5.9: Particulate water (light blue) clearly shows a sudden increase out of proportion with the other species at the beginning of this pollution episode and the subsequent decrease on 21 July as the difference in ambient and room temperature decreased.

complicate this matter further, the concentration increase due to focusing occurred in short episodes when the dew point approached the ambient temperature (i.e., close to 100% relative humidity) and was not consistent throughout the whole period. In order to account for this, the concentration during these periods was decreased approximately proportional to the measured particulate water content and the difference between the room and ambient temperatures. It also became apparent in the middle of this episode that this was an issue, so the temperature inside the laboratory building was raised approximately 5°C and this decreased the effect for the rest of this episode and subsequent episodes, but did not completely eliminate the issue. The disparity in temperatures did not significantly affect measurements during the cleaner periods because of the much lower water content.

The last three episodes were much shorter than the first one: July 30 to midday August 2, August 5 to midday August 7, and midday August 8 to evening August 9. However, they all exhibited similar behavior; increased temperatures and dew points, O_3, CO, and NO_x; and particulate chemical composition and size.

All of these episodes are caused by air that came from the southwest or southeast and the lack of any major urban areas for hundreds of kilometers appears to have smeared out any distinctive characteristics. They all have the features of aged, well-mixed air, which is consistent given the homogeneity of the landscape it passes over.

5.4 Northerly Flow

Northerly flow was characterized by lower temperature and water vapor content and very low levels of almost all chemical species, including ozone, NO_x, CO, and aerosols. The sulfate concentration was very low, with only a few small increases related to small particle events that will be discussed in the next section. During these cleaner periods organics dominate the mass loading, although the concentrations are also low, no higher than 1 $\mu g/m^3$.

July 12 was a fairly typical northerly flow day with air traveling across mostly uninhabited land in Canada. The average total aerosol mass loading was approximately 0.5 $\mu g/m^3$, with the exception of one event in the afternoon, and the inorganic aerosol species concentrations were very low. The largest contribution to the aerosol mass on this day was organic species, perhaps biogenic in origin. In an attempt to find some distinctive marker for biogenic species, pinic acid, a $C_9H_{14}O_4$

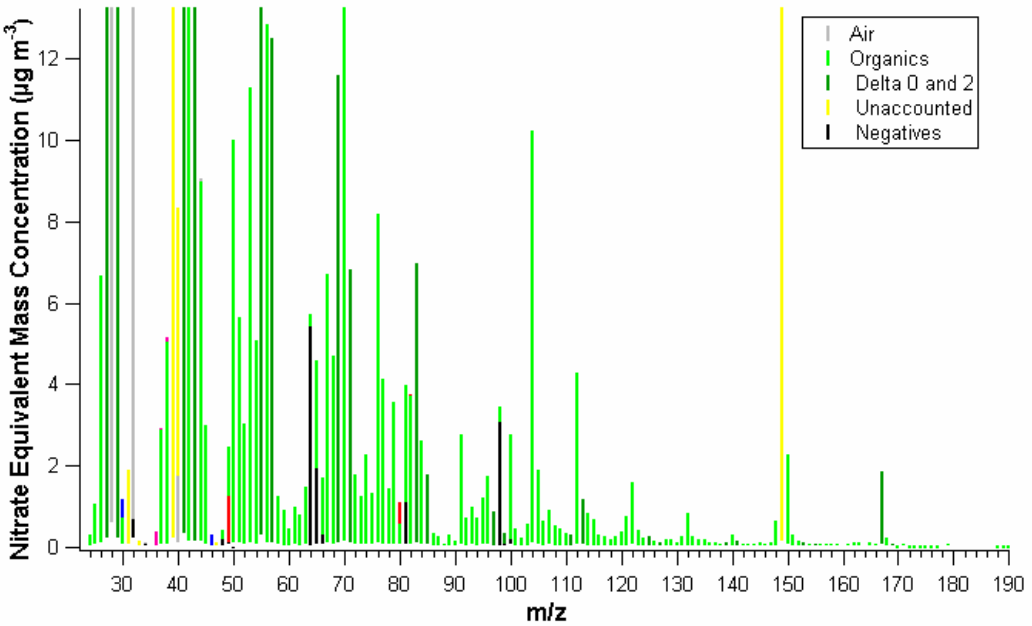

Figure 5.10: Averaged AMS mass spectrum from laboratory-generated pinic acid showing possible marker fragments.

(MW 186) dicarboxylic acid formed from the oxidation of the common terpene α-pinene by ozone, was tested with an AMS to generate a mass spectrum that could be used for comparison as shown in Figure 5.10. Distinctive markers are usually found at higher mass numbers (greater than *m/z* 60) because the most of the organic species observed in ambient air have fragments at the lower mass numbers. Some mass numbers that might be used as markers include 69, 70, 71, 76, 83, 104, 112, 149, 150, and 167. Unfortunately, dicarboxylic acids are common anthropogenic species as well, so these mass numbers would not provide conclusive identification. In addition, there are a large number of other biogenic oxidation products and these have not been tested to provide comparison mass spectra.

As averaged mass spectrum for this period (10 July 1125 to 12 July 0515 local time), shown in Figure 5.11, clearly shows very low levels of all species. Of the small mass concentrations, the organics are largest with no signal at *m/z* 44, but signals for the ion series 0 and 2. This implies that these aerosols are completely

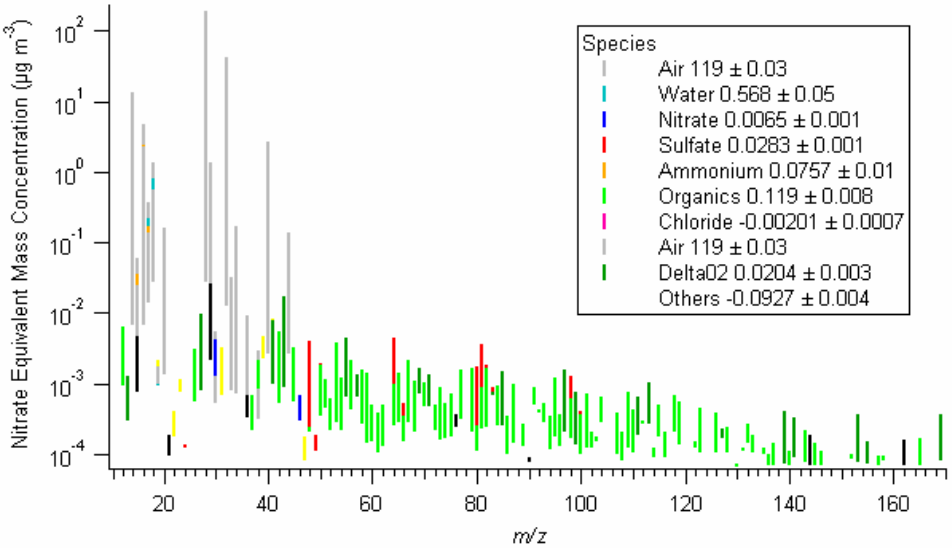

Figure 5.11: Averaged mass spectrum (10 July 1125 – 12 July 0515) showing very low concentration of aerosols.

unoxidized. The averaged size distribution shown in Figure 5.12 is consistent with the mass spectrum, showing very low levels of sulfate and nitrate, but no ammonium, and a larger concentration of organics, all at smaller sizes than those observed during the pollution episodes. The noise in this average despite the long averaging time is one more indication that the signals are very low. The ammonium is especially noisy and some of the contribution from gas-phase species is apparent, demonstrating that the ammonium calculation is not as reliable at low mass concentrations.

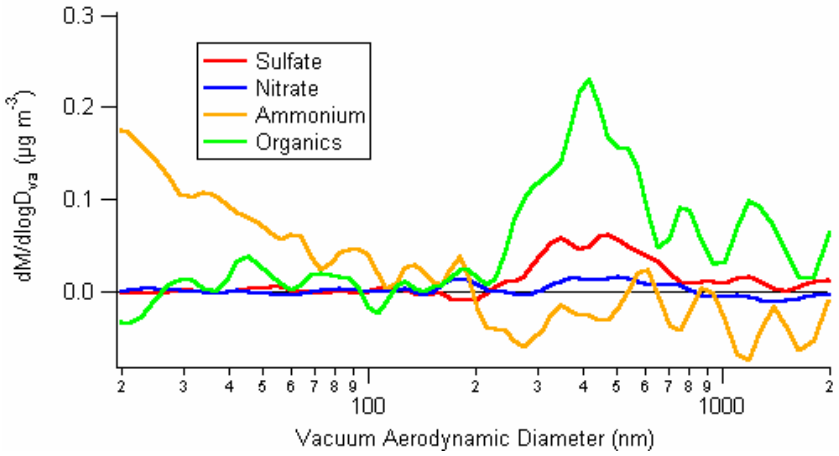

Figure 5.12: Averaged size distribution for the same period as Figure 5.11.

Another type of event observed on several occasions, 5, 6, and 12 July, during northerly flow were short periods, approximately one hour that consisted almost entirely of organics, again dominated by the ion series 0 and 2 as shown in an averaged mass spectrum in Figure 5.13. From empirical evidence at several urban locations, this pattern with pronounced ion series 0 and 2 is indicative of diesel exhaust. It is thought these events were the result of deliveries to the site. Although there was no road access to the tower during the study, the road was only about 100 meters away.

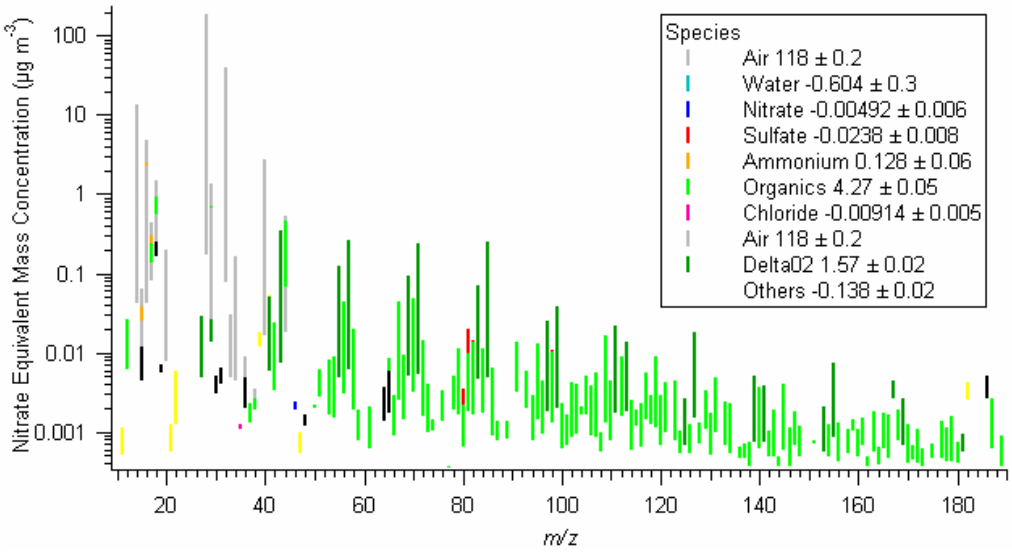

Figure 5.13: Averaged mass spectrum from organic event 12 July showing pronounced ion series 0 and 2 pattern typical of diesel exhaust.

5.5 Small Particle Events

One of the most interesting, and unexpected, results observed during the PROPHET study was the occurrence of several small particle growth events. These always occurred during the morning of days with low aerosol concentrations and can be observed in the sulfate size distribution in Figure 5.5 on 6, 7, 14, 26, 27, and 28 July. Sulfate and organics were the primary species involved in all of the events, although it is difficult to determine which of these species initiated the events. The observed growth events may have occurred subsequent to the actual formation of new particles, but instruments capable of measuring ultrafine particles (<10 nm) were not available for this study, so the actual particle formation cannot be discussed.

The most distinct growth event occurred on 26 July, beginning at about 0930 and ending approximately 1330. A very clean air mass had moved into the area the day before and the background levels of almost all the gas-phase species measured

were low on this day, with the primary exception of OH and H_2SO_2 as indicated in Table 5.1. The winds were from the northeast at approximately 3-4 m/s all day. The temperature was approximately 20°C and the relative humidity was about 60% in the morning, falling to 40% later in the day.

Table 5.1: Gas-phase concentrations of relevant species on 26 July.

Species	Concentration	Relative Amount
O_3 (M.A. Carroll, U Mich)	20 ppb	Low
NO_x (M.A. Carroll, U Mich)	300 ppt	Typical
CO (M.A. Carroll, U Mich)	100 ppb	Typical
Light hydrocarbons (V. Young, Ohio State)	None	Low
Isoprene (S. Pressley, U. Washington	1-2 ppb	Low
OH (G. Huey/D. Tanner, G. Tech)	2-3x10^6 molecules/cm^3	High
H_2SO_2 (G. Huey/D. Tanner, G. Tech)	3x10^7 molecules/cm^3	High

The back trajectories in Figure 5.14 show that the air was moving into northern Michigan from the northeast with no vertical mixing. Increasingly high levels of sulfuric acid marked this air mass on the morning of July 26. At approximately 0930 there was a sudden increase in the particle number concentration as measured by the SMPS system from approximately 900 to 5000 particles/cm^3, as illustrated in Figure 5.15. There followed a gradual increase in the volume/mass

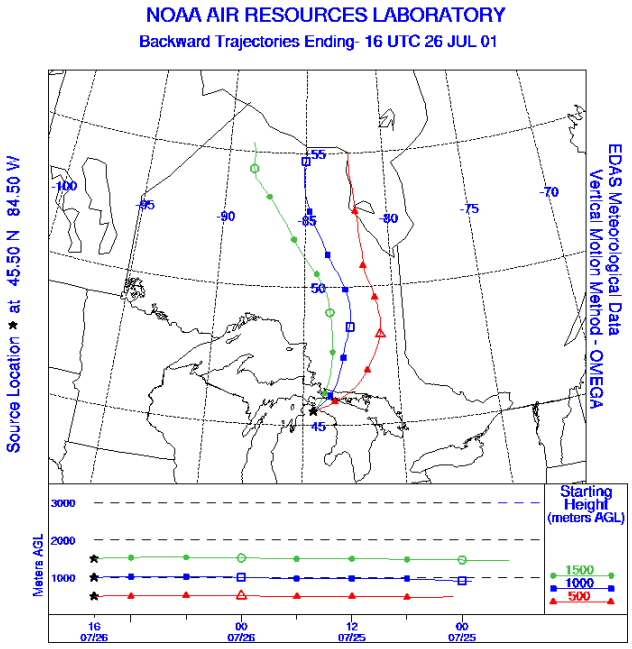

Figure 5.14: Back trajectory for 26 July generated by NOAA Air Resources Laboratory Hysplit model.

concentration of the particles, but the number concentration stabilized until 1100, when both the number and volume concentrations began increasingly rapidly until first the number and then the volume concentrations peaked just before 1200 and then began decreasing.

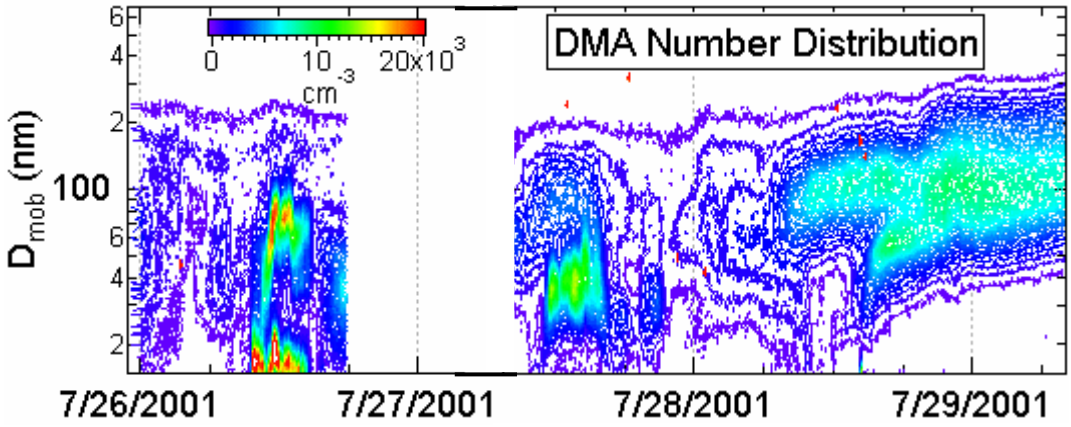

Figure 5.15: SMPS number distribution showing small particles on 26 July and slightly larger particles on 27 and 28 July.

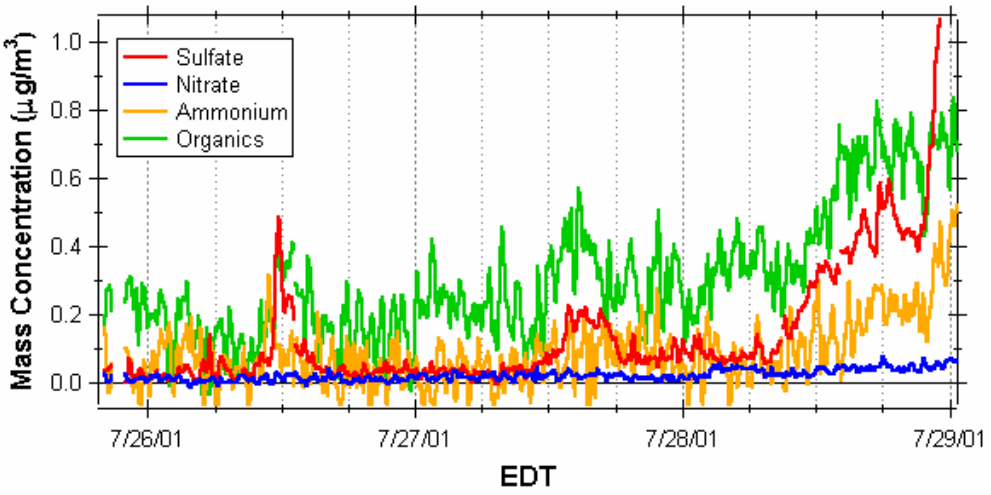

Figure 5.16: AMS mass concentrations for three small particle growth events.

During the same time period, the AMS detected a sudden increase in the particle mass just before noon as shown in Figures 5.16. Size distributions before, during, and after this event, Figure 5.17, show both a small and large mode of sulfate and organics of varying proportions. It appears that there was a small mode of

organics, starting at 50 nm, before this event, but most of the sulfate was in a larger mode of 300 nm. During the event peak the sulfate increases significantly and the primary mode shifts to a smaller size, beginning at about 40 nm. There is also some nitrate and ammonium, but not enough to neutralize the aerosols. The sulfate concentration decreases again after the peak and shifts back to a mode centered at 300 nm, but the organics remain in the small mode, which shifts even further to begin at 30 nm. Both ammonium and nitrate also decrease.

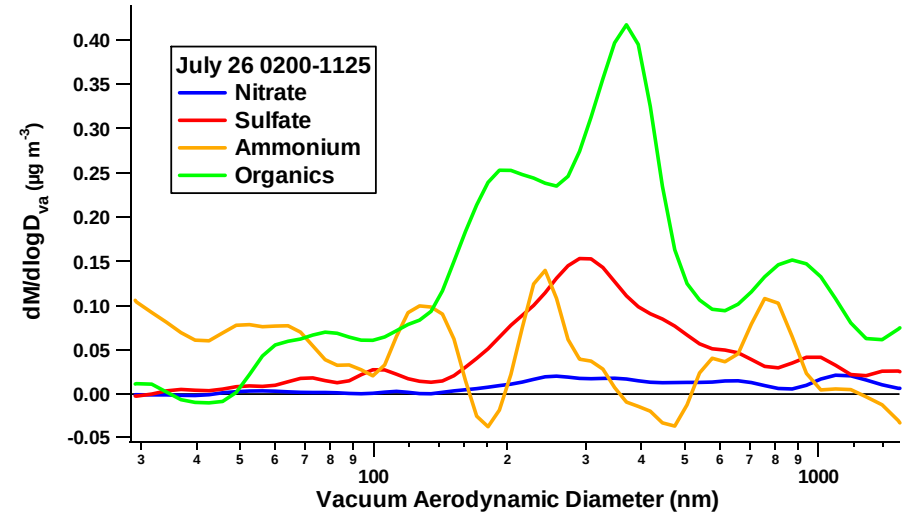

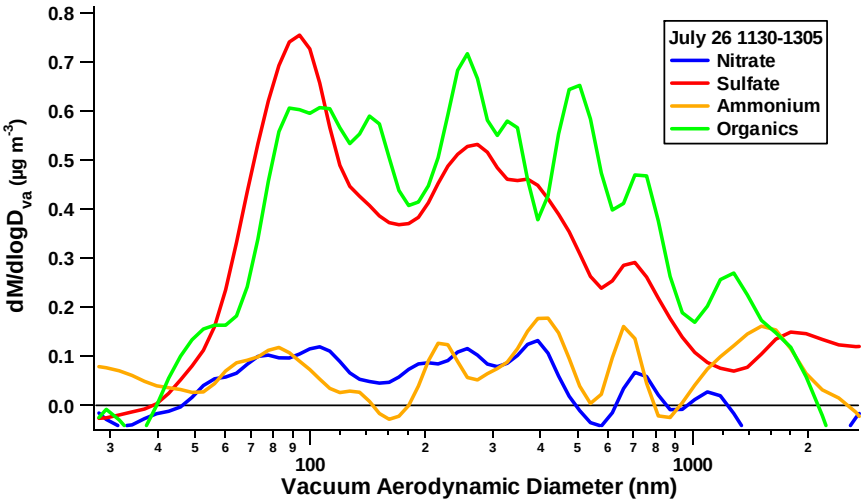

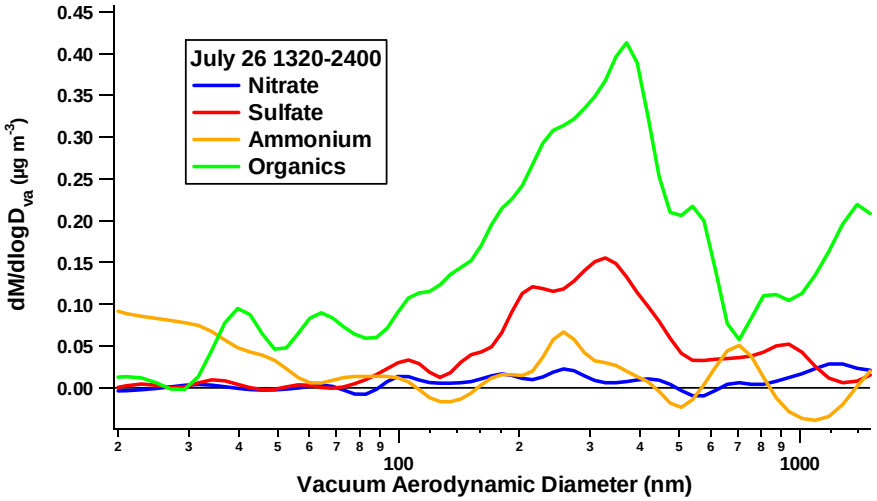

Figure 5.17: Averaged size distributions before (top), during (middle), and after (bottom) the 26 July small particle growth event.

An examination of the differences in the mass spectrum before and during this event shown in Figure 5.18 clearly illustrates the much higher sulfate levels during the peak of the mass loading. The increase in the organic mass concentration appears to be the result of increases in the signal at a few of the smaller fragments, primarily *m/z* 27, 39, 43, 53, and 55, indicating the presence of carbonyl or alkene species.

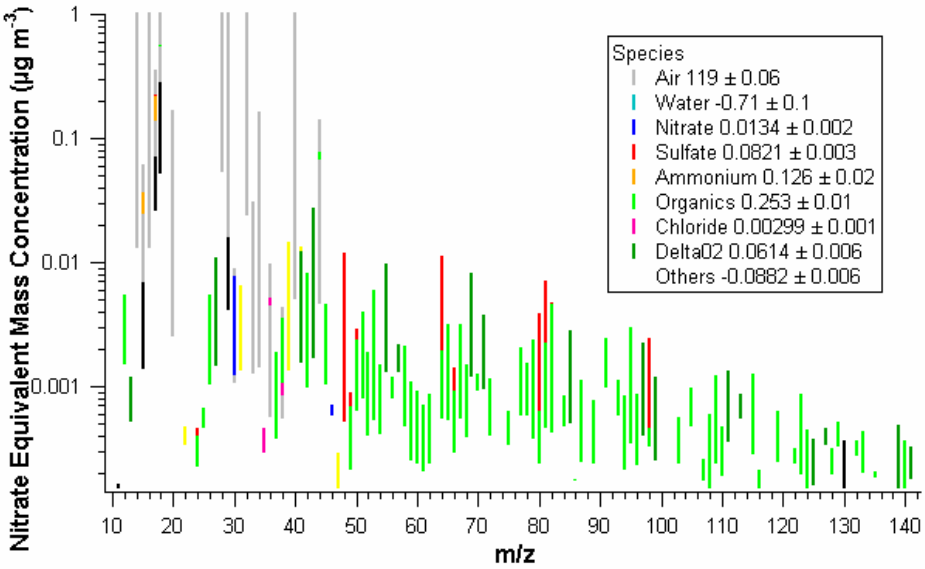

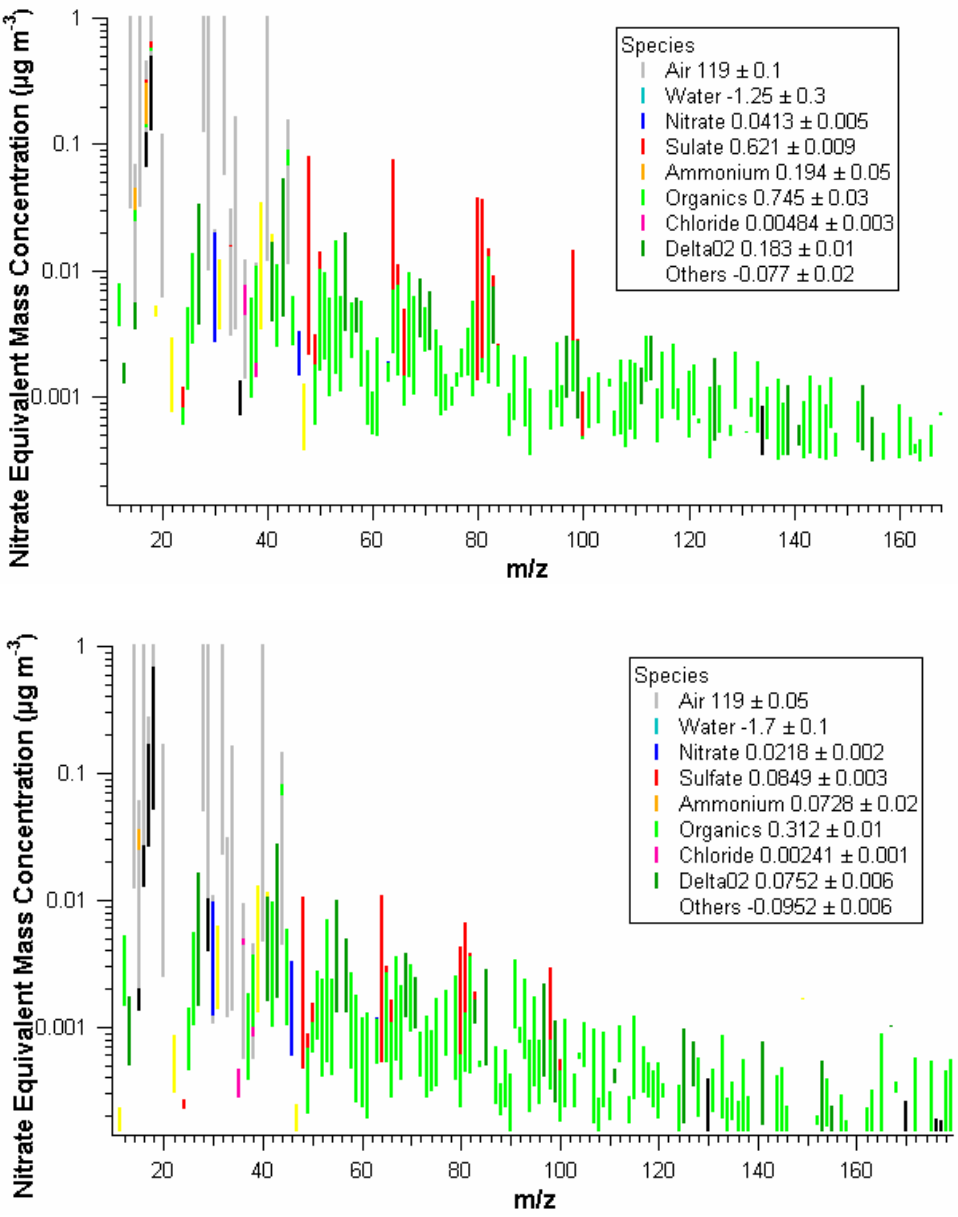

Figure 5.18: Averaged mass spectra before (top), during (middle), and after (bottom) of the growth event.

It appears that the air mass that arrived in northern Michigan on the morning of July 26 passed over the city of Sudbury in Ontario, Canada during the previous night. Sudbury is the site of several nickel smelting facilities, which produce large amounts of sulfur dioxide in the process of purifying the nickel, approximately 75

tons of sulfur dioxide each day according to Falconbridge, Inc., one of the smelting operations. [Falconbridge website, 2001] When the air arrived over northern Michigan in the morning of July 26 and OH levels began to rise, the sulfur dioxide was converted to sulfuric acid. Since the background aerosol level was very low as a result of the clean air transported from Canada, the sulfuric acid began form new particles rather than condensing onto pre-existing particles.

The other growth events were similar in nature to that on 26 July, but much less intense. They started with larger particles and smaller concentrations. Also, few of these events resulted in any actual increase in particles – they grew and then disappeared. It may be that these were extremely localized events and the newly grown particles were quickly blown away.

5.6 Gradient Measurements

Although measuring the gradients was one of the main objectives for this study, the system was not fully implemented to acquire data until 1 August. Figure 5.19 shows the results from these measurements. It was difficult to detect significant variations between the three heights, even after a three hour running averages was applied. However, there appears to be an increase in organics at midnight of 1 August in the lowest inlet and an increase in nitrates from the same inlet approximately 3 hours later. This may be some kind of emission from the soil. There also appears to be some variation on 7 and 8 August, particularly in the nitrate at 0200 from the top of tower inlet. On 9 August at approximately 1700, there is a decrease in the top of tower inlet compared to the other two in sulfate. There are

other smaller variations, but it is difficult to state conclusively that these are significant given the inherent variations in the data.

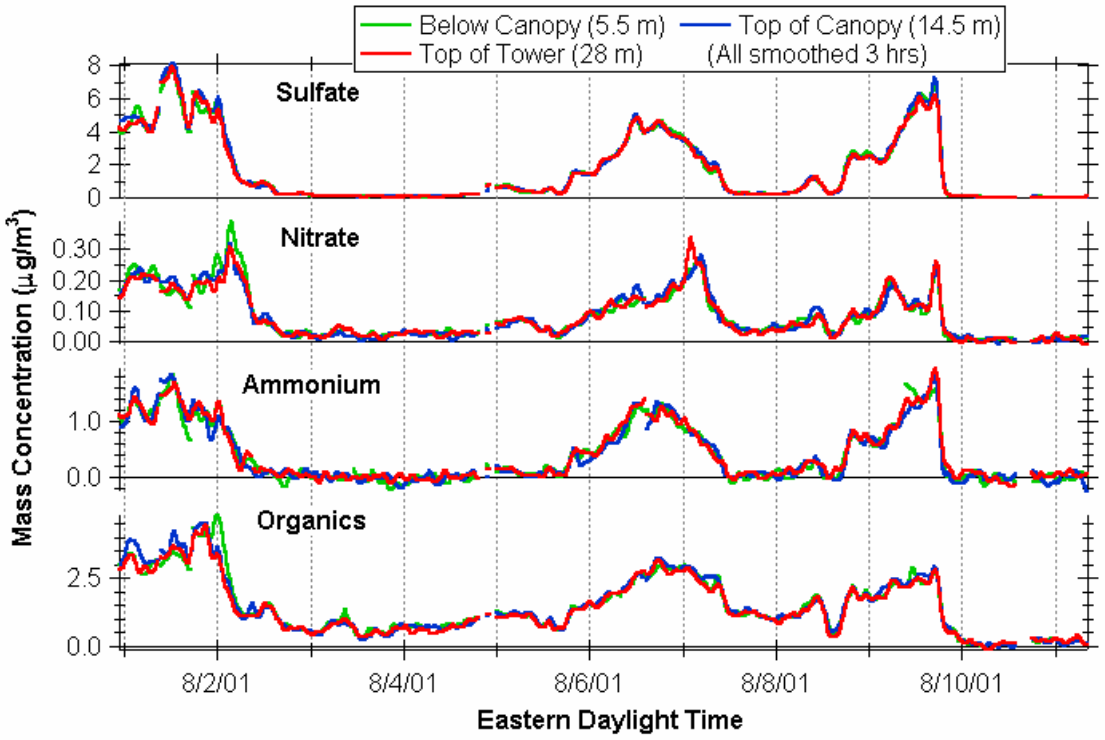

Figure 5.19: Gradient measurements at PROPHET. A running average of 3 hours was applied.

5.7 Conclusions

The PROPHET 2001 field campaign was the first study in a remote location where AMS measurements were made. There was little influence on the aerosol population from the local environment, so transported air masses caused most of the aerosol loading. Due to the distance of the site from any significant urban centers, the aerosols were well-aged by the time they arrived at the site as indicated by the consistent ratio of organics to sulfate, the oxidation level 0.12, and the accumulation mode of approximately 400 nm of all species.

One of the most interesting aspects of this study was the appearance of several small particle events. Although we were unable to measure the ultrafine particles that defined the nucleation events, we did measure their growth and detected only sulfate and organic in the smallest mode of 30-40 nm. There was some ammonium present during this event, but not enough to fully neutralize the sulfate and nitrate.

In addition to the first AMS measurements at a remote site, this was also one of the first successful field campaigns where an AMS was deployed. As a result, there were several issues that were not apparent before this study, including the importance of a properly aligned lens, correct evaluation of sampling line losses, and, most importantly, the impact of temperature and humidity gradients on particle transmission.

Following the problems with the temperature/humidity gradients in this study, several versions of temperature and/or humidity control on the inlet just upstream of the critical orifice have been implemented that clearly show the increased particle transmission at low temperature or high humidities (Allan, unpublished results). However, controlling the temperature and/or humidity raises the additional issue of possible alteration of the particles. At a minimum, the temperature should be measured carefully both outside and inside whatever building or facility in which the aerosol measurements are being made. These measurements allow determination of those time periods when special attention should be given to the aerosol measurements so that any changes due to variations of water can be accounted for. In addition, the widespread use of the beam width probe to quantitatively measure the focusing through the critical orifice and lens was implemented to address this issue.

CHAPTER 6: CELTIC Field Campaign

The **C**hemical **E**mission, **L**oss, **T**ransformation and **I**nteractions within **C**anopies (CELTIC) study took place during July 2003. This study was designed to improve the ability to predict regional air quality and climate through a quantitative understanding of trace gases and aerosols between the atmosphere and vegetation canopies [CELTIC website, 2004].

The main objectives for the aerosol measurements were similar to those at PROPHET: to gain an understanding of the bulk aerosol population, study the effect of transported aerosols on local conditions, and determine what, if any, effect biogenic aerosols may have and examine the interaction of aerosols with the forest canopy.

6.1 Site Description

CELTIC was based at the Forest-Atmosphere Carbon Transfer and Storage (FACTS-I) facility located in the Blackwood Division of Duke Forest (35° 58' 41.430" N, 79° 05' 39.087" W), near Durham, North Carolina (Figure 6.1). FACTS-I consists of six free-air CO_2 enrichment (FACE) rings, three of which provide elevated atmospheric CO_2 concentrations, and three are ambient control rings. The purpose of this system is to permit the experimental exposure of tall vegetation, such as stands of forest trees, and a wide range of forest stand and ecosystem processes to elevated atmospheric CO_2 concentrations without enclosures that alter tree microenvironment.

Figure 6.1: CELTIC site and surrounding area. Created by Microsoft Streets & Trips.

The forest in the immediate study area is composed primarily of loblolly, shortleaf and Virginia pine, established after clear cutting and burning in 1983. In addition to the coniferous trees, sweetgum, elm, red maple, dogwood, and oak-hickory species are also common. [FACTS website] These types of trees emit both isoprene and terpenes, and are therefore more likely to produce condensable material than the forests at the PROPHET site.

6.2 Measurements Overview

There were two AMSs involved in this study. As described earlier, the CIRES AMS (J. Jimenez and A. Huffman, CIRES, University of Colorado) was primarily focused on making eddy flux covariance measurements of a small number of mass fragments above the forest canopy. However, that instrument was operated in a mode that alternated between the more common MS and TOF modes and the newly developed fast Jump MS mode for the fluxes every 30 minutes, so some of this data was used to fill in data gaps caused by instrument issues of the AMS measuring concentrations at the beginning of the study.

The concentration measurements were split into two types: the profile measurement as performed in the PROPHET study from the beginning to 19 July late afternoon and measurements to determine the particle beam width within the instrument 19 to 23 July. The results from these separate experiments will be discussed in detail later; meanwhile these measurements have been combined to provide a complete view of the entire study.

The combined aerosol mass loading is shown in Figure 5.2, including the CIRES results from 10-15 July. The wind direction at the site as measured by the Davis weather system is also included. The wind is predominantly from the southwest or west, with short periods of airflow from the northwest. Figure 5.3 shows other meteorological parameters as well as NO_x and O_3 concentrations. The temperature typically reaches 25-30°C during the day and falls to 18-21°C at night. The dew point temperature is also high, causing 100% relative humidity every night and 60-70% relative humidity during most days. The ozone generally reached

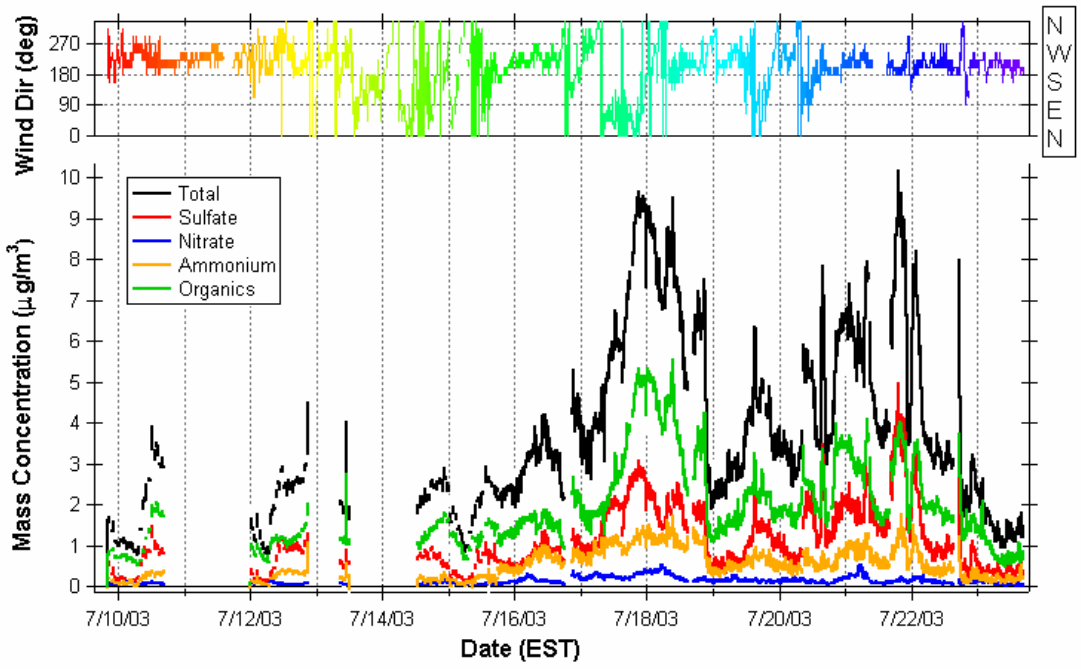

Figure 6.2: Wind direction (top) and AMS mass concentrations of major species (bottom) for entire CELTIC field campaign.

approximately 50 ppbv in late morning or early afternoon and the NO_x usually varied between two and five ppbv with the notable exceptions of 14, 15, 16, 17, and 19 July. The strong diurnal pattern observed in the gas-phase measurements clearly shows that the air is stagnant every night after the daytime boundary layer collapses.

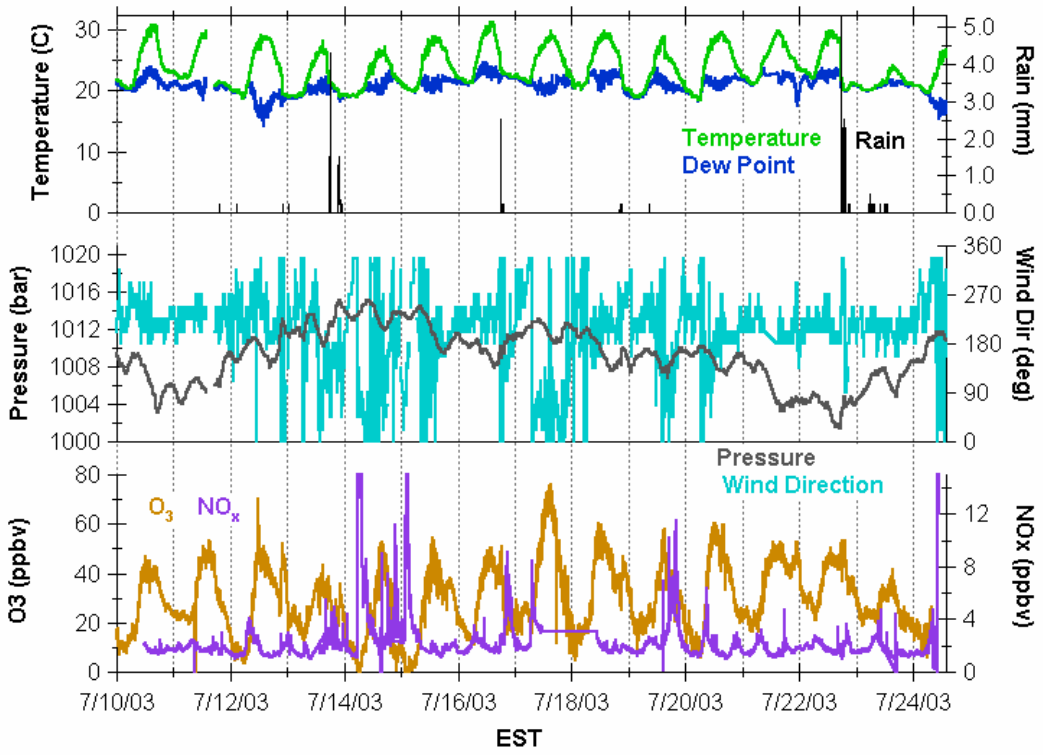

Figure 6.3: Meteorological conditions (Davis weather system) and gas-phase behavior.

It is difficult to determine if any of these parameters had a direct effect on the aerosol concentrations. However, there is clearly a change in the air mass at approximately 0900 17 July as seen in the size distribution plots shown in Figure 6.4. Back trajectories, Figure 6.5, show that the air was coming from the west and southwest prior to this time, but changes to the northwest on 17 July. Prior to this date, the size mode for all species was fairly narrow and large, peaking at approximately 600 nm for most species, slightly larger at 700 nm for sulfate, indicating that there were few fresh particles, as would be implied by smaller particle sizes. For the next day and a half, the mode is much broader, extending from below 200 nm to 600 nm, and the concentrations reach their highest continuous values of the

study until rain late on 18 July removes the accumulated aerosol population. The highest ozone concentration of approximately 80 ppbv also marked 17 July.

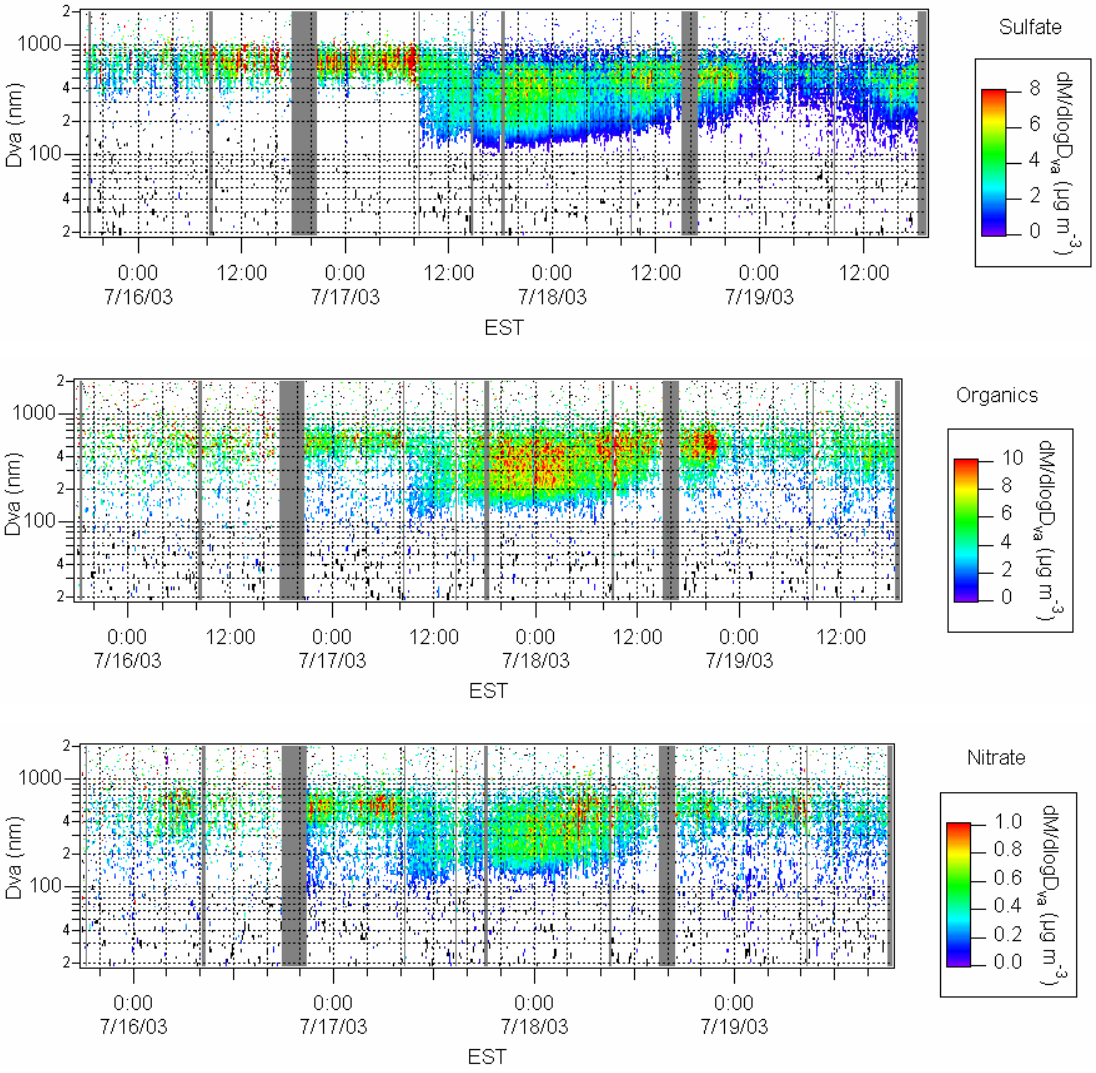

Figure 6.4: Size distributions showing change in air mass on 17 July. Small particles are also visible in the nitrate size distributions.

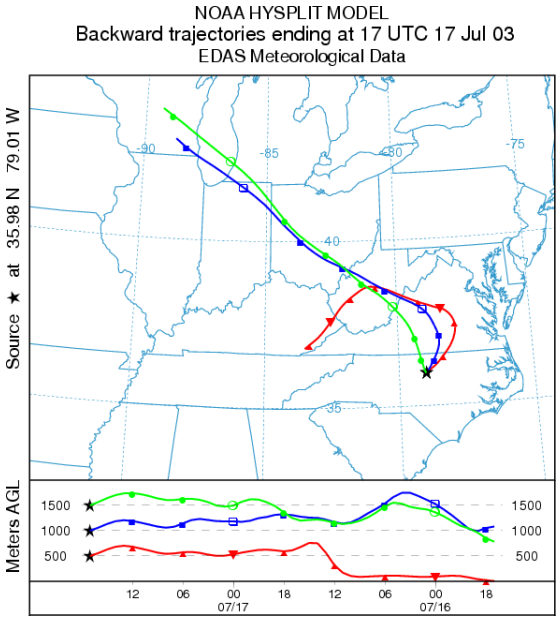

Figure 6.5: Back trajectory for 17 July at the beginning of more polluted period. Generated by NOAA Air Resources Laboratory Hysplit model.

Compositionally, the organic aerosols are the dominant species with sulfate the next most abundant. The only exception to this occurs late on 21 July when the sulfate briefly exceeds the organics. Figure 6.6 shows the relationship between these species. The overall ratio is approximately one, but there is an offset in the organic concentration of 0.8. There are two notable exceptions to this ratio. The period denoted by the size change described above, 17-18 July, is also marked by a change in the organic to sulfate ratio to approximately 2. An average mass spectrum from this period, Figure 6.7, primarily displays the signature of saturated hydrocarbons as identified with ion series 0 and 2 [McLafferty and Turecek, 1993] and some contribution from oxygenated species as indicated by the size of the *m/z* 44 (CO_2^+ ion). There may also be some aromatic species, ion series –5 (*m/z* 92 and 106), but these are very small signals.

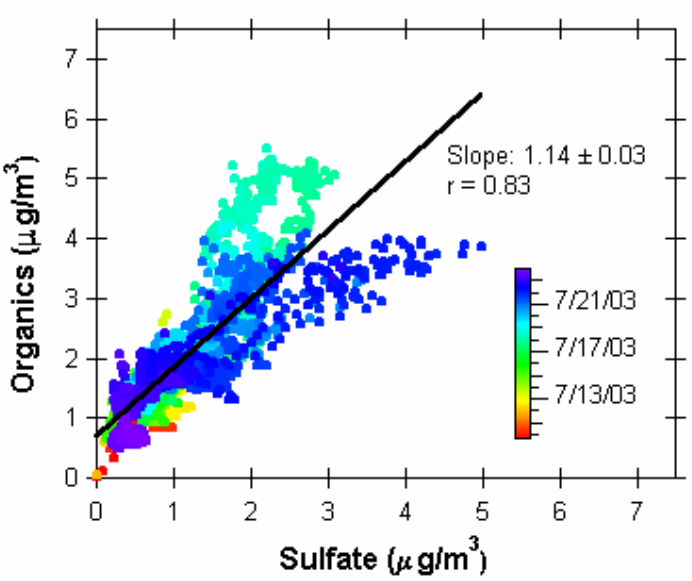

Figure 6.6: Relationship between organics and sulfate for the entire study.

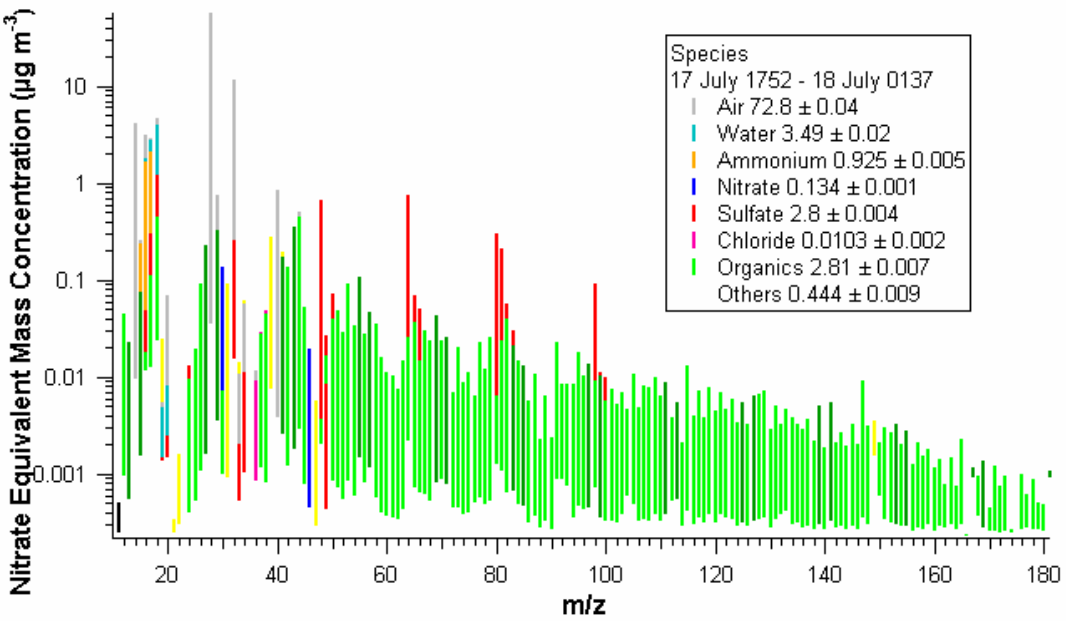

Figure 6.7: Averaged mass spectrum for 17-18 July.

The second exception occurs late on 21 and early on 22 July where the sulfate briefly exceeds the organic concentration. The air was coming from the southwest during this period and there was an atypical ozone increase at approximately 2300 on 21 July. Figure 6.8 shows the averaged mass spectrum for this period where the sulfate and organics have about the same concentration. The ion series 0 and 2 are not particularly prominent in this mass spectrum and the *m/z* 44 signal is larger than the *m/z* 43 signal, so the organics probably include a mixture of species from several categories, not just unsaturated hydrocarbons.

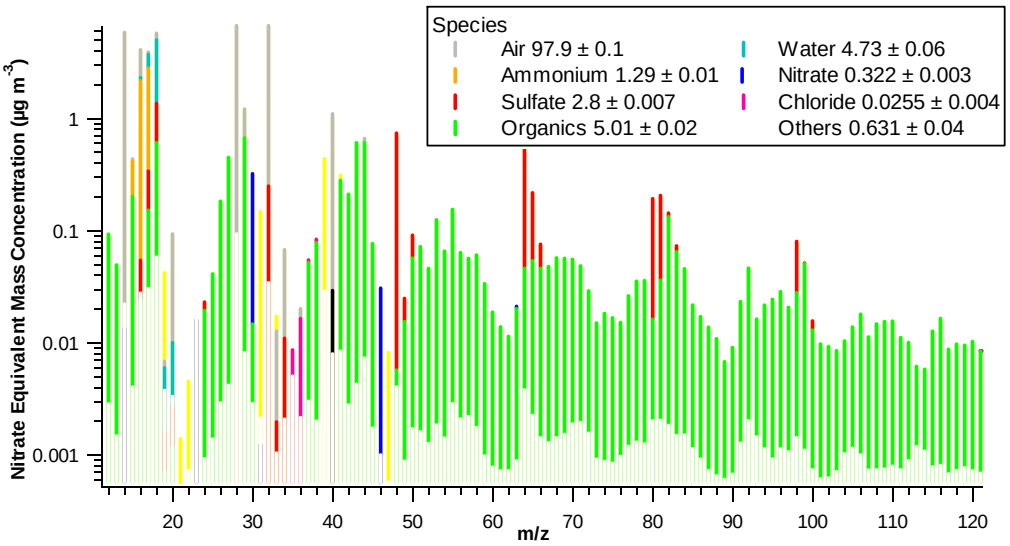

Figure 6.8: Averaged mass spectrum for 21/22 July.

The size distribution for this period shows a broad, consistent mode centered at approximately 550 nm, indicating a well-mixed aerosol population with few fresh particles.

The ratio of ammonium to nitrate and sulfate is key to determining the level of neutralization of the particles, as discussed previously. The measured and predicted ammonium, shown in Figure 6.9, establishes that the bulk particle mass is often close to neutralized, but brief periods on 20 and 21 July (1700-1810 and 2000-2340

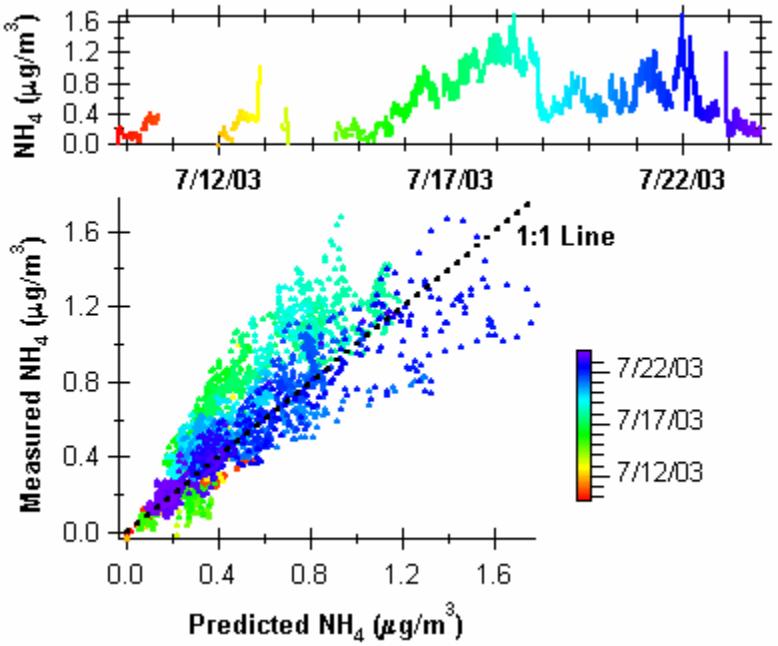

Figure 6.9: Relationship between measured ammonium and that predicted based on the concentration of nitrate, sulfate, and chloride.

respectively) exhibit under-neutralization. In contrast, a substantial period, 15 July 1800 to 18 July 2330, reveals more ammonium than can be accounted for by the measured nitrate and sulfate concentrations. It is not yet understood where this excess ammonium is coming from. One possibility is the presence of organic acids, but there is no definitive evidence for this.

As described earlier, the AMS cannot generally identify specific organic species, however it can provide information about the level of oxidation. Since *m/z* 44 (the CO_2^+ ion) is the only mass fragment without the possibility of interferences from other ions, it is used as the marker for oxidation. Therefore, a plot of *m/z* 44 vs total organics, as shown in Figure 6.10, provides a qualitative estimate of oxidation. AMS data from field studies around the world has provided a reasonable empirical formula for determining the level of oxidation: a ratio of 0.03 indicates very little

oxidation and a ratio of 0.15 indicates highly oxidized aerosols. A ratio of 0.095, as determined for this study, is therefore a middle value, signifying a mixture of types.

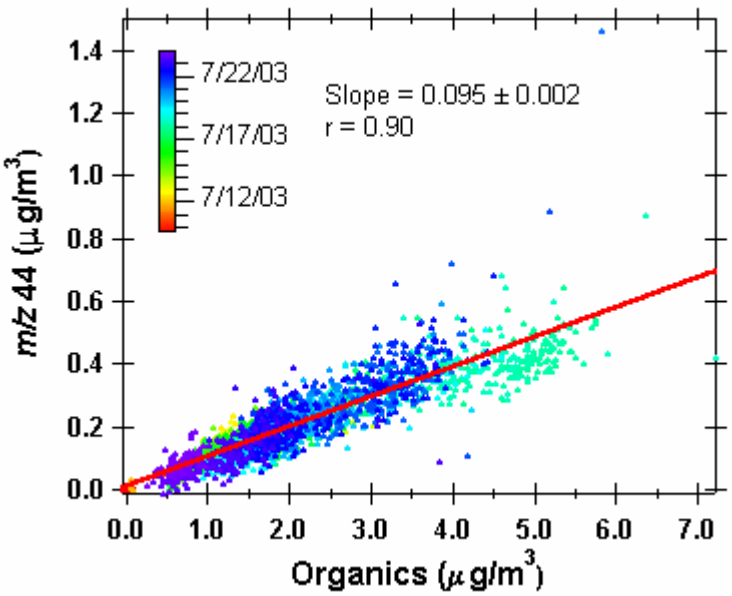

Figure 6.10: Relationship between m/z 44 and total organics gives an estimate of an above average level of oxidation.

A new instrument was tested during this study, the Classical Scattering Aerosol Spectrometer Probe (CSASP-200-S) developed by Particle Metrics, Inc. This instrument sizes particles using optical scattering from a classical He-Ne 632.8 nm laser. The CSASP can detect particles 0.2 to 20 μm in diameter, so it complements the AMS by providing data on coarse mode particles and larger growth events.

Unfortunately, the CSASP was only in operation for the last four days of the study, but it did confirm the accumulation mode of 300-500 nm and shows growth to 4 μm early on 21 July and late on 22 July as shown in Figure 6.11. There were a few

hundred particles in the supermicron size bins during the higher concentration periods, but very few particles greater than 10 μm in diameter.

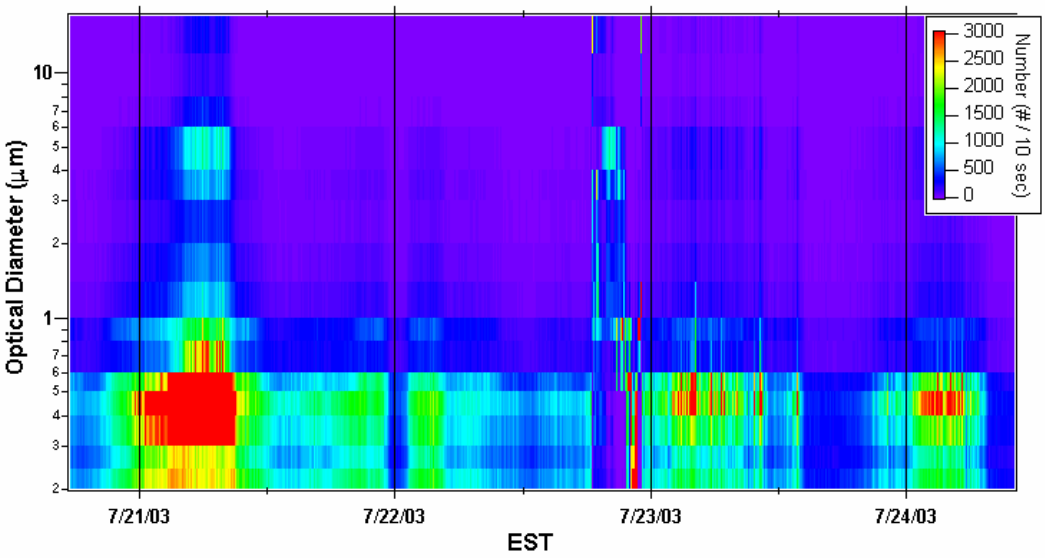

Figure 6.11: CSASP data for last 4 days of the study showing larger particles

6.3 Profile Experiment

One of the goals of this study was to determine the level of interaction of the aerosols with the forest. The profile, or gradient, measurements are one method of measuring the emission or deposition of aerosols from the forest canopy. The measurement of fluxes, as performed by the CIRES group, is another means of obtaining this information.

As described in section 4.1, the sampling inlets were placed at three heights on the tower to provide a variety of sampling environments. The inlet below the canopy was placed to measure interactions with the ground/soil and any human influences. The inlet at the top of the canopy was designed to measure the atmosphere/biosphere interface and the inlet at the top of the tower was intended to

measure the regional contribution. Data for this experiment was collected for approximately four days.

The data for each inlet was separated out and a running mean of two hours was applied to eliminate small-scale variations. The results are summarized in Figure 6.12 for each species and inlet. It does not appear that there are large differences for most of the species. The measurements from the below canopy and top of canopy inlets are especially similar. However, it appears that there is a regular deviation in the nitrate concentration in the early morning, where the two canopy inlets detect larger concentrations than the top of the tower inlet. On three of the four days the anomaly occurs approximately 0350 to 0730 with a peak at about 0530, but on 19 July it occurs at 0610 to 0915 with the peak at 0745.

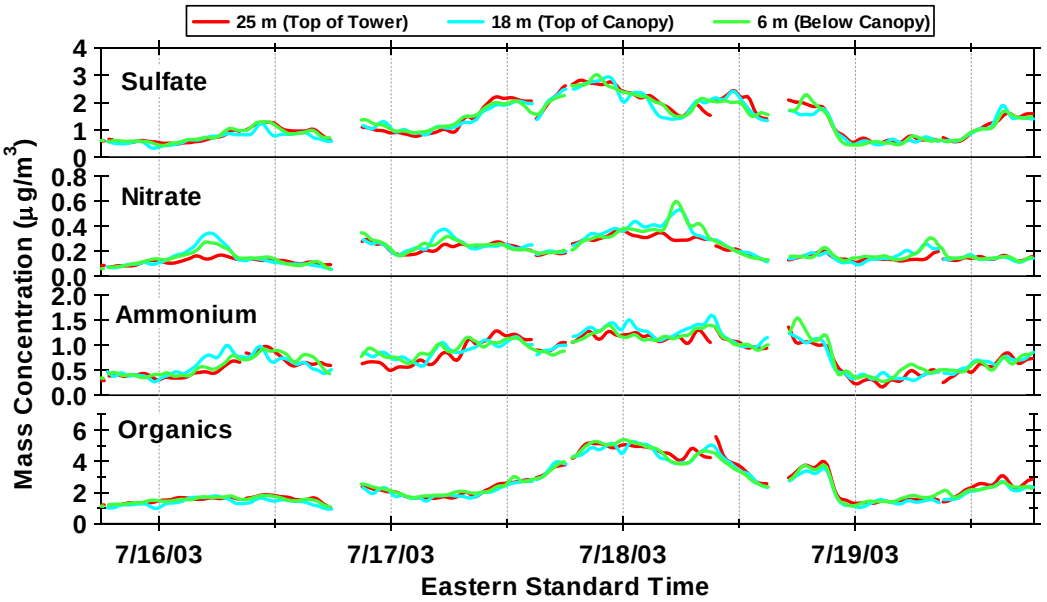

Figure 6.12: Results from gradient measurements for the main species. Running average of 2 hours applied to decrease small scale variability.

The cause of this variance is not yet clear. It could be caused by the release or formation of HONO within the canopy or some other nighttime nitrate chemistry. It may also be the result of release of NOx from the soil, since there is a peak slightly

after the particulate nitrate gradient. Since the majority of these events occur before sunlight, it seems unlikely that the volatility of ammonium nitrate is an issue. However, the air at this time was also saturated, as shown in Figure 6.3, which may have had some effect.

There do not appear to be any other significant discrepancies between the inlets. There is some variability in the ammonium measurements, but this is most likely due to noise in the data, rather than real gradients in concentration. Given the lack of sources for sulfate compounds in the forest, there are no notable differences in the sulfate concentrations as expected. However, variability in the organic concentrations would be expected given the many species produced by the forest, but, with the possible exception of the morning of 18 July, do not emerge.

6.4 Beam Width Experiment

A persistent problem with AMS data is not being able to determine the collection efficiency of the instrument, i.e., how many of the particles that enter the instrument actually reach the vaporizer and are detected. Without information regarding this parameter, it is impossible to ascertain how representative the AMS measurements are. The importance of this issue was first realized during the PROPHET campaign as described in Chapter 5, where different air masses brought either dry or moist air and the lack of other aerosol measurements made it difficult to determine the focusing efficiency.

The beam width probe was described in detail in Chapter 2, but to review briefly, it consists of a thin wire, 0.5 mm diameter in this case, positioned on the

upstream side of the detection chamber entrance aperture and controlled by a servo motor that moves the wire to preset positions in front of the entrance. Five wire positions were used for this experiment: two at the edge of the vaporizer, two halfway between the center and edge of the vaporizer and one at the center of the vaporizer. These positions were chosen to provide a compromise between adequate coverage of the vaporizer and avoiding complication by not using additional wire positions that would provide more detailed information on the exact beam shape. The program controlling the servo motor (J. Jayne, ARI) was set to alternate between an edge and non-edge position so that the "real" data would not be lost and the two positions could be easily compared to determine the level of attenuation. Since the non-wire data was set to save every five minutes, the wire data was set to save every 2.5 minutes so that the edge, or "real" data would also be available on a five-minute time scale.

Although all three inlets could have been used during this period, it was decided that could have induced a level of complexity inappropriate for the first use of this technique. Therefore, only the inlet at the top of the tower was used for this experiment.

The results in Figure 6.13 clearly show that the particle beam was well focused for the period measured. Comparison of the wire measurements showing the attenuation at each position and the data showing only the edge positions clearly show that the attenuation at the center position is the largest by approximately 30% and the middle position attenuation is much lower. This clearly confirms that the beam is well focused and that the collection efficiency should be set to one for the

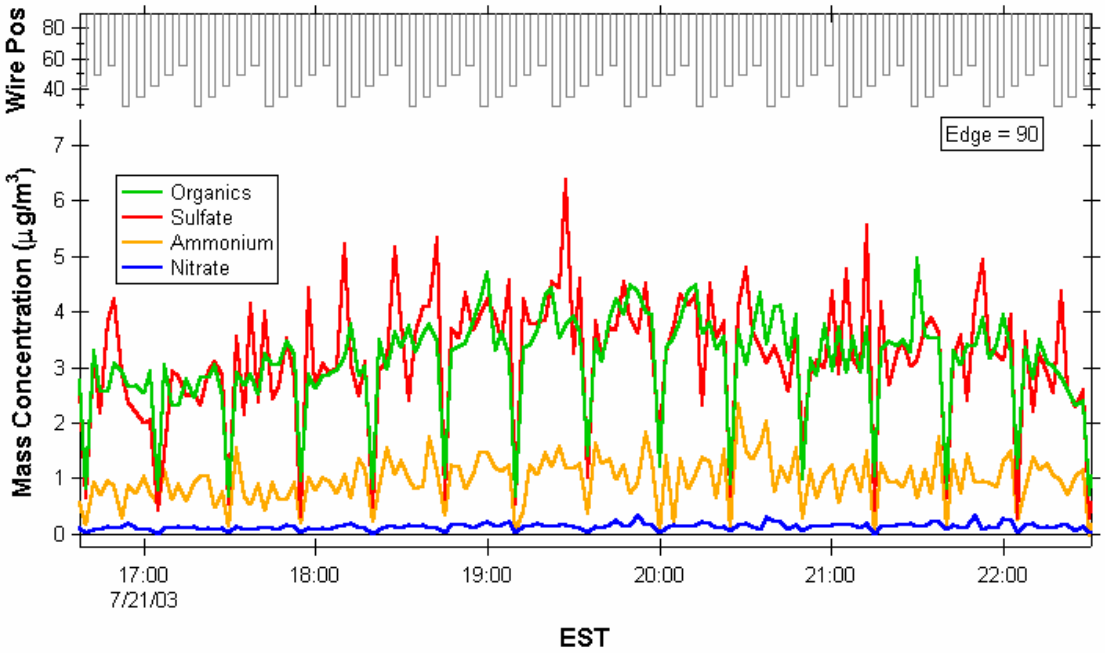

Figure 6.13: Beam width results showing sharp attenuation when the wire blocked the center of the beam, indicating a well-focused particle beam.

whole study since the humidity level was high for the whole study and there was always measurable particulate water.

6.5 Events

There were several interesting events during this study. One of the most intriguing was the appearance of several particle growth events during the evening or night where nitrate is involved. The AMS cannot measure ultrafine particles that are representative of particle formation and initial growth, but there were two SMPS systems, one nano (5-63 nm) and one long (20-550 nm), that were capable of detecting these events and comparison with AMS data at these times gives compositional information on the growth. Figure 6.14 shows the SMPS data for the whole study as measured and compiled by Craig Stroud and Sreela Nandi (NCAR,

Boulder, CO). This data shows particle growth in the morning on 11, 12, 13, 14, 17, and 20 July and in the late afternoon or evening on 13, 14, and 19 July.

The event on the morning of 17 July is different from those observed during the PROPHET study. The organics and nitrate appear to be the primary species involved in the growth, as shown in Figure 6.14, with the small mode in both species

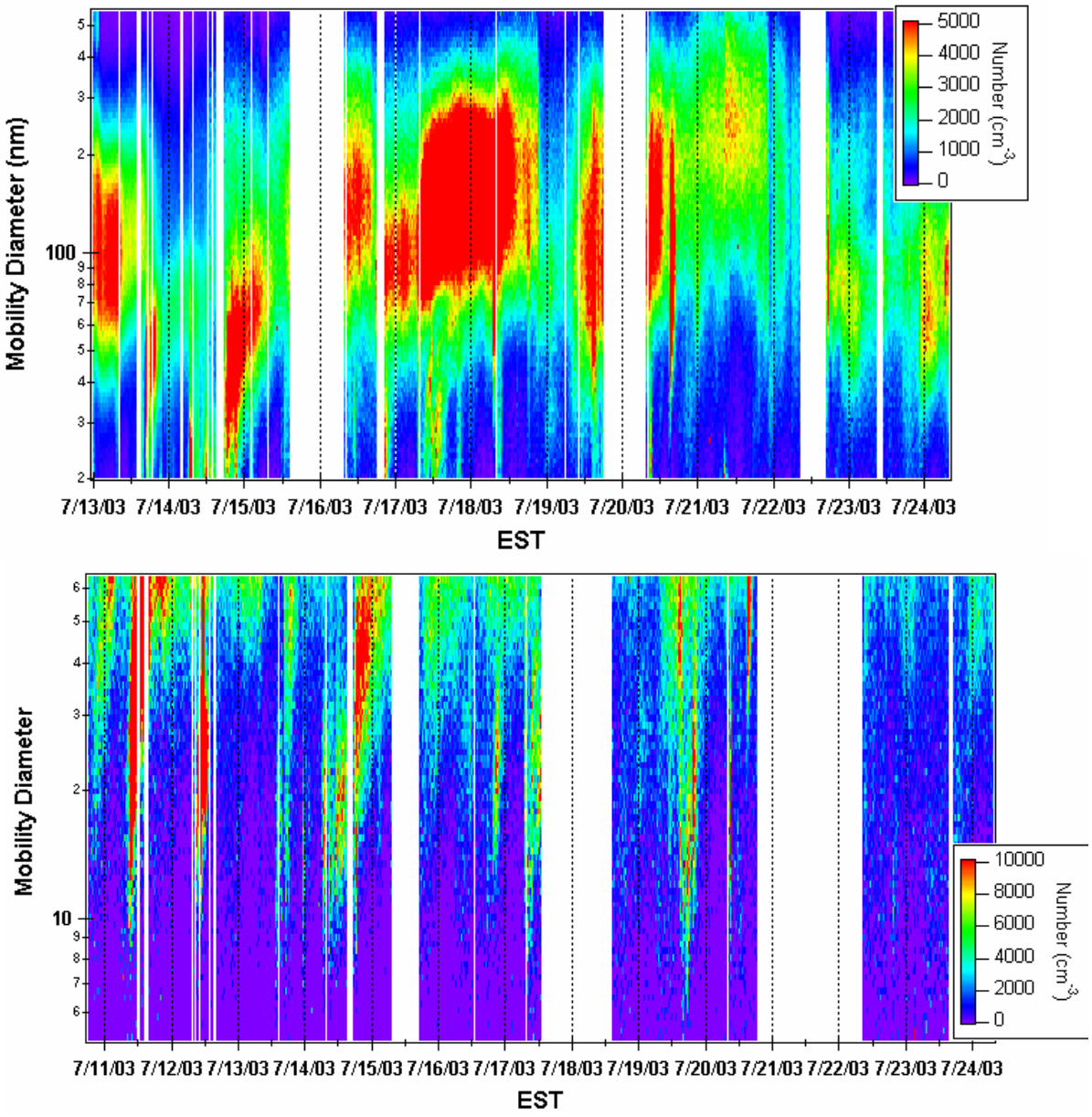

Figure 6.14: Long (top) and nano (bottom) SMPS number distributions. Craig Stroud and Sreela Nandi, NCAR, Boulder, CO.

beginning at about 70 nm and peaking at approximately 150 nm and a larger mode centered at approximately 550 nm. The sulfate exhibited different behavior, with a single mode peaking at approximately 700 nm and a small size tail extending down to 130 nm. The ammonium appears to share characteristics with both the nitrate and sulfate, indicating that they are at least partially neutralized.

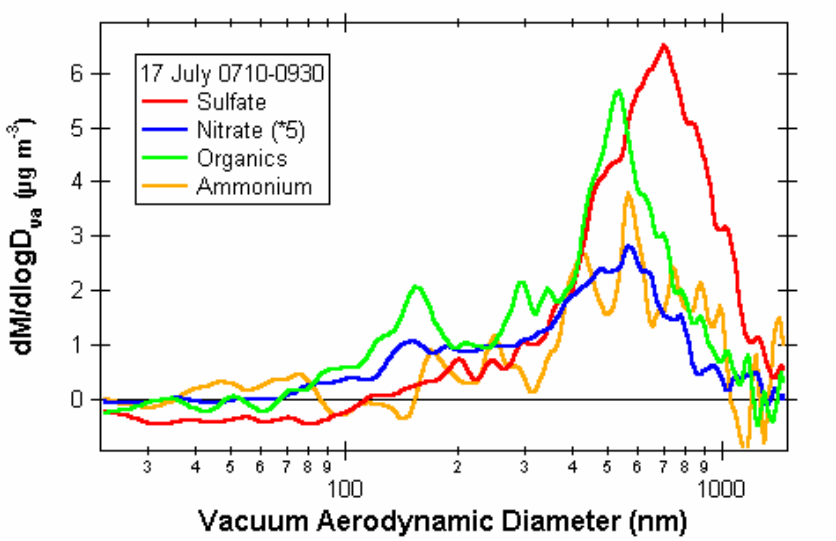

Figure 6.15: Averaged size distribution for the growth event on 17 July showing particles of ~70 nm. Nitrate has been multiplied by 5 for viewing.

The organics in the averaged mass spectrum for this same period, Figure 6.15, do not exhibit any readily distinguished pattern, but have approximately equal concentrations of *m/z* 43 and 44, indicating a mixture of species. A few of the mass fragments are noticeable, such as *m/z* 53, 55, and 99, but none of the *m/z* tentatively identified from the laboratory pinic acid mass spectrum (*m/z* 69, 70, 71, 76, 83, 104, 112, 149, 150, and 167) are conspicuous.

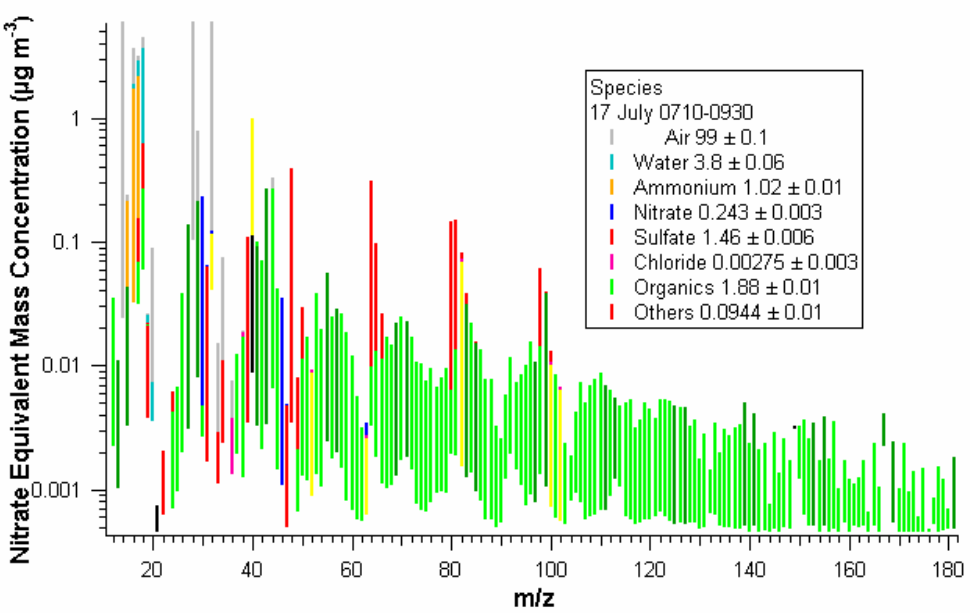

Figure 6.16: Averaged mass spectrum of 17 July growth episode.

Unfortunately, most of the growth events that occurred in the late afternoon or evening were not measured by either of the AMSs. However, the initial part of the episode on 19 July was observed. The averaged size distribution, Figure 6.16, exhibits very different behavior from the 17 July event; there is no distinct small mode, only a large mode that is maximized at approximately 450 nm with a tail down to 70 nm for sulfate and nitrate and 60 nm for organics. All species appear to display the same behavior, so these aerosols are probably well mixed.

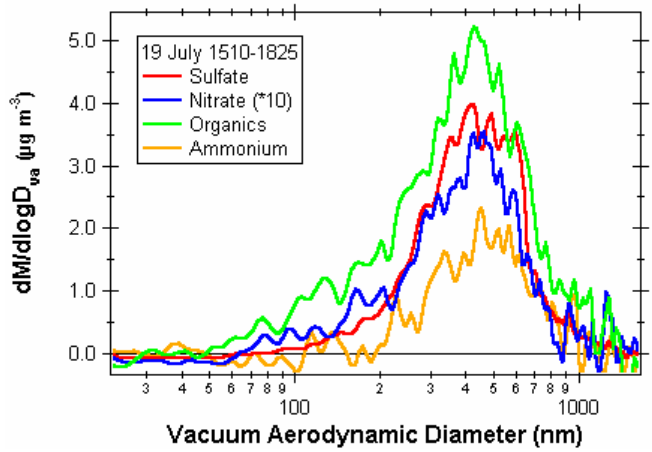

Figure 6.17: Averaged size distribution for 19 July growth event.

The averaged mass spectrum for this period, Figure 6.17, is very similar to the one for the 17 July growth episode, with the same prominent *m/z*. There is a slight increase in the *m/z* 44 signal over *m/z* 43, indicating a slightly higher oxidation state.

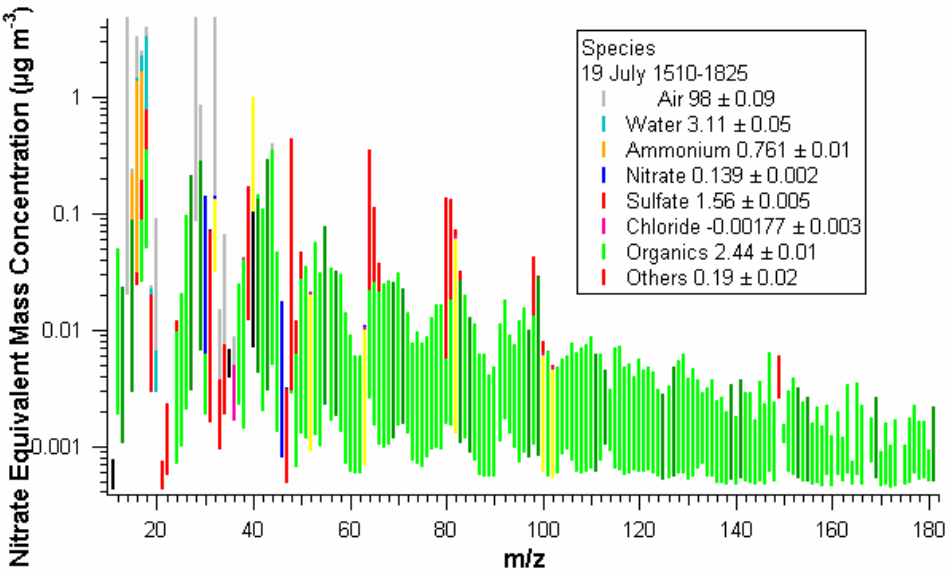

Figure 6.18: Averaged mass spectrum for 19 July growth event.

6.6 Summary

The aerosols measured during the CELTIC field campaign exhibited a combination of features from more regional aerosols (i.e., aged aerosols with substantial sulfate and organic, but low nitrate concentrations) and aerosols influenced by local conditions that displayed smaller sizes, indicating younger particles, and more varied chemical proportions.

There was a strong diurnal pattern caused by the stagnation of the air every night and high levels of humidity (saturation every night). The high humidity caused uptake of water by the aerosols, which allowed them to be well focused in the AMS

lens, but did not cause an overwhelming increase in the particulate water that would indicate condensation in the sampling lines, as was apparent at PROPHET. The air was predominantly from the southwest, but the wind direction did not appear to have an overwhelming influence on the aerosols.

Several interesting incident occurred during this study. There was a strong emission of nitrate from the forest canopy or soil very early every morning. The cause of this has not yet been identified. Also, a number of particle growth events were observed in the morning, late afternoon, and evening. Of particular interest is that the chemical composition of the smallest particles during these episodes was organics and nitrate, but not sulfate. This may represent a new particle growth mechanism.

CHAPTER 7: CONCLUSIONS

There has been a lot of concern about the effects of anthropogenically-produced aerosols on air quality, health, climate and the interactions with other atmospheric components. However, biogenic aerosols exist almost everywhere, simply because there is always plantlife with its own processes that release thousands of compounds capable of forming or interacting with aerosols. The effect of the anthropogenic aerosols is impossible to assess without information about the underlying biogenic aerosols. In addition, aerosols are exposed to different conditions as they are advected.

The research described in this dissertation addresses several issues associated with both biogenic aerosols and aerosols in general.

7.1 Instrument Operation and Development

The AMS provides quantitative measurement of the size and chemical composition of submicron non-refractory aerosols with standard quadrupole mass spectrometry as described in Chapter 2. It is a relatively new instrument, first deployed in 1999, that has proven itself a valuable addition to the suite of aerosol instruments currently available, since no other instrument can measure the size and chemical composition simultaneously. However, it is a complex instrument that requires careful calibration and quality control. Over the past five years, a comprehensive set of calibrations has been developed to ensure the highest quality measurement. There have also been a number of improvements to both the hardware

and software that have increased the sensitivity while decreasing the noise: an adjustable lens system, the addition of a fourth vacuum chamber that reduces transmission of stray ions to the detector, a small volume ionizer that increases the ionization efficiency, higher definition in the deflection voltages that direct the ions to the detector, and the beam width probe that measures the focusing of the particle beam. There have been improvements to the data acquisition software to increase the quality of the recorded data and facilitate presentation of the data to make it more comprehensible for real-time evaluation. There have also been impressive improvements to the analysis software so that the data can be processed almost instantaneously with a high standard of quality and several diagnostics that provide general information about the general characteristics of a data set have been developed.

Chapter 3 describes the development of a procedure to determine the ammonium concentration. This measurement is complicated by the interference of gas-phase nitrogen, oxygen, and water and particulate nitrate, sulfate, organics, and water at the same masses at which the ammonium fragments appear. Many of these interferences are much larger than the portion caused by ammonium, making this a difficult calculation, especially at low concentrations. This effort was motivated by the need to determine the neutralization of the aerosols during a particle growth event during the PROPHET 2001 field study and was developed over the next year and a half.

7.2 General Results

This dissertation focuses on two field studies in forested environments. The PROPHET 2001 study took place at a remote site in northern Michigan far from any large urban centers. The transport at this site determined the aerosol composition. Air from the south carried a well-mixed, aged aerosol population dominated by sulfate and organics in uniform proportions and accumulation mode sizes of approximately 400 nm. In contrast, air from the north brought very clean, dry air with low mass concentrations dominated by organics. There was little variability in the aerosol populations within the boundaries of the transport direction and little local influence to complicate the analysis. Several instances of small particle growth and variations in the height concentrations will be discussed in the next section.

The CELTIC field campaign was located near Chapel Hill, North Carolina, at the Duke Forest research site. This area was termed an urban forest because of its proximity to the population centers or Chapel Hill and Durham, but many of the markers of urban environments, such as the unsaturated organic signature of rush hour traffic were not obvious. This site was less influenced by simple transport and appeared to be more chemically active locally. Small particle growth events were observed at this location as well and there were clear variations in the nitrate concentrations with height on several occasions.

7.3 Scientific Issues

There were several scientific questions posed at the beginning of this dissertation: what is the mixing state (internal or external) of the aerosols; what, if

any, effect did biogenic aerosols have on the composition and behavior of the aerosols; how does transport affect aerosols; how do the forest and aerosols interact; and what factors affect the formation and growth of aerosols.

One of the issues over which there has been much debate is whether each aerosol is chemically uniform and compositional differences exist only in separate particles (external mixture) or whether each aerosol is a mixture of chemical species (internal mixture). In some ways, the single particle measurement techniques are better suited to address this question since they detect all, or most, of the chemical components of a particle, but they cannot address the mixing state of an entire aerosol population, only that of a few members of that population. While the AMS cannot prove this definitively, an examination of the trends of the species over time, their relative ratios, and most importantly, their size distributions can provide a lot of support for the determination of internal or external mixtures.

From the data collected in Michigan, it appears that the older, more processed aerosols from the south had plenty of time to interact with their surroundings and each other and become mixed internally, but the aerosols from the north did not have either enough time or a variety of environments to allow them to become internally mixed. While there was undoubtedly a mixture of organic species, there was almost no contribution from any other species. The North Carolina data, in contrast, appeared to contain both internal and external mixtures at the same time. For example, the sulfate concentration decreased almost every night, but the organic concentration often increased, or decreased more slowly, indicating that these species were not reacting in the same way. Also, they often exhibited different size modes,

with the organics more prevalent in the small mode and the sulfate in a much larger mode.

Another issue is the presence of biogenic aerosols. Although some concentration of biogenic aerosols must exist at these sites, it was very difficult to specifically identify them. Much of this difficulty arose because of the fragmentation caused by the electron impact ionization of the AMS. Most of the organic compounds have similar structures, or portions of structures, that cause them to fragment in the same way and makes identification difficult unless they have a distinct subgroup that produces an equally mass fragment. Another impediment is the thousands of possible organic species. Even if a distinct marker can be identified, the concentration of that species is often so small that it is indistinguishable from the general confusion of organic mass fragments.

The most common gas phase organic species emitted by plant life are isoprene (C_5H_8), which is usually too volatile to condense onto particles even after it has been oxidized, and terpenes ($C_{10}H_{16}$) and sesquiterpenes ($C_{15}H_{24}$). The terpenes are usually emitted by coniferous trees and have a low enough vapor pressure to condense, especially after they have been oxidized to ketones, aldehydes, and acids, which occurs rapidly because of the carbon-carbon double bond.

The PROPHET study was in an area dominated by isoprene-producing trees and high levels of biogenic aerosols was not expected or detected, as evidenced by the extremely low levels of organics during those periods not dominated by the processed aerosols. However, the CELTIC study was located in a coniferous forest and should have shown signs of the presence of biogenic aerosols. However, the

difficulty in identifying organics recurred here. A sample of pinic acid, one of the products of the oxidation of α-pinene, the most common terpene, by ozone [Calogirou et al., 1999], was obtained and measured by the AMS to attempt to identify some mass fragments that could be used to distinguish some of the biogenic species from anthropogenic. While several masses did appear to stand out, and a combination of these masses (*m/z* 69, 70, 71, 76, 83, 104, 112, 149, 150, and 167) might be sufficient for identification, none of these combinations were clearly observed. This does not mean that biogenic aerosols were not present, as this is only one of thousands of possible compounds, however, it does limit the possibility of useful identification of biogenic species with an AMS. It may be that the only way to identify these compounds is in conjunction with another measurement, such as a filter, that can chemically resolve these species.

Given the lack of widespread measurements at remote sites, one of the main goals of these studies was simply to determine the properties of remote aerosols. It is clear that the composition of these aerosols depends highly both on the local environment and the air advected into the area. At PROPHET the local environment produced very few particles, so almost all of the aerosol population was transported from other locations and was consistent in both proportions of chemical composition and size. That was not the case at CELTIC. While there was a clear influence on the aerosol population from various air masses, as evident from the large change in both concentration and size distribution on 17 and 18 July, it was not necessarily direction-dependent and there was also an effect from local conditions. There was almost no mixing at night as verified by the ozone and carbon dioxide measurements, yet there

was an increase in organic aerosol concentration almost every night, in contrast to a decrease or smaller increase of the sulfate aerosols. This had to be a result of either deposition or chemical interactions in contrast to increases expected from the decreased boundary layer and/or production of organic aerosols.

The issue of what, if any, interaction the particles have with the forest canopy is one of great interest. At both PROPHET and CELTIC, gradient measurements were made to address this issue. The aerosols were sampled at one of three inlets at different heights on the tower and changed inlets every five minutes, so a complete cycle of all three inlets was completed every 15 minutes. This gradient data was then averaged to 2-3 hours so that any short-term variability was reduced and the larger trends would be more apparent. At PROPHET, there were noticeable gradients in nitrate, organics, and sulfate, although they were not frequent. There were also several smaller variations, but it is not clear how meaningful these are.

During CELTIC, there were very clear gradients in nitrate concentration early every morning, with larger concentrations in the canopy than in the free air above the canopy. Three of the four of these events began well before sunrise, so some kind of nighttime chemistry or emission must be involved, although the cause is not yet apparent. Again, there were a number of smaller variations, but it is not clear how significant these are. Comparison of these results with the flux measurements performed by the CIRES group may provide more information as to the relevance of the variations.

One of the more surprising results from these studies was the common occurrence of particle growth events. Particle formation and growth has generated a

lot of interest and study, but is still one of the least understood aerosol processes [Kulmala et al., 2002; Clement and Ford, 1999; Leaitch et al., 1999; Birmili et al., 2000; Verheggen and Mozurkewich, 2002]. Nucleation bursts are known in many remote environments, including the free troposphere, marine boundary layer and coastal sites, boreal forests, and Arctic and Antarctic areas [Kulmala et al., 2002] and can subsequently grow to sizes large enough to have both a chemical and radiative effect. Neither of the locations in this research is known for particle nucleation and/or growth like the Smoky or Blue Ridge Mountains, but small particle growth was observed at both locations. It is not clear if the particles actually formed at these sites since measurements capable of detecting nucleation particles, those approximately 3 nm in diameter, were available or operating properly. There were differences in the growth events at these two locations that indicate that different causes or mechanisms were at work.

The events at PROPHET all occurred on clean days when the particle number was very low and there was not enough surface area for the condensable material to simply adsorb to the existing particles. However, the small particles that presumably formed and then grew did not remain. They were either disbursed or re-evaporated since they disappeared within a few hours. Also, they all occurred in the morning when photochemistry converted any SO_2 in the air to H_2SO_4, which then condensed. Ammonia was also involved in at least one event, the most distinct occurrence on 26 July, but the noisy ammonium signal on the other days precludes any conclusion as to the involvement of ammonia generally in these growth events.

The contribution of ammonia is an important issue because of the theories of binary and ternary nucleation. Only sulfuric acid and water are involved in binary nucleation, while ternary nucleation also includes ammonia. The calculated rates for binary nucleation [Kumala et al., 2000] make it unlikely to be the prime mechanism. Therefore, ternary nucleation is much more likely, but it has not been measured often enough to provide substantial evidence.

The particle growth events observed at CELTIC appear more variable than those at PROPHET. There were several events in the morning (11, 12, 14, 17, and 20 July) that are probably photochemically driven, but there were never such low concentrations at CELTIC as were observed at PROPHET, so the basic conditions are not quite the same. Also, the species that were primarily involved in the growth (i.e., smallest sizes) were consistently the organics and nitrate. There were also several events that occurred in the late afternoon or evening (13, 14, 16, and 19 July) where organics and nitrate were the main contributors, but the small mode was much less distinct during these events.

7.4 Next Steps

Both of these field campaigns provided a wealth of information about the general aerosol population and conditions at each site, how transport and weather patterns affected the aerosols, and the importance of fully understanding all aspects of the instrumentation and sampling process. However, there were several questions that were not fully addressed.

The issue of the presence and interaction of biogenic aerosols remains unresolved and will probably require a more extensive set of measurements to find any answers. The exact nature of the forest-aerosol interactions is still not apparent. A more in-depth analysis of the data already recorded may yield some more insights, but this issue will probably also require better information on the nature and reactions of the biogenic species. And finally, the particle formation and growth mechanisms require additional study. It seems clear that ternary ($H_2SO_4/NH_3/H_2O$) and binary (H_2SO_4/H_2O) nucleation are not the only mechanisms capable of forming particles, given the evidence of organic/nitrate involvement at CELTIC.

BIBLIOGRAPHY

Allan, J.D., J.L. Jimenez, H. Coe, K. N. Bower, P.I. Williams, J.T. Jayne, and D.R. Worsnop, 2003, Quantitative sampling using an Aerodyne aerosol mass spectrometer 1. Techniques of data interpretation and error analysis. *J. Geophys. Res.* doi:10.1029/2002JD002358.

Allan, J.D., A.E. Delia, H. Coe, K.N. Bower, M.R. Alfarra, J.L. Jimenez, A.M. Middlebrook, F. Drewnick, T.B. Onasch, M.R. Canagaratna, J.T. Jayne, D.R. Worsnop. A generalised method for the extraction of chemically resolved mass spectra from aerodyne aerosol mass spectrometer data. *J. of Aerosol Science*, in press.

Andersen, H.V., M.F. Hovmand, P. Hummelshoj, N.O. Jensen, 1999. Measurements of ammonia concentrations, fluxes, and dry deposition velocities to a spruce forest 1991-1995. *Atm. Environment*, 33, 1367-1383.

Baron, P.A. and K. Willeke. Aerosol Measurement. Van Nostrand Reinhold, New York. 2001.

Bley, W.G. 1988 Quantitative Measurements with Quadrupole Mass Spectrometers: Important Specifications for Reliable Measurements. *Vacuum*. 38 (2) 103-109.

Birmili, W., A. Wiedensohler, C. Plass-Dulmer, H. Berresheim, 2000: Evolution of Newly Formed Aerosol Particles in the Continental Boundary Layer: A Case Study Including OH and H_2SO_4 Measurements. *Geophys. Res. Lett.*, **27**, 2205-2208.

Blando, J.D., R.J. Porcja, T-H Li, D. Bowman, P.J. Lioy, B.J. Turpin, 1998: Secondary Formation and the Smoky Mountain Organic Aerosol: An Examination of Aerosol Polarity and Functional Group Composition During SEAVS. *Environ.Sci. Technol.*, **32**, 604-613.

Caligorou, A., B.R. Larsen, and D. Kotzias. 1999. Gas-phase terpene oxidation products: a review. Atm. Environ. 33. 1423-1439.

Carroll, M.A., S.B. Bertman, P. Shepson. 2001. Overview of the Program for Research on Oxidants: PHotochemistry, Emissions, and Transport (PROPHET) summer 1998 measurements intensive. *J. Geophys. Res*.

CELTIC website. http://acd.ucar.edu/~cstroud/CELTIC/, Accessed 2004.

Clement, C.F. and I.J. Ford, 1999. Gas-to-particle conversion in the atmosphere: I. Evidence from empirical atmospheric aerosols. *Atm. Environ*. 33, 475-487.

Draxler, R.R. and Rolph, G.D., 2003. HYSPLIT (HYbrid Single-Particle Lagrangian Integrated Trajectory) Model access via NOAA ARL READY Website (http://www.arl.noaa.gov/ready/hysplit4.html). NOAA Air Resources Laboratory, Silver Spring, MD.

EPA Office of Air Quality Planning and Standards: National Ambient Air Quality Standards (NAAQS), http://www.epa.gov/airs/criteria.html, Accessed November, 2001.

Forest Atmosphere Carbon Dioxide Transfer and Storage-1 (FACTS-1), http://www.face.bnl.gov/facts1.html. Accessed 2004.

Falconbridge, Ltd., http://www.falconbridge.com/, Accessed September 2001.

Finlayson-Pitts, B.J., J.N. Pitts, 1999: Chemistry of the Upper and Lower Atmosphere. Academic Press, San Diego.

Flaim, T.A. and P.D. Ownby, 1971. Observations on Bayard-Alpert Iion Gauge Sensitivities to Various Gases. *J. Vacuum Science and Technology*. 8 (5) 861.

FLUENT, 1995: Version 4.47, Fluent, Inc., Lebanon, New Hampshire.

Glasius, M. M. Duane, B.R. Larsen, 1999: Determination of polar terpene oxidation products in aerosols by liquid chromatography-ion trap mass spectrometry. *J. Chrom. A*, **833**, 121-135.

Griffin, R.J., D.R. Cocker III, R.C. Flagan, J.H. Seinfeld, 1999: Organic aerosol formation from the oxidation of biogenic hydrocarbons. *J. Geophys. Res.*, **104**, 3555-3567.

International Panel on Climate Change 2001 Technical Summary, http://www.ipcc.ch/, Accessed November, 2001.

Jacobson, M.C., H.-C. Hansson, K.J. Noone, R.J. Charlson, 2000: Organic Atmospheric Aerosols: Review and State of the Science. *Rev. Geophys.*, **38**, 267-294.

Jayne, J.T., D.C. Leard, X. Zhang, P. Davidovits, K.A. Smith, C.E. Kolb, D.W. Worsnop, 2000: Development of an Aerosol Mass Spectrometer for Size and Composition Analysis of Submicron Particles. *Aerosol Sci and Tech.,* **33**, 49-70.

Jimenez, J.L., J.T. Jayne, Q. Shi, C.E. Kolb, D.R. Worsnop, I. Yourshaw, J.H. Seinfeld, R.C. Flagan, X. Zhang, K.A. Smith, J.W. Morris, and P. Davidovits.

2003. Ambient aerosol sampling using the Aerodyne Aerosol Mass Spectrometer. *J. Geophys. Res*. doi:10.1029/2002JD002452.

Kulmala M., P. Korhonen, I. Napari, A. Karlsson, H. Berresheim, and C.D. O'Dowd. 2002, Aerosol formation during PARFORCE: Ternary nucleation of H_2SO_4, NH_3, and H_2O. *J. Geophys. Res.* doi: 10.1029/2001JD0009000.

Leaitch, W.R., J.W. Bottenheim, T.A. Biesenthal, S.M. Li, P.S.K. Liu, K. Asalian, H. Dryfhout-Clark, F. Hopper, 1999: A case study of gas-to-particle conversion in an eastern Canadian forest. *J. Geophys. Res.*, **104**, 8095-8111.

Liu, P. P.J. Ziemann, D.B. Kittelson, P.H. McMurry, 1995: Generating Particle Beams of Controlled Dimensions and Divergence: I. Theory of Particle Motion in Aerodynamic Lenses and Nozzle Expansions. *Aerosol Science and Technology.,* **22,** 293-313 .

Liu, P. P.J. Ziemann, D.B. Kittelson, P.H. McMurry, 1995: Generating Particle Beams of Controlled Dimensions and Divergence: II. Experimental Evaluation of Particle Motion in Aerodynamic Lenses and Nozzle Expansions. *Aerosol Science and Technology.,* **22,** 314-324.

McLafferty, F.W., F. Tureček, 1993: Interpretation of Mass Spectra. University Science Books, Sausalito, CA.

NIST Chemistry WebBook (http://webbook.nist.gov/chemistry, Accessed 2004.

PROPHET website, http://data.engin.umich.edu/PROPHET/, Accessed 2004.

Rolph, G.D., 2003. Real-time Environmental Applications and Display sYstem (READY) Website (http://www.arl.noaa.gov/ready/hysplit4.html). NOAA Air Resources Laboratory, Silver Spring, MD.

Seinfeld, J.H., S.N. Pandis, 1998: Atmospheric Chemistry and Physics: From Air Pollution to Climate Change. John Wiley & Sons, New York.

Summers, R.L. 1969. NASA Technical Note TND 5285, Ionization Gauge Sensitivities as Reported in the Literature, Lewis Research Center, National Aeronautics and Space Administration.

TSI Product Information: Model 3936-Series Scanning Mobility Particle Sizer, http://www.tsi.com/particle/product/pdf/3936scr.pdf, Accessed March 2001.

Verheggen, B. and M. Mozurkewich, 2002. Determination of nucleation and growth rates from observation of a SO_2 induced atmospheric nucleation event. *J. Geophys. Res*. doi: 10.1029/2001JD000683.

Whitby, K.T. and D. Cantrell. 1976. Fine Particles. International Conference on Environmental Sensing and Assessment, Las Vegas, NV, Institute of Electrical and Electronic Engineers.

Yokouchi, Y., Y. Ambe, 1985: Aerosols Formed from the Chemical Reaction of Monoterpenes and Ozone. *Atmos. Env.*, **19**, 1271-1276.

Zhang X., K.A. Smith, D.R. Worsnop, J. Jimenez, J.T. Jayne, and C.E. Kolb. 2002. A numerical characterization of particle beam collimation by an aerodynamic lens-nozzle system: Part I. An individual lens or nozzle. *Aerosol Sci and Tech*. 36. 617-631.

APPENDIX A

DATA DIAGNOSTICS PROCEDURE (version 1.1.7a)

Written in IgorPro, this procedure creates graphs that display the fragmentation patterns of the major species, as well the ammonium neutralization based on the concentrations of sulfate, nitrate, and chloride, and as estimate of the organics oxidation based on the ration of *m/z* 44 to total organics

```
#pragma rtGlobals=1                    // Use modern global access method.

// Modified for combinrd waves

//& Version 1.1.7a - Kludged version by James Allan 2 May 03
//& Compatibility fixes put in for revised batch with shortened wave names
//& All changes have the '//&' comment line

// DATA DIAGNOSTICS v1.1.7
//   Alice Delia, December 19 2002
//   For use with James Allan's AMS Analysis Toolkit (Deluxe v1.25 or higher)

//   Many thanks for contributions from Doug Worsnop, Tim Onasch, Manjula Canagaratna,
//     Jose-Luis Jimenez, Qi Zhang, and James Allan

// INSTRUCTIONS
//  You must have loaded the "general" frag list available on James' website:
//      AMSbatch.11.29.02.itx or later to use this panel.
//            (http://cloudbase.phy.umist.ac.uk/people/allan/ja_igor.htm)
//  After opening panel, press "Calc Std Batch" button to create all of the necessary waves
//  Plot data diagnostics after choosing:
//   -number ofpoints to smooth
//   -which species to plot diagnostics for (All, Ammonium, Sulfate, Nitrate, Organics)
//   -how to color species (Time-default, Ammonium, Sulfate, Nitrate, Organics, ratios)

//   IMPORTANT NOTICE!!!
//   I have not yet gotten the colorscale tick labels to print out the correct units.
//     It doesn't have a problem with the numeric waves, but does not recognize date/time units
//     So if you want the date/time recognizable, use the following command on the command line
//        and then resize the graph a little (so it updates). I'm working on this, but haven't quite managed
//        to get it right yet. Hopefully, it will work properly in the next version.
//   SetScale d 0,0,"dat", waveforcolor

// Minor change from 1.1.6 to 1.1.7 complete by Tim Onasch per Alice's request:  Function call
// to MakeLines() has been moved from function MakeDDPanel() to

MENU "Panels"
          "Alice's", get_win("Data_Diags", "MakeDDPanel()")
END

MENU "Forward"
          "Mass Trend", DoWindow/F Mass_Trend
          "Instrument Diagnostics", DoWindow/F diag_graph
          "Instrument Corrections", DoWindow/F corr_graph
          "Ammonium", DoWindow/F NH4_Fragment; DoWindow/F NH4_Meas_Pred
          "Sulfate", DoWindow/F SO4_Fragment
          "Nitrate", DoWindow/F NO3_Fragment
          "Organics", DoWindow/F Org_Fragment
END

FUNCTION MakeDDPanel()
          MakeGlobals()
          Execute ("Data_Diags()")              // makes panel
END
```

```
//  ----------------------  Data Diagnostics Panel ---------------------
Window Data_Diags() : Panel
	PauseUpdate; Silent 1		// building window...
	NewPanel /W=(12.75,53.75,309.75,425.75) as "Data Diagnostics"
	SetDrawLayer UserBack
	SetDrawEnv fsize= 18,textrgb= (0,15872,65280)
	DrawText 14,32,"AMS Data Diagnositcs v1.1.7"
	SetDrawEnv linethick= 2,linefgc= (0,39168,0)
	DrawLine 14,238,251,238
	DrawText 29,49,"Alice Delia, University of Colorado"
	SetDrawEnv textrgb= (65280,0,0)
	DrawText 157,73,"1) Load general frag lists"
	SetDrawEnv textrgb= (65280,0,0)
	DrawText 157,88,"2) Run 'Calc Std Batch'"
	SetDrawEnv textrgb= (65280,0,0)
	DrawText 157,103,"3) Set graph options"
	Button button_calcbatch,pos={15,64},size={84,20},proc=Butt_CalcStdBatch,title="Calc Std
Batch"
	PopupMenu popup_ChooseDiagnostics,pos={14,132},size={117,21},title="Diagnostics"
	PopupMenu popup_ChooseDiagnostics,mode=1,popvalue="All",value=
#"\"All;Ammonium;Sulfate;Nitrate;Organics;MassTrend\""
	SetVariable setvar_smth_dd_pts,pos={23,104},size={99,16},title="Smooth Pts"
	SetVariable setvar_smth_dd_pts,value= smth_dd
	PopupMenu popup_ColorDiags,pos={16,166},size={112,21},title="Color by"
	PopupMenu popup_ColorDiags,mode=1,popvalue="Time",value=
#"\"Time;Ammonium;Sulfate;Nitrate;Organics;Org_SO4;Water_SO4;NO3_SO4;NH4_SO4;NH4_NO
3\""
	Button button_CalcDiags,pos={58,202},size={133,19},proc=Butt_CalcDiags,title="Plot Data
Diagnostics"
EndMacro
//  ------------------------------------------------------------------------------

//   Button functions for panel
Function Butt_CalcStdBatch(ctrlName) : ButtonControl
	string ctrlName
	MakeLines()                                                    //makes lines for graphs (needs
revision)
	GenerateFragTrends()
	MakeRatios()		// this makes some useful ratios for plotting, must have calculated
the batch list first
End

Function Butt_CalcDiags(ctrlName) : ButtonControl
	String ctrlName

	NVAR smth_dd		// reads smooth pts
	controlinfo/w=Data_Diags setvar_smth_dd_pts
	if (smth_dd > 0)
		smth_dd = v_value
	else
		smth_dd = 1
	endif

	SVAR colorby	// reads wave for coloring
```

```
	string
colorwaves="t_series_comb;NH4_comb_sm;SO4_comb_sm;N03_comb_sm;Org_comb_sm;ratio_O_S
;ratio_W_S;ratio_N_S;ratio_A_S;ratio_A_N"
	controlinfo/w=Data_Diags popup_ColorDiags
	if (v_value==1)
		colorby=stringfromlist(0, colorwaves)
	elseif (v_value==2)
		colorby=stringfromlist(1, colorwaves)
	elseif (v_value==3)
		colorby=stringfromlist(2, colorwaves)
	elseif (v_value==4)
		colorby=stringfromlist(3, colorwaves)
	elseif (v_value==5)
		colorby=stringfromlist(4, colorwaves)
	elseif (v_value==6)
		colorby=stringfromlist(5, colorwaves)
	elseif (v_value==7)
		colorby=stringfromlist(6, colorwaves)
	elseif (v_value==8)
		colorby=stringfromlist(7, colorwaves)
	elseif (v_value==9)
		colorby=stringfromlist(8, colorwaves)
	elseif (v_value==10)
		colorby=stringfromlist(9, colorwaves)
	endif

	controlinfo/w=Data_Diags popup_ChooseDiagnostics
	if (v_value==1)
		OrganicDiagnostics()
		NitrateDiagnostics()
		SulfateDiagnostics()
		AmmoniumDiagnostics()
		Plot_MassTimeTrend()
	elseif (v_value==2)
		AmmoniumDiagnostics()
	elseif (v_value==3)
		SulfateDiagnostics()
	elseif (v_value==4)
		NitrateDiagnostics()
	elseif (v_value==5)
		OrganicDiagnostics()
	elseif (v_value==6)
		Plot_MassTimeTrend()
	endif

END

FUNCTION WaveScaling(colorby)
	string colorby
	wave ts = t_series
	wave sulphate
	make/o/n=(numpnts(t_series)) waveforcolor
	wave waveforcolor = $colorby

	controlinfo/w=Data_Diags popup_ColorDiags		// this part works
	if (v_value==1)
```

```
		setscale d 0,0,"dat", waveforcolor
		                                                                //print "dat"
	else
		setscale d 0,0,"", waveforcolor
		                                                                //print "numeric"
	endif

END

FUNCTION MakeGlobals()

variable/g smth_dd=1
variable/g axis_min,axis_max
string/g colorby

END FUNCTION


FUNCTION GenerateFragTrends()		// Pushes James' "Batch Calculate" for species listed
below
	SVar ms2_speclist=root:ms2_speclist
	String
NewMassList="Sulphate,Nitrate,Organics,Ammonium,Chloride,Water,NH4_16,NH4_17,"
	NewMassList +=
"SO4_48,SO4_64,SO4_80,SO4_81,SO4_98,NO3_30,NO3_46,m43,m44,m57"
	String OldMassList=ms2_specList
	ms2_speclist=NewMassList
	butt_ugcalc("ms2_ugcalc")			// calculates species
	ms2_specList=OldMassList		// puts whatever was originally in batch species
list back
END FUNCTION


FUNCTION Axis(xwave,ywave)			//determines values for autoscale both axes
WAVE xwave,ywave
NVAR axis_min,axis_max
axis_min=0
axis_max=0

variable V_min_x,V_max_x,V_min_y,V_max_y
WaveStats/Q xwave
V_min_x = V_min
V_max_x = V_max
WaveStats/Q ywave
V_min_y = V_min
V_max_y = V_max
	if (V_min_x < V_min_y)  //determines min scale
		axis_min = V_min_x
	else
		axis_min = V_min_y
	endif
	if (axis_min < 0)			// sets axis to 0 if min is > 0
		axis_min = axis_min
	else
		axis_min = 0
	endif
```

```
	if (V_max_x > V_max_y) //determines max scale
		axis_max = V_max_x
	else
		axis_max = V_max_y
	endif

END FUNCTION


FUNCTION AmmoniumDiagnostics()

Wave t_series_comb
//&Wave ammonium,sulphate,nitrate,chloride
Wave NH4_comb_sm,SO4_comb_sm,NO3_comb_sm
	//ammonium=nh4,sulphate=so4,nitrate=no3,chloride=chl
NVAR smth_dd
NVAR axis_min,axis_max

// Compare measured ammonium with predicted ammonium
duplicate/o NH4_comb_sm NH4_meas,NH4_predict                    //ammonium
NH4_meas,NH4_predict
NH4_predict = (36/98)*SO4_comb_sm + (18/63)*NO3_comb_sm         // + (18/35)*Chloride
smooth_nans(NH4_meas,smth_dd)
smooth_nans(NH4_predict,smth_dd)

DoWindow/k NH4_Meas_Pred                // Kills/makes graph
Execute ("NH4_Meas_Pred()")
Axis(NH4_predict,NH4_meas)
SetAxis y_nh4_meas axis_min,axis_max ;DelayUpdate
SetAxis x_nh4_pred axis_min,axis_max

//// NH4 17 to 16 ratio
//Wave NH4_17,NH4_16
//duplicate/o  NH4_17 NH4_ratio,NH4_17dd
//duplicate/o  NH4_16 NH4_16dd
//NH4_ratio /= NH4_16
//smooth_nans(NH4_ratio,smth_dd)
//smooth_nans(NH4_16dd,smth_dd)
//smooth_nans(NH4_17dd,smth_dd)
//
//DoWindow/k NH4_Fragment                 // Kills/makes graph
//Execute ("NH4_Fragment()")
//Axis(NH4_16dd,NH4_17dd)
//SetAxis y_nh4_17 axis_min,axis_max ;DelayUpdate
//SetAxis x_nh4_16 axis_min,axis_max

END FUNCTION


FUNCTION SulfateDiagnostics()
NVAR smth_dd
NVAR axis_min,axis_max
//&Wave t_series,sulphate
Wave t_series,sulphate=so4
duplicate/o sulphate SO4_dd
```

```
smooth_nans(SO4_dd,smth_dd)
// Determine sulfate ratios 48/64/80/81/98
Wave SO4_48,SO4_64,SO4_80,SO4_81,SO4_98
duplicate/o SO4_48 ratio64_48,ratio80_48,ratio81_48,ratio98_48
duplicate/o SO4_48 SO4_48dd
duplicate/o SO4_64 SO4_64dd
duplicate/o SO4_80 SO4_80dd
duplicate/o SO4_81 SO4_81dd
duplicate/o SO4_98 SO4_98dd
ratio64_48 = SO4_64 / SO4_48
ratio80_48 = SO4_80 / SO4_48
ratio81_48 = SO4_81 / SO4_48
ratio98_48 = SO4_98 / SO4_48
smooth_nans(ratio64_48,smth_dd)
smooth_nans(ratio80_48,smth_dd)
smooth_nans(ratio81_48,smth_dd)
smooth_nans(ratio98_48,smth_dd)
smooth_nans(SO4_48dd,smth_dd)
smooth_nans(SO4_64dd,smth_dd)
smooth_nans(SO4_80dd,smth_dd)
smooth_nans(SO4_81dd,smth_dd)
smooth_nans(SO4_98dd,smth_dd)

DoWindow/k SO4_Fragment                    // Kills/makes graph
Execute ("SO4_Fragment()")
Axis(SO4_48dd,SO4_64dd)
SetAxis y_so4_ratio_scatter axis_min,axis_max ;DelayUpdate
SetAxis x_so4_48 axis_min,axis_max

END FUNCTION


FUNCTION NitrateDiagnostics()
NVAR smth_dd
NVAR axis_min,axis_max
//& Wave t_series,nitrate              //,m31
Wave t_series,nitrate=no3              //,m31
duplicate/o nitrate NO3_dd
smooth_nans(NO3_dd,smth_dd)
//duplicate/o m31 m31_dd
//smooth_nans(m31_dd,smth_dd)

// Determine nitrate ratios 30/46
Wave NO3_30,NO3_46
duplicate/o NO3_30 ratio30_46,ratio46_30,NO3_30dd
duplicate/o NO3_46 NO3_46dd
ratio46_30 = NO3_46 / NO3_30
smooth_nans(ratio46_30,smth_dd)
ratio30_46 /= NO3_46
smooth_nans(ratio30_46,smth_dd)
smooth_nans(NO3_30dd,smth_dd)
smooth_nans(NO3_46dd,smth_dd)

DoWindow/k NO3_Fragment                    // Kills/makes graph
Execute ("NO3_Fragment()")
Axis(NO3_30dd,NO3_46dd)          // set axes
```

```
SetAxis y_no3_46 axis_min,axis_max ;DelayUpdate
SetAxis x_no3_30 axis_min,axis_max
//KillVariables/Z V_min_30,V_max_30,V_min_46,V_max_46

END FUNCTION


FUNCTION OrganicDiagnostics()
NVAR smth_dd
NVAR axis_min,axis_max

// m/z 44 : Total Organic
//&Wave t_series,m44,Organics
Wave t_series,m44,Organics=org
duplicate/o Organics Org_dd
duplicate/o m44 m44_dd
smooth_nans(Org_dd,smth_dd)
smooth_nans(m44_dd,smth_dd)

// m43 : m57
wave m43,m57
duplicate/o m43 m43_dd
duplicate/o m57 m57_dd
smooth_nans(m43_dd,smth_dd)
smooth_nans(m57_dd,smth_dd)

DoWindow/k Org_Fragment                 // Kills/makes graph
Execute ("Org_Fragment()")

END FUNCTION


FUNCTION Plot_MassTimeTrend()

DoWindow/k Mass_TimeTrend               // Kills/makes graph
Execute ("Mass_TimeTrend()")

END FUNCTION


FUNCTION MakeRatios()                   // Must have calculated batch to run this
NVAR smth_dd
//&Wave Sulphate,Organics,Nitrate,Ammonium,Water
Wave Sulphate=so4,Organics=org,Nitrate=no3,Ammonium=nh4,Water

make/o/n=(numpnts(t_series)) ratio_O_S,ratio_W_S,ratio_N_S,ratio_A_S,ratio_A_N
ratio_O_S = Organics / Sulphate
smooth_nans(ratio_O_S,smth_dd)

ratio_W_S = Water / Sulphate
smooth_nans(ratio_W_S,smth_dd)

ratio_N_S = Nitrate / Sulphate
smooth_nans(ratio_N_S,smth_dd)

ratio_A_S = Ammonium / Sulphate
```

```
smooth_nans(ratio_A_S,smth_dd)

ratio_A_N = Ammonium / Nitrate
smooth_nans(ratio_A_N,smth_dd)

END FUNCTION


FUNCTION MakeLines()              // lines for graphs, need to change for log scale
wave t_series_comb

make/o/n=2 unity
unity[0]=0
unity[1]=10
SetScale/I x 0,10,"", unity              // 1:1 line

make/o/n=2 line_1pt1_1
line_1pt1_1[0]=0
line_1pt1_1[1]=11
SetScale/I x 0,10,"", line_1pt1_1     //1.1:1 line (for NH4)

make/o/n=2 line_at1pt1_time                    // 1.1 line over time (for NH4)
line_at1pt1_time[0]=1.1
line_at1pt1_time[1]=1.1
SetScale/I x t_series_comb[0],t_series_comb[numpnts(t_series_comb)],"", line_at1pt1_time

make/o/n=2 line_at1_time
line_at1_time[0]=1
line_at1_time[1]=1
SetScale/I x t_series_comb[0],t_series_comb[numpnts(t_series_comb)],"", line_at1_time // 1 line over
time

make/o/n=2 line_at2_time
line_at2_time[0]=2
line_at2_time[1]=2
SetScale/I x t_series_comb[0],t_series_comb[numpnts(t_series_comb)],"", line_at2_time // 2 line over
time (NO3)

make/o/n=2 line_atpt5_time
line_atpt5_time[0]=0.5
line_atpt5_time[1]=0.5
SetScale/I x t_series_comb[0],t_series_comb[numpnts(t_series_comb)],"", line_atpt5_time          //
0.5 line over time (NO3)

make/o/n=2 line_1_2
line_1_2[0]=0
line_1_2[1]=5
SetScale/I x 0,10,"",line_1_2          // 0.5:1 or 1:2 line

make/o/n=2 line_1_4
line_1_4[0]=0
line_1_4[1]=2.5
SetScale/I x 0,10,"",line_1_4                    // 0.25:1 or 1:4 line

make/o/n=2 line_1_8
line_1_8[0]=0
```

```
line_1_8[1]=1.25
SetScale/I x 0,10,"",line_1_8                    // 0.125:1 or 1:8 line

make/o/n=2 line_2_1
line_2_1[0]=0
line_2_1[1]=10
SetScale/I x 0,5,"",line_2_1                     // 2:1 line

make/o/n=2 line_3_1
line_3_1[0]=0
line_3_1[1]=10
SetScale/I x 0,3.3,"",line_3_1                   // 3:1 line

make/o/n=2 line_4_1
line_4_1[0]=0
line_4_1[1]=40
SetScale/I x 0,10,"",line_4_1                    // 4:1 line

make/o/n=2 line_5_1
line_5_1[0]=0
line_5_1[1]=10
SetScale/I x 0,2,"",line_5_1                     // 5:1 line

END FUNCTION


//  ------------------------  Data Diagnostics Graphs ----------------------

Window NH4_Fragment() : Graph
        PauseUpdate; Silent 1                    // building window...
        make/o/n=(numpnts(t_series)) waveforcolor
        waveforcolor = $(colorby)

        Display /W=(13.5,68,596.25,529.25)/L=y_nh4_time/B=x_time NH4_meas vs t_series
        AppendToGraph/L=y_nh4_ratio/B=x_time NH4_ratio vs t_series
        AppendToGraph/L=y_nh4_17/B=x_nh4_16 NH4_17dd vs NH4_16dd
        AppendToGraph/L=y_nh4_17/B=x_nh4_16 line_1pt1_1
        AppendToGraph/L=y_nh4_ratio/B=x_time line_at1pt1_time
        ModifyGraph margin(left)=72,margin(bottom)=36
        ModifyGraph mode(NH4_17dd)=3,marker(NH4_17dd)=19
        ModifyGraph lsize(NH4_meas)=2
        ModifyGraph lsize(NH4_ratio)=2
        ModifyGraph lSize(line_1pt1_1)=2,lSize(line_at1pt1_time)=2
        ModifyGraph lStyle(line_1pt1_1)=2,lStyle(line_at1pt1_time)=2
        ModifyGraph rgb(line_1pt1_1)=(0,0,0),rgb(line_at1pt1_time)=(0,0,0)
        ModifyGraph msize(NH4_17dd)=1
        ModifyGraph
zColor(NH4_meas)={waveforcolor,*,*,Rainbow},zColor(NH4_17dd)={waveforcolor,*,*,Rainbow}
        ModifyGraph tick=1
        ModifyGraph
zero(y_nh4_time)=1,nticks(x_time)=10,minor(x_time)=1,sep(x_time)=10,fStyle(x_time)=1
        ModifyGraph mirror(y_nh4_time)=1,mirror(x_time)=1,mirror(y_nh4_ratio)=1
        ModifyGraph
lblPos(y_nh4_time)=58,lblPos(y_nh4_ratio)=53,lblPos(y_nh4_17)=52,lblPos(x_nh4_16)=75
        ModifyGraph lblLatPos(y_nh4_time)=4,lblLatPos(y_nh4_17)=-2,lblLatPos(x_nh4_16)=-16
        ModifyGraph freePos(y_nh4_time)=0,freePos(x_time)={0,y_nh4_ratio}
```

```
	ModifyGraph
freePos(y_nh4_ratio)=0,freePos(y_nh4_17)=0,freePos(x_nh4_16)={0,y_nh4_17}
	ModifyGraph axisEnab(y_nh4_time)={0.85,1},axisEnab(y_nh4_ratio)={0.47,0.8}
	ModifyGraph axisEnab(y_nh4_17)={0,0.4},axisEnab(x_nh4_16)={0,0.4}
	ModifyGraph dateInfo(x_time)={0,0,0}
	ModifyGraph mirror(x_time)=1
	ModifyGraph mirror(y_nh4_time)=1
	ModifyGraph mirror(y_nh4_ratio)=1
	Label y_nh4_time "\\f01NH\\B4\\M (\\F'Symbol'm\\F'Arial'g/m\\S3\\M)"
	Label x_time " "
	Label y_nh4_ratio "\\f01NH\\B4\\M Ratio: m/z 17 / 16"
	Label y_nh4_17 "\\f01NH\\B4\\M at m/z 17"
	Label x_nh4_16 "\\f01NH\\B4\\M at m/z 16"
	SetAxis y_nh4_ratio 0,2
	ShowInfo
	TextBox/N=text0/F=0/B=1/A=MC/X=21.15/Y=-18.08 "\\f01\\Z14Data Diagnostics:
Ammonium\r\\Z12Fragmentation Patterns\r\r\\f00Line 1.1:1"
	ColorScale/N=text1/F=0/B=1/A=MC/X=44.48/Y=-37.12 trace=NH4_meas, heightPct=40
	ColorScale/C/N=text1 width=7, nticks=10, fsize=10, minor=1
	AppendText " "
EndMacro

Window NH4_Meas_Pred() : Graph
	PauseUpdate; Silent 1		// building window...
	make/o/n=(numpnts(t_series_comb)) waveforcolor
	waveforcolor = $(colorby)

	Display /W=(70.5,59.75,630,478.25)/L=y_nh4_meas/B=x_nh4_pred unity
	AppendToGraph/L=y_nh4_meas/B=x_nh4_pred NH4_meas vs NH4_predict
	AppendToGraph/L=y_nh4_time/B=x_time NH4_meas vs t_series_comb
	ModifyGraph margin(top)=43,margin(left)=50,margin(bottom)=43
	ModifyGraph mode(NH4_meas)=2
	ModifyGraph lsize=2
	ModifyGraph lSize(unity)=2,lSize(NH4_meas)=2
	ModifyGraph lStyle(unity)=2,rgb(unity)=(0,0,0)
	ModifyGraph
zColor(NH4_meas)={waveforcolor,*,*,Rainbow},zColor(NH4_meas#1)={waveforcolor,*,*,Rainbow
}
	ModifyGraph nticks(y_nh4_meas)=10,nticks(x_nh4_pred)=10,nticks(x_time)=10
	ModifyGraph minor(x_time)=1
	ModifyGraph tick=1
	ModifyGraph sep(y_nh4_time)=10,sep(x_time)=10
	ModifyGraph fStyle(x_time)=1,lblMargin(y_nh4_meas)=9
	ModifyGraph lblPos(y_nh4_meas)=52,lblPos(x_nh4_pred)=44,lblPos(y_nh4_time)=52
	ModifyGraph lblLatPos(y_nh4_meas)=1
	ModifyGraph
freePos(y_nh4_time)=0,freePos(x_time)={0,y_nh4_time},freePos(x_nh4_pred)=0,freePos(y_nh4_mea
s)=0
	ModifyGraph axisEnab(y_nh4_meas)={0,0.70},axisEnab(x_nh4_pred)={0,0.70}
	ModifyGraph axisEnab(y_nh4_time)={0.75,1},dateInfo(x_time)={0,0,0}
	ModifyGraph mirror(x_time)=1
	ModifyGraph mirror(y_nh4_time)=1
	Label y_nh4_meas "\\f01Measured NH\\B4\\M (\\F'Symbol'm\\F'Arial'g/m\\S3\\M)"
	Label x_nh4_pred "\\f01Predicted NH\\B4\\M (\\F'Symbol'm\\F'Arial'g/m\\S3\\M)"
	Label y_nh4_time "\\f01NH\\B4\\M (\\F'Symbol'm\\F'Arial'g/m\\S3\\M)"
	Label x_time " "
```

```
	ShowInfo
	TextBox/N=text1/F=0/B=1/A=MC/X=-25.96/Y=58.19 "\\Z14\\f01Data Diagnostics:
Ammonium\r\\Z12Measured vs. Predicted"
	TextBox/N=text2/F=0/A=MC/X=40.34/Y=9.64 "Line 1:1"
	ColorScale/N=text0/F=0/B=1/A=MC/X=44.59/Y=-23.79 trace=NH4_meas, heightPct=50,
width=6
	ColorScale/C/N=text0 nticks=10, fsize=10, minor=1
	AppendText " "
EndMacro


Window SO4_Fragment() : Graph
	PauseUpdate; Silent 1		// building window...
	make/o/n=(numpnts(t_series)) waveforcolor
	waveforcolor = $(colorby)

	Display /W=(-2.25,37.25,588.75,514.25)/L=y_so4_time/B=x_time SO4_dd vs t_series
	AppendToGraph/L=y_so4_ratio/B=x_time ratio64_48,ratio80_48,ratio81_48,ratio98_48 vs
t_series
	AppendToGraph/L=y_so4_ratio_scatter/B=x_so4_48
SO4_64dd,SO4_80dd,SO4_81dd,SO4_98dd vs SO4_48dd
	AppendToGraph/L=y_so4_ratio_scatter/B=x_so4_48 unity,line_1_2,line_1_4,line_1_8
	ModifyGraph margin(left)=72,margin(bottom)=43
	ModifyGraph lsize(SO4_dd)=2
	ModifyGraph lsize(ratio64_48)=2
	ModifyGraph lsize(ratio80_48)=2
	ModifyGraph lsize(ratio81_48)=2
	ModifyGraph lsize(ratio98_48)=2
	ModifyGraph
mode(SO4_64dd)=3,mode(SO4_80dd)=3,mode(SO4_81dd)=3,mode(SO4_98dd)=3
	ModifyGraph
marker(SO4_64dd)=19,marker(SO4_80dd)=19,marker(SO4_81dd)=19,marker(SO4_98dd)=19
	ModifyGraph lSize(unity)=2,lSize(line_1_2)=2,lSize(line_1_4)=2,lSize(line_1_8)=2
	ModifyGraph lStyle(unity)=2,lStyle(line_1_2)=2,lStyle(line_1_4)=2,lStyle(line_1_8)=2
	ModifyGraph
rgb(ratio80_48)=(44032,29440,58880),rgb(ratio81_48)=(0,52224,0),rgb(ratio98_48)=(0,9472,39168)
	ModifyGraph
rgb(SO4_80dd)=(44032,29440,58880),rgb(SO4_81dd)=(0,52224,0),rgb(SO4_98dd)=(0,9472,39168)
	ModifyGraph
rgb(unity)=(0,0,0),rgb(line_1_2)=(0,0,0),rgb(line_1_4)=(0,0,0),rgb(line_1_8)=(0,0,0)
	ModifyGraph
msize(SO4_64dd)=1,msize(SO4_80dd)=1,msize(SO4_81dd)=1,msize(SO4_98dd)=1
	ModifyGraph zColor(SO4_dd)={waveforcolor,*,*,Rainbow}
	ModifyGraph tick=1
	ModifyGraph zero(y_so4_time)=1
	ModifyGraph mirror(y_so4_time)=1,mirror(x_time)=1,mirror(y_so4_ratio)=1
	ModifyGraph nticks(x_time)=10,minor(x_time)=1,sep(x_time)=10,fStyle(x_time)=1
	ModifyGraph
lblPos(y_so4_time)=58,lblPos(y_so4_ratio)=51,lblPos(y_so4_ratio_scatter)=53,lblPos(x_so4_48)=41
	ModifyGraph lblLatPos(y_so4_ratio_scatter)=8,lblLatPos(x_so4_48)=-14
	ModifyGraph freePos(y_so4_time)=0,freePos(x_time)={0,y_so4_ratio}
	ModifyGraph freePos(y_so4_ratio)={0,x_time},freePos(y_so4_ratio_scatter)=0
	ModifyGraph freePos(x_so4_48)={0,y_so4_ratio_scatter}
	ModifyGraph axisEnab(y_so4_time)={0.85,1},axisEnab(y_so4_ratio)={0.45,0.8}
	ModifyGraph axisEnab(y_so4_ratio_scatter)={0,0.4},axisEnab(x_so4_48)={0,0.4}
	ModifyGraph dateInfo(x_time)={0,0,0}
```

```
	Label y_so4_time "\\f01SO\\B4\\M (\\F'Symbol'm\\F'Arial'g/m\\S3\\M)"
	Label x_time " "
	Label y_so4_ratio "\\f01SO\\B4\\M Ratios: Fragment / 48"
	Label y_so4_ratio_scatter "\\f01SO\\B4\\M Ratios: Fragment / 48"
	Label x_so4_48 "\\f01SO\\B4\\M at m/z 48"
	SetAxis y_so4_ratio 0,2
	ShowInfo
	TextBox/N=text0/F=0/A=MC/X=22.32/Y=-17.56 "\\f01\\Z14Data Diagnostics:
Sulfate\r\\Z12Fragmentation Patterns"
	TextBox/N=text1/F=0/A=MC/X=20.49/Y=-37.59 "\\f01Sulfate Ratios\r\\K(65280,0,0)m/z 64
/ 48"
	AppendText "\\K(44032,29440,58880)m/z 80 / 48\r\\K(0,52224,0)m/z 81 /
48\r\\K(0,9472,39168)m/z 98 / 48"
	TextBox/N=text4/F=0/A=MC/X=0.46/Y=-36.09 "\\f01Lines 1:1\r		1:2\r		1:4\r
1:8"
	TextBox/N=text2/F=0/A=MC ""
	ColorScale/N=text3/F=0/B=1/A=MC/X=45.72/Y=-38.72 trace=SO4_dd, heightPct=40
	ColorScale/C/N=text3 width=7, nticks=10, fsize=10, minor=1
	AppendText " "
EndMacro

Window NO3_Fragment() : Graph
	PauseUpdate; Silent 1		// building window...
	make/o/n=(numpnts(t_series)) waveforcolor
	waveforcolor = $(colorby)

//WaveScaling(colorby)		//changes wave units

	Display /W=(154.5,49.25,733.5,503)/L=t_no3_time/B=x_time NO3_dd vs t_series
	AppendToGraph/L=y_no3_ratio/B=x_time ratio46_30 vs t_series
	AppendToGraph/L=y_no3_46/B=x_no3_30 NO3_46dd vs NO3_30dd
	AppendToGraph/L=y_no3_46/B=x_no3_30 line_1_2
	AppendToGraph/L=y_no3_ratio/B=x_time line_atpt5_time
//	AppendToGraph/R=y_no3_31/B=x_no3_30 m31_dd vs NO3_30dd
	ModifyGraph margin(left)=58,margin(bottom)=36
	ModifyGraph mode(NO3_46dd)=3
	ModifyGraph marker(NO3_46dd)=19
	ModifyGraph lsize(NO3_dd)=2
	ModifyGraph lsize(ratio46_30)=2
//		ModifyGraph lSize(m31_dd)=2
//		ModifyGraph mode(m31_dd)=2
	ModifyGraph lSize(line_1_2)=2,lSize(line_atpt5_time)=2
	ModifyGraph lStyle(line_1_2)=2,lStyle(line_atpt5_time)=2
	ModifyGraph rgb(line_1_2)=(0,0,0),rgb(line_atpt5_time)=(0,0,0)
	ModifyGraph msize(NO3_46dd)=1
	ModifyGraph
zColor(NO3_dd)={waveforcolor,*,*,Rainbow},zColor(NO3_46dd)={waveforcolor,*,*,Rainbow}
	ModifyGraph zero(t_no3_time)=1
	ModifyGraph mirror(t_no3_time)=1,mirror(x_time)=1,mirror(y_no3_ratio)=1
	ModifyGraph nticks(x_time)=10
	ModifyGraph minor(x_time)=1
	ModifyGraph tick=1
	ModifyGraph sep(x_time)=10,sep(y_no3_ratio)=10
	ModifyGraph fStyle(x_time)=1
	ModifyGraph
lblPos(t_no3_time)=55,lblPos(y_no3_ratio)=50,lblPos(y_no3_46)=55,lblPos(x_no3_30)=40
```

```
//                      ModifyGraph lblPos(y_no3_31)=50
        ModifyGraph lblLatPos(t_no3_time)=3,lblLatPos(y_no3_ratio)=3,lblLatPos(y_no3_46)=1
//                      ModifyGraph lblLatPos(x_no3_30)=-13,lblLatPos(y_no3_31)=2
        ModifyGraph freePos(t_no3_time)=0
        ModifyGraph freePos(x_time)={0,y_no3_ratio}
        ModifyGraph freePos(y_no3_ratio)=0
        ModifyGraph freePos(y_no3_46)=0
        ModifyGraph freePos(x_no3_30)={0,y_no3_46}
//                      ModifyGraph freePos(y_no3_31)=-290
        ModifyGraph axisEnab(t_no3_time)={0.85,1}
        ModifyGraph axisEnab(y_no3_ratio)={0.47,0.82}
        ModifyGraph axisEnab(y_no3_46)={0,0.4}
        ModifyGraph axisEnab(x_no3_30)={0,0.4}
        ModifyGraph dateInfo(x_time)={0,0,0}
//                      ModifyGraph axisEnab(y_no3_31)={0,0.4}
        Label t_no3_time "\\f01NO\\B3\\M (\\F'Symbol'm\\F'Arial'g/m\\S3\\M)"
        Label x_time " "
        Label y_no3_ratio "\\f01NO\\B3\\M Ratio: m/z 46 / 30"
        Label y_no3_46 "\\f01NO\\B3\\M at m/z 46"
        Label x_no3_30 "\\f01NO\\B3\\M at m/z 30"
//                      Label y_no3_31 "\\f01m/z 31 (no nitrate)"
        SetAxis y_no3_ratio 0,2
        ShowInfo
        TextBox/N=text0/F=0/A=MC/X=28.00/Y=-19.00 "\\f01\\Z14Data Diagnostics:
Nitrate\r\\Z12Fragmentation Patterns\r"
        AppendText "\\f00Line 1:2"
        ColorScale/N=text1/F=0/B=1/A=MC/X=35.50/Y=-35.88 trace=NO3_dd, side=2
        ColorScale/C/N=text1 heightPct=40, width=7, fsize=10, minor=1
        AppendText " "
EndMacro

Window Org_Fragment() : Graph
        PauseUpdate; Silent 1                   // building window...
        make/o/n=(numpnts(t_series)) waveforcolor
        waveforcolor = $(colorby)

        Display /W=(98.25,44,657,512.75)/L=y_org_time/B=x_time Org_dd vs t_series
        AppendToGraph/L=y_m44/B=x_org m44_dd vs Org_dd
        AppendToGraph/L=y_m43/B=x_m57 m43_dd vs m57_dd
        ModifyGraph margin(left)=58,margin(bottom)=43
        ModifyGraph mode(m44_dd)=3,mode(m43_dd)=3
        ModifyGraph marker(m44_dd)=19,marker(m43_dd)=19
        ModifyGraph msize(m44_dd)=1,msize(m43_dd)=1
        ModifyGraph lsize(Org_dd)=2
        ModifyGraph
zColor(Org_dd)={waveforcolor,*,*,Rainbow},zColor(m44_dd)={waveforcolor,*,*,Rainbow}
        ModifyGraph zColor(m43_dd)={waveforcolor,*,*,Rainbow}
        ModifyGraph nticks(x_time)=10
        ModifyGraph minor(x_time)=1
        ModifyGraph sep(x_time)=20
        ModifyGraph mirror(y_org_time)=1,mirror(x_time)=1
        ModifyGraph tick=1
        ModifyGraph
lblPos(y_org_time)=48,lblPos(y_m44)=52,lblPos(x_org)=49,lblPos(y_m43)=48
        ModifyGraph lblPos(x_m57)=41
        ModifyGraph lblLatPos(y_org_time)=3,lblLatPos(y_m44)=3,lblLatPos(x_org)=-6
```

```
	ModifyGraph freePos(y_org_time)=0
	ModifyGraph freePos(x_time)={0,y_org_time}
	ModifyGraph freePos(y_m44)={0,x_org}
	ModifyGraph freePos(x_org)={0,y_m44}
	ModifyGraph freePos(y_m43)={0,x_m57}
	ModifyGraph freePos(x_m57)={0,y_m43}
	ModifyGraph axisEnab(y_org_time)={0.65,1}
	ModifyGraph axisEnab(y_m44)={0,0.4}
	ModifyGraph axisEnab(x_org)={0,0.4}
	ModifyGraph axisEnab(y_m43)={0,0.4}
	ModifyGraph axisEnab(x_m57)={0.6,1}
	ModifyGraph dateInfo(x_time)={0,0,0}
	Label y_org_time "Organics (\\F'Symbol'm\\F'Arial'g/m\\S3\\M)"
	Label x_time " "
	Label y_m44 "m/z 44"
	Label x_org "Organics"
	Label y_m43 "m/z 43"
	Label x_m57 "m/z 57"
	ShowInfo
	ColorScale/N=text0/F=0/B=1/A=MC/X=32.22/Y=-3.65 trace=Org_dd, vert=0, height=7
	ColorScale/C/N=text0 widthPct=40, tickLblRot=90, fsize=9, minor=1
	AppendText " "
	TextBox/N=text1/F=0/B=1/A=MC/X=-32.38/Y=1.92 "\\f01\\Z14Data Diagnostics:
Organics\rOxidation"
EndMacro

Window Mass_TimeTrend() : Graph
	PauseUpdate; Silent 1		// building window...
//&	Display /W=(75.75,59.75,753.75,312.5) Ammonium,Sulphate,Organics,Nitrate vs t_series
	Display /W=(75.75,59.75,753.75,312.5) nh4,so4,org,no3 vs t_series
	ModifyGraph lSize=2
//&	ModifyGraph
rgb(Ammonium)=(65280,43520,0),rgb(Organics)=(0,52224,0),rgb(Nitrate)=(0,15872,65280)
	ModifyGraph rgb(nh4)=(65280,43520,0),rgb(Org)=(0,52224,0),rgb(No3)=(0,15872,65280)
	ModifyGraph zero(left)=1
	ModifyGraph mirror(left)=1,mirror(bottom)=1
	ModifyGraph nticks=10
	ModifyGraph minor=1
	ModifyGraph tick=1
	ModifyGraph sep=20
	ModifyGraph fSize=12
	ModifyGraph grid(bottom)=1,gridRGB(bottom)=(43520,43520,43520)
	ModifyGraph lblMargin(left)=5,lblMargin(bottom)=3
	ModifyGraph lblLatPos(left)=10,lblLatPos(bottom)=-15
	ModifyGraph dateInfo(bottom)={0,0,-
1},dateFormat(bottom)={Default,1,1,1,2,"Month/DayOfMonth/Year",1}
	Label left "\\f01\\Z12Mass Concentration (\\F'Symbol'm\\F'Arial'g/m\\S3\\M)"
	Label bottom "\\f01\\Z12Date"
	ShowInfo
//&	Legend/N=text0/J/A=MC/X=-33.56/Y=25.00 "\\Z12\\s(NH4_meas)
Ammonium\r\\Z12\\s(SO4_dd) Sulfate"
//&	AppendText "\\Z12\\s(NO3_dd) Nitrate\r\\Z12\\s(Org_dd) Organic"
	Legend/N=text0/J/A=MC/X=-33.56/Y=25.00 "\\Z12\\s(NH4) Ammonium\r\\Z12\\s(SO4)
Sulfate"
	AppendText "\\Z12\\s(NO3) Nitrate\r\\Z12\\s(Org) Organic"
EndMacro
```